THE UNIVERSITY OF MICHIGAN

INDUSTRY PROGRAM OF THE COLLEGE OF ENGINEERING

OXYGEN TRANSFER AT COBALT FERRITE SURFACE

Ching-Rong Huang

A dissertation submitted in partial fulfillment
of the requirements for the degree of
Doctor of Philosophy in the
University of Michigan
Department of Chemical and Metallurgical Engineering
1966

October, 1966

IP-750

ACKNOWLEDGEMENTS

The author wishes to express his appreciation to the members of his doctoral committee, Professors G. Parravano, J. F. Verdieck, J. D. Goddard, E. E. Hucke and G. B. Williams, for their guidance during the course of his work. The author is especially grateful to his Chairman, Professor Parravano who suggested the topic for this research, for his numerous helpful suggestions and invaluable criticism. The author is also grateful to Professor Hucke who served as the acting Chairman in the latter part of this work while Professor Parravano was on sabbatical leave.

The author is indebted to the National Science Foundation for its financial support for four years.

Finally the author would like to thank Mr. W. C. Gates, Jr. for reading the manuscript, to thank the staff of the Industry Program of the College of Engineering for typing and printing this manuscript, and to express my deep gratitude to my devoted wife for her constant encouragement and for the typing of the rough draft of this manuscript.

TABLE OF CONTENTS

	Page
ACKNOWLEDGMENTS	ii
LIST OF TABLES	iv
LIST OF FIGURES	v
LIST OF APPENDICES	vii
NOMENCLATURE	viii
ABSTRACT	ix
I. INTRODUCTION	1
II. THEORY	4
III. SURVEY OF LITERATURE	19
IV. EXPERIMENTAL APPARATUS AND PROCEDURE	26
V. EXPERIMENTAL RESULTS	35
VI. DISCUSSION OF RESULTS	59
VII. CONCLUSIONS	69
APPENDICES	71
BIBLIOGRAPHY	109

LIST OF TABLES

Table		Page
1	Summary of Experimental Results of the Exchange Reaction of CO_2 and CO on $Co_{3-x}\ Fe_x\ O_4$	37
2	Activation Energy of the Exchange Reaction of CO_2 and CO on $Co_{3-x}\ Fe_x\ O_4$	37
3	Summary of Experimental Results of the Adsorption of Oxygen on $Co_{3-x}\ Fe_x\ O_4$	44
4	Summary of Experimental Results of the Desorption of Oxygen on $Co_{3-x}\ Fe_x\ O_4$	50
5	Experimental Data on the Formation of ^{14}CO catalyzed by 1.000 gram of $Co_{3-x}\ Fe_x\ O_4$	71
6	Experimental Data on the Adsorption of Oxygen by 50.000 grams of Cobalt Ferrite	82
7	Experimental Data of Oxygen Desorption from 50.000 grams of Cobalt Ferrite	90
8	The Result of Run 17-21 of the Exchange Reaction of CO_2 and CO	98

LIST OF FIGURES

Figure		Page
1	Apparatus for the Exchange Reaction of CO_2 and CO ...	28
2	Geigen Counter and Accessaries	30
3	Apparatus for the Adsorption and Desorption of Oxygen..	32
4	Formation of ^{14}CO Versus Times on $Co_{0.901}Fe_{2.099}O_4$ with A=2.48 x 10^4 cm^2 and T=350°C	36
5	The Value m from $k(a_o)$ Versus a_o	39
6	Activation Energy of the Exchange Reaction from $k(a_o)$ Versus $\frac{1}{T}$, a_o=0.464	45
7	Adsorption of Oxygen on $Co_{0.994}Fe_{2.006}O_4$	46
8	Activation Energy of Oxygen Adsorption from $K_{ads.}$ Versus $\frac{1}{T}$.....	48
9	Rate Constant $k(a_o)$ of the Exchange Reaction Versus Composition x, T=350°C and a_o=0.464	51
10	Activation Energy of the Exchange Reaction Versus Composition x, a_o=0.464	52
11	Amount of Oxygen Adsorbed in 24 Hours Versus Composition x, t=300°C	53
12	Initial Rate of Oxygen Adsorption on $Co_{3-x}Fe_xO_4$ Versus Composition x, T=300°C and p_{ai}=100 microns of Hg	55
13	Initial Rate Constant of Adsorption $K_{ads.}$ Versus Composition x on $Co_{3-x}Fe_xO_4$ at T=300°C	56
14	Initial Rate of Desorption from $Co_{3-x}Fe_xO_4$ Versus Composition x at 300°C	57
15	Amount of Oxygen Desorbed from $Co_{3-x}Fe_xO_4$ in 24 Hours Versus Composition x at 300°C	58
16	$p_{^{14}CO}/p^i_{^{14}CO_2}$ Versus t for Run 17-21 and initial slope	97

LIST OF FIGURES (CONT'D)

Figure		Page
17	$p_{^{14}CO}/p^{i}_{^{14}CO_2}$ Versus t for Run 17-21 and results from the Computer Simulating Method	100
18	p_a Versus t for Run 10-14 and Results from the Computer Simulating Method	103
19	Composition of (100), (110) and ($\bar{1}$10) Planes in $CoFe_2O_4$.....	107

LIST OF APPENDICES

Appendix		Page
I	Experimental Data.....	71
II	Sample Calculation.....	96
III	Structure of Cobalt Ferrite.....	106

NOMENCLATURE

a	lattice parameter of cobalt ferrite
a_o	ratio of $\frac{P_{CO_2}}{P_{CO}}$
A	surface area of the catalyst
$\|A\|$	tetrahedral site in the spinel structure
$\|B\|$	octahedral site in the spinel structure
C_1, C_2	constants
$C_o^{+2} \|B\|$	C_o^{+2} ion on the tetrahedral site
$C_o^{+3} \|B\|$	C_o^{+3} ion on the tetrahedral site
$C_o^{+2} \|B\| - Fe^{+3} \|B\|$	the ion pair, the proposed active center on the catalyst surface
e^-	free electron
E_a	activation energy
F	Gibbs free energy
$Fe^{+2} \|B\|$	Fe^{+2} ion on the tetrahedral site
$Fe^{+3} \|B\|$	Fe^{+3} ion on the tetrahedral site
h^+	free hole
$k(a_o)$	forward rate constant of the exchange reaction defined by equation (16)
$k'(a_o)$	backward rate constant of the exchange reaction defined by equation (16)
$k_{ads.}$	adsorption rate constant defined by equation (40)
$k_{des.}$	desorption rate constant defined by equation (49)
k_p	pre-exponential factor defined by equation (28)
k_f	rate constant defined by equation (30)
K_1	equilibrium constant

K_{ads}	overall rate constant of adsorption defined in equation (39)
m	a constant defined in equation (25)
n	n-type semiconductor
$n_{^{14}CO}$	gm-mole of ^{14}CO
n_a	gm-mole of oxygen in the adsorption reservoir
n_d	gm-mole of oxygen in the desorption reservoir
N	Avogadro's number
p	partial pressure
R	gas constant
t	time
T	temperature
V	volume of reactor or reservoir
x	a parameter which defines the composition of $CO_{3-x}\ Fe_x\ O_4$
z	concentration of CO^{+3} $\|B\|$ in cobalt ferrite
α	a constant defined in equation (25)
β	number of the active center CO^{+2} $\|B\|$ - Fe^{+3} $\|B\|$ per unit surface area
γ	a constant defined by equation (47)
ξ	a constant defined by equation (54)

Subscripts and Superscripts

a	refer to adsorption
b	refer to the bare site
d	refer to desorption
f	denote the final condition

i	denote the initial condition
o	refer to the occupied site
r	indicate the reference state of adsorption
t	refer to total

ABSTRACT

Semiconductors are commonly used catalysts. Cobalt ferrite, $Co_{3-x}Fe_xO_4$, was very suitable to be chosen for studying catalysis. It can be made a n-type or p-type semiconductor by changing slightly the ratio of iron and cobalt. Therefore it gives an opportunity to study the effect of composition on the catalytic activity without introducing impurities into the catalyst.

The exchange reaction between carbon dioxide and carbon monoxide was investigated on cobalt ferrite catalysts, $Co_{3-x}Fe_xO_4$, with four different compositions x ranging from 1.903 to 2.099. The reaction occurred in a constant volume reactor. The reaction rate was measured at temperatures ranging from 250° to 410°C with carbon^{-14} dioxide as the tracer. One feature of the catalyzed exchange reaction is that the reaction rate is studied under equilibrium condition. There is no net increase nor decrease of carbon dioxide and carbon monoxide in the gas phase. The thermodynamic activity of the catalytic intermediate on the surface remains constant during the reaction.

The adsorption and desorption of oxygen was investigated on five different cobalt ferrite catalysts with the same range of x as the exchange reaction. The adsorption occurred in a constant volume reactor with initial pressure of oxygen near 0.1 mm of mercury. The desorption of oxygen was under high vacuum with pressure less than 1×10^{-5} mm of mercury. The rate was measured by the pressure change of the system with the ionization gauge at temperatures ranging from 100° to 500°C.

The experimental results show that the rate constant of the exchange reaction and the initial rate of oxygen adsorption are at their maximum when x is near two. This can not be explained by the conventional electronic defect mechanism which is based on the electronic defect, electron donor for the n-type semiconductor or electron acceptor for the p-type semiconductor, as the active center of the reactions. But the result can be explained by the proposed mechanism of cyclic electron-hole transfer of the cation pair which can supply an electron and an electron hole to the catalytic intermediate and act as the active center of the reactions.

This study has not only furnished basic data for the exchange reaction of carbon dioxide and carbon monoxide and for the oxygen adsorption - desorption on cobalt ferrite, but also has proposed a new concept for studying the mechanism of heterogeneous catalysis.

I. INTRODUCTION

Catalysis plays an important role in many chemical processing industries. Let us imagine that a solid - the catalyst - is introduced into a mixture of reacting gases. The rate of reaction increase by hundreds or thousands of times. In the absence of a catalyst the reaction either hardly occurs or proceeds very slowly. Catalysis provides a new path of stepwise reactions which are associated with the interaction between reactants and catalyst. The catalyst participates in the formation of an catalytic intermediate on its surface and returns to its original state after the completion of the chemical reaction. The increase in the reaction rate, caused by the fact that the reaction follows the path of intermediate steps with the catalyst, has been made possible by the decrease in activation energy due to a more favorable form of the bonds between the reactants.

Semiconductors, like metals, are commonly used catalysts. The catalytic action of semiconductors was discovered and used in the chemical processing industry long before the concept of a semiconductor itself appeared. It is now obvious that the catalytic activity of semiconductors is very closely connected with the electronic properties inside and on the surface of semiconductors. For examples, the influence of impurities of a semiconductor on its catalytic activity has been investigated; the correlation between the electrical conductivity or thermolelectric power of a semiconductor and its catalytic activity has been discovered. In order to investigate the mechanism of the catalytic reaction, it is necessary to understand the solid state reactions of the semiconductor.

The object of this research was to study the catalytic activity of cobalt ferrite as a function of its composition. The first part of the research was the study of catalytic exchange reaction of carbon monoxide and carbon dioxide by using carbon-14 as the tracer. The second phase of the research was the study of the chemisorption and desorption of oxygen on cobalt ferrite.

Cobalt ferrite, $Co_{3-x}Fe_xO_4$, was chosen as the catalyst for the following six reasons. (1) It can be made a n-type or p-type semiconductor by changing slightly the ratio of iron and cobalt. Therefore it gives an opportunity to study the effect of composition on the catalytic activity without introducing impurities into the catlyst. (2) The crystal structure and electronic properties of cobalt ferrite has been investigated extensively. (3) It is chemically stable up to 1100°C in the atmosphere due to its close-packed, face-centered cubic arrangement of the spinel structure. With composition ranging from $1.84 < x < 2.34$, the spinel is found stable in one phase. (4) It does not contain an appreciable number of lattice vacancies - Schottky type defect, or of interstitial ions - Frenkel type defect; the ratio of cations to anions can be regarded as a constant of 3:4. The characteristic defects of cobalt ferrite are Fe^{+2}, which replaces Co^{+2} in case of $x > 2$, and Co^{+3} which replaces Fe^{+3} in case of $x < 2$. (5) The thickness of the space charge layer is smaller than the interatomic distance between lattice ions. The small thickness gives the advantage of permitting the electronic boundary phenomena to be neglected and appropriate equilibrium assumptions to be used in later derivations. With experimental results, we can compare the theoretical explanation on the mechanism

of the catalytic reaction by the electronic defect and by the cyclic electron transfer of the cation pairs.

The exchange reaction between carbon dioxide and carbon monoxide was investigated on cobalt ferrite catalysts, $Co_{3-x}Fe_xO_4$, with four different compositions x ranging from 1.954 to 2.099. The reaction occurred in a constant volume reactor. The reaction rate was measured at temperatures ranging from 250° to 410°C with carbon-14 dioxide as the tracer. One feature of the catalyzed exchange reaction is that the reaction rate is studied under equilibrium condition. There is no net increase nor decrease of carbon dioxide and carbon monoxide in the gas phase. The thermodynamic activity of the catalytic intermediate on the surface remains constant during the reaction.

The adsopption and desorption of oxygen was investigated on five different cobalt ferrite catalysts with the same range of x as the exchange reaction. The adsorption occurred in a constant volume reactor with initial pressure of oxygen near 0.1 mm of mercury. The desorption of oxygen was under high vacuum with pressure less than 1×10^{-5} mm of mercury. The rate was measured by the pressure change in the system with the ionization gauge at temperatures ranging from 100° to 500°C.

II. THEORY

A. Properties of Cobalt Ferrite

(a) Structure

Cobalt ferrite $Co_{3-x}Fe_xO_4$ is one of many composite oxides having the gereral formula AB_2O_4 which crystallize with the crystal structure called spinel [73]. The spinel structure is characterized by face-centered cubic close packing of O^{-2} ions and A^{+2} and B^{+3} metallic ions in certain interstices [9] [55]. A unit cell of spinel crystal contains eight molecules of AB_2O_4 and, therefore, thirty-two O^{-2} ions. The close packed unit cell contains sixty-four interstices surrounded by four O^{-2} ions (coordination number 4, tetrahedral) and thirty-two interstices surrounded by six O^{-2} ions (coordination number 6, octahedral). In the spinel unit cell, eight of these tetrahedral sites, denoted as $|A|$, and sixteen of the octahedral sites, denoted as $|B|$, are occupied by these metallic ions.

The metallic ions A^{+2} and B^{+3} are distributed among the cation sites in different ways [4]. In "normal" spinel, all sixteen B^{+3} ions occupy the sixteen octahedral sites and all eight A^{+2} ions occupy the tetrahedral sites. In "inverse" spinel, the sixteen octahedral sites are occupied half by A^{+2} and half by B^{+3}. This has been determined by x-ray diffraction.

Cobalt ferrite exists in a structure [48] which is very close to the structure of the "inverse" spinel, $Fe^{+3}|A|[Co^{+2}|B|Fe^{+3}|B|]O_4$ (see Appendix III).

(b) Composition

Stoichiometric cobalt ferrite, $CoFe_2O_4$, hardly exists. The non-stoichiometric cobalt ferrite, $Co_{3-x}Fe_xO_4$, has been investigated [47] with x ranging from 1.84 to 2.34. When x is larger than 2.34, a new phase of Fe_2O_3 will co-exist with the spinel phase. Also when x is less than 1.84, a new phase of wustite will co-exist with the spinel phase. When x is in the vicinity of 2, if $x < 2$, indicating an excess of cobalt, Fe^{+3} on the octahedral sites is essentially replaced by Co^{+3} ion. If, on the other hand, $x > 2$, indicating an excess of iron, Co^{+2} on the octahedral sites is essentially replaced by Fe^{+2} ions.

Using this disorder model and appropriate assumptions, it is possible to obtain the concentration of each cation on different sites as a function of the composition x [48]. There are eight possibilities of cations which may occupy the lattice sited |A| and |B|. These are Fe^{+3} |A|, Fe^{+2} |A|, Co^{+3} |A|, Co^{+2} |A|, Fe^{+3} |B|, Fe^{+2} |B|, Co^{+3}|B| and Co^{+2} |B|.

(i) Fe and Co balance:

$$[Fe^{+3}|A|] + [Fe^{+2}|A|] + [Fe^{+3}|B|] + [Fe^{+2}|B|] = x \qquad (1)$$

$$[Co^{+3}|A|] + [Co^{+2}|A|] + [Co^{+3}|B|] + [Co^{+2}|B|] = 3-x \qquad (2)$$

(ii) tetrahedral and octahedral sites balance:

$$[Fe^{+3}|A|] + [Fe^{+2}|A|] + [Co^{+3}|A|] + [Co^{+2}|A|] = 1 \qquad (3)$$

$$[Fe^{+3}|B|] + [Fe^{+2}|B|] + [Co^{+3}|B|] + [Co^{+2}|B|] = 2 \qquad (4)$$

(iii) charge ratio balance:

$$[Fe^{+3}|A|] + [Fe^{+3}|B|] + [Co^{+3}|A|] + [Co^{+3}|B|]$$
$$= 2\{[Fe^{+2}|A|] + [Fe^{+2}|B|] + [Co^{+2}|A|] + [Co^{+2}|B|]\} \qquad (5)$$

$[Fe^{+3}|A|]$, denoted as concentration of Fe^{+3} in the tetrahedral sites, is assumed to be unity and independent of x, if we designate the concentration $[Co^{+3}|B|]$ by z.

Solving equations (1) to (5), yields

$$[Co^{+2}|B|] = 3-x-z \tag{6}$$

$$[Fe^{+2}|B|] = x-2+z \tag{7}$$

$$[Fe^{+3}|B|] = 1-z \tag{8}$$

(c) Electronic Property

The semiconducting properties of $Co_{3-x}Fe_xO_4$ have been investigated with x ranging from 1.9 to 2.1[35]. Electrons or electron holes can be introduced into cobalt ferrite to obtain n-type or p-type semiconductivity by varying x values. When $x > 2$, the excess Fe is added to $CoFe_2O_4$ to replace Co, it enters the crystal structure as $Fe^{+2}|B|$, which acts as an electron donor and causes the ferrite to become a n-type semiconductor. In a similar way, when $x < 2$, the Co is added to $CoFe_2O_4$ to replace Fe, it enteres the crystal structure as $Co^{+3}|B|$, which acts as an electron acceptor, causing the ferrite to become a p-type semiconductor. Therefore it gives an opportunity to study the catalytic activity of an oxide catalyst having a single substrate with either electrons (n-type catalyst) or electon holes (p-type catalyst) in excess without adding foreign impurities to the ferrite. Also the validity of the electronic defect explanation to catalysis can be investigated.

Since catalytic reaction may involve the electron transfer from the catalyst surface to the catalytic intermediate, so it is necessary to look into the defect reaction of cobalt ferrite from its characteristic defects.

Let us first define the characteristic defect of cobalt ferrite. The characteristic defect of cobalt ferrite is defined as $Fe^{+2}|B|$ or $Co^{+3}|B|$ in the lattice structure. In the range of $1.9 < x < 2.1$, Jonker [35] has shown that the characteristic defects $Fe^{+2}|B|$ and $Co^{+3}|B|$ are completely ionized. This means that the activition energy of ionization is very close to zero. Therefore, we may write the predominate solid phase reactions from the characteristic defects as following:

$$\text{For n-type, } Fe^{+2}|B| \rightarrow Fe^{+3}|B|_i + e^- \tag{9}$$

$$\text{For p-type, } Co^{+3}|B| \rightarrow Co^{+2}|B|_i + h^+ \tag{10}$$

where $Fe^{+3}|B|_i$ is the ionized donor in n-type cobalt ferrite. It is important to note that the electron can also be generated by the normal cations $Co^{+3}|B|$ and Fe^{+3} on the solid surface,

$$Co^{+2}|B| \rightarrow Co^{+3}|B|_i + e^- \tag{11}$$

$$\text{also } Fe^{+3}|B| \rightarrow Fe^{+2}|B|_i + h^+ \tag{12}$$

if the solid is in contact with gas molecules with high electron or hole affinity. Jonker has found that the activation energies for equations (11) and (12) are 10.94 to 11.75 Kcal. and 4.4 to 4.73 Kcal. respectively [35]. The next sections are the analysis of the catalyzed exchange reaction of CO_2 and CO and of the adsorption and desorption of oxygen on cobalt ferrites based on the solid state reaction of the solid phase.

B. CO_2 - CO Exchange Reaction

(a) Description of Model

The kinetics of the catalyzed exchange reaction on cobalt ferrite between carbon dioxide and carbon monoxide was investigated in

a constant volume reactor. Radioactive carbon-14 dioxide was employed as the tracer. An important feature of the exchange reaction of CO_2 and CO is that the gas phase, composed of a fixed ratio of CO_2 and CO, is in equilibrium with the catalyst surface. The following reaction was studied,

$$^{14}CO_2(g) + CO(g) \underset{\leftarrow}{\rightarrow} {}^{14}CO(g) + CO_2(g) \qquad (13)$$

with a small amount of $^{14}CO_2$ introduced in the gas phase.

It is assumed that reaction (13) follows the sequence of steps:

$$^{14}CO_2(g) \underset{\leftarrow}{\rightarrow} {}^{14}CO(g) + O_{ads.} \qquad (14)$$

$$CO(g) + O_{ads.} \rightleftarrows CO_2(g) \qquad (15)$$

Since there is no net formation of either CO_2 or CO, the activity of oxygen atom adsorbed on the surface is constant. It is obvious that the activity of oxygen on the catalyst surface depends on the ratio of CO_2 and CO in the gas phase. The next three sections are the analysis of the correlation of this dependence with the properties of cobalt ferrite.

(b) Evaluation of Rate Constants

Since the activity of oxygen on the catalyst surface is a constant for a prefixed CO_2/CO ratio, the rate of formation of ^{14}CO can be written as

$$\frac{dn^{14}CO}{Adt} = k(a_o)\, p_{^{14}CO_2} - k'(a_o)\, p_{^{14}CO} \qquad (16)$$

$$\text{where } a_o = \frac{p_{CO_2}}{p_{CO}} \qquad (17)$$

and A = surface area of the catalyst.

The forward and backward rate constants $k(a_o)$ and $k'(a_o)$ are defined by equation (16). Note that at constant temperature for a

catalyst with fixed x, $k(a_o)$ or $k'(a_o)$ is a function of a_o only. The net rate of formation of ^{14}CO becomes zero, when equation (16) reaches equilibrium. It yields

$$\left(\frac{p\ ^{14}CO_2}{p\ ^{14}CO}\right)_{eq.} = \frac{p\ CO_2}{p\ CO} = \frac{k'\ (a_o)}{k\ (a_o)} = a_o \qquad (18)$$

Eliminating $k'(a_o)$ from equation (16) with equation (18), it follows that

$$\frac{d\ n\ ^{14}CO}{A\ d\ t} = k(a_o)\ (p_{^{14}CO_2} - a_o\ p_{^{14}CO}) \qquad (19)$$

In a constant volume reactor, the total amount of radioactive ^{14}C is constant, so

$$p_{^{14}CO_2} + p_{^{14}CO} = p^i_{^{14}CO_2} \qquad (20)$$

where $p^i_{^{14}CO_2}$ is the initial partial pressure of $^{14}CO_2$ in the reactor at $t=0$. There is no ^{14}CO in the gas mixture at $t=0$.

Combining equations (19) and (20) to eliminate $p_{^{14}CO_2}$, and applying ideal gas law;

$$\frac{V}{RTA}\ \frac{dp\ ^{14}CO}{dt} = k(a_o)\ [p^i_{^{14}CO_2} - (1 + a_o)\ p_{^{14}CO}] \qquad (21)$$

In a constant volume reactor at constant temperature with prefixed CO_2/CO ratio, a_o and $k(a_o)$ are constants, so that equation (21) can be integrated with the initial condition $p_{^{14}CO} = 0$ at $t = 0$.

$$\int_o^{\frac{p\,^{14}CO}{p^i\,^{14}CO_2}} \frac{d\ \frac{p\,^{14}CO}{p^i\,^{14}CO}}{\frac{1}{1+a_o} - \frac{p\,^{14}CO}{p^i\,^{14}CO_2}} = \frac{k(a_o)\ RTA(1+a_o)}{V} \int_o^t dt \qquad (22)$$

$$\text{In}\ \left[1 - (1+a_o)\ \frac{p_{14}CO}{p^i\,^{14}CO_2}\right] = -\ \frac{k(a_o)RTA(1+a_o)t}{V} \qquad (23)$$

or

$$\frac{p_{14}CO}{p^i\,^{14}CO_2} = \frac{1}{1+a_o}\ \left\{1 - \exp.\left[\frac{-k(a_o)\ RTA\ (1+a_o)\ t}{V}\right]\right\} \qquad (24)$$

At a given temperature and CO_2/CO ratio, the rate constant $k(a_o)$ can be calculated by equation (24) from the experimental data of the percentage of ^{14}CO formation and time.

(c) Dependence of the Rate Constant as a Function of CO_2/CO ratio and Temperature

The most commonly postulated mechanism to explain the catalytic reaction is based on the assumption that reacting molecules rearange themselves on the active centers of the catalyst surface. The adsorbed fragment of the reacting molecule on the active center is called the catalytic intermediate. Although there are widely different opinions on the exact catalytic intermediate and on the active center in a reacting system, this does not disprove their existence.

The proposed catalytic intermediate for this exchange reaction of CO_2 and CO is $O_{ads.}$ The employing of $O_{ads.}$ as the catalytic intermediate was postulated by Wagner [75] [76] for the CO_2 - CO exchange reaction on Wustite. And it was applied by Grabke [26] [27] to study the rate of oxygen transfer from CO_2 to the surface of the

oxides $Fe_{1-x}O$, Fe_2O_4, CoO, ZnO and MgO. There are various states in which O_{ads} may exist. It may exist as chemisorbed oxygen atom, chemisorbed O^- ion or chemisorbed O^{-2} ion. The state of the catalytic intermediate is dependent on the properties of the oxide. Under equilibrium condition and assuming that the mass action law holds, we may express, in general, the thermodynamic activity of the active center as a linear function of $(p_{CO_2}/p_{CO})^{-m}$ which is equal to a_o^{-m} as defined in equation (17). m is a positive constant which is dependent on the electronic property of the active center and on the existing state of O_{ads}. Consider the phenomenological derivation of equation (16), it is desirable to correlate the dependence of $k(a_o)$ on a_o with the mechanistic expression of the thermodynamic activity of the active center. The dependence can be described by

$$k(a_o) = \alpha\, a_o^{-m} \tag{25}$$

where α is a function of temperature. The constant m will be discussed in detail in the next section. The value of m can be obtained experimentally from the known values of $k(a_o)$ as following,

$$\ell n\ [k(a_o)] = -\, m\ \ell n\ a_o + \ell n\ \alpha \tag{26}$$

$$\left(\frac{\partial\ \ell n\ [k(a_o)]}{\partial\ \ell n\ a_o}\right)_T = -m \tag{27}$$

at fixed a_o, the temperature dependence of $k(a_o)$ follows the relation

$$k(a_o) = k_p e^{-E_a/RT} \tag{28}$$

where k_p is the pre-exponential factor, and E_a is the activation energy of the reaction which can be obtained by plotting log $k(a_o)$ versus $\frac{1}{T}$.

$$\left(\frac{\partial \ell n\,[k(a_o)]}{\partial\, \ell n\, \frac{1}{T}}\right)_{a_o} = -\frac{E_a}{R} \qquad (29)$$

(d) The Proposed Active Center and Catalytic Intermediate

The proposed active center for the CO_2 - CO exchange reaction is the ion pair $Co^{+2}|B|$ - $Fe^{+3}|B|$. The ion pair $Co^{+2}|B|$-$Fe^{+3}|B|$ appears on plane (100) of the "inversed" spinel structure of cobalt ferrite. The average inter-ionic distance of the pair is 2.97A. (see Appendix III). The characteristic feature of the pair is that they can supply to the catalytic intermediate $O_{ads.}$ an free electron and an electron hole with which the simultaneous catalyzed oxidation of CO and reduction of CO_2 in the exchange reaction can proceed. An electron donor itself, for example, the characteristic defect $Fe^{+2}|B|$ is not qualified as an effective active center. The reason is that without an hole supplied from the active center the O_{ads} is very strongly bound to the active center and usually hinder the course of catalysis. The hindered effect by the strongly bound catalytic intermediate was also shown in many other catalyzed reactions [2]. It was established long time ago that molecules possessing an electron donor group and a hole donor group may act as catalysts in homogeneous catalysis. It was known as the dual theory of catalysis [7]. Taylor [68] [69] bases his support of the dual theory on the rate of hydrolysis of various esters in presence of acids with and without the addition of salts. He has found that the addition of 1N KCl to 0.1N HCl causes a 24% increase of reaction rate. From conductivity data, the degree of dissociation of 0.1N HCl is

about 90% and this is reduced to 75% by the addition of 1N KCl. Taylor, therefore, concludes that the increase in the reaction rate caused by the addition of KCl is due to the formation of more undissociated HCl which acts as a catalyst by having an electron donor group H and a hole donor group Cl. Recently, the mechanism of alkylations of diazoalkanes catalyzed with fluoroboric acid was based on the complex formation of the diazoalkane and HBF_4 with H as the electron donor group and BF_4 as the hole donor group [5] [46].

There are other pairs, eg. free electron - free electron hole pair, pairs of the characteristic defect and the normal lattice cations ____ $Fe^{+2}|B|$ - $Fe^{+3}|B|$ or $Co^{+2}|B|$ - $Co^{+3}|B|$ ____ and pair of two different types of characteristic defects $Fe^{+2}|B|$ - $Co^{+3}|B|$ which may supply an electron and a hole to the catalytic intermediate. But they are rejected as the active center in the following discussion. The free electron - free electron hole pair are difficult to be found on the surface of semiconductor with the inter-particle distance in the order of magnitute of angstrom. The two opposite charged particles of the pair tend to collide with each other at that distance. The pairs $Fe^{+2}|B|$ - $Fe^{+3}|B|$ and $Co^{+2}|B|$ - $Co^{+3}|B|$ are rejected because of their unbalanced ability of gererating a free electron and a free hole, which was discussed in Section A(c). the electronic property. The overall electronic characteristics of the pairs are an electron donor and a hole donor respectively. The pair of characteristic defects $Fe^{+2}|B|$ - $Co^{+3}|B|$ are extremely unstable because each defect is completely ionized to form a free electron or a free hole. After the reaction of the electron and the hole, the pair become Fe^{+3}- Co^{+2} which is the proposed active center.

It is worth noting that although the characteristic defects $Fe^{+2}|B|$ and $Co^{+3}|B|$ are rejected as active centers, they may effect the activation energy of ionization of the proposed active center. Any characteristic defect located next to the proposed active center (see Appendix III) may alter the polarity of the center so that the potential field, which effects the activation energy of ionization, is changed.

With the proposed $Co^{+2}|B| - Fe^{+3}|B|$ as the active center for the exchange reaction, we may write the rate expression of the forward reaction of equation (16) as the following:

$$\frac{d\, n\, {}^{14}CO}{A\, d\, t} = -k_f\, [Co^{+2}|B| - Fe^{+3}|B|]\; p_{{}^{14}CO_2} \tag{30}$$

where k_f is the forward reaction rate constant, and $[Co^{+2}|B| - Fe^{+3}|B|]$ is the activity of the bare active center $Co^{+2}|B| - Fe^{+3}|B|$ on the catalyst surface.

Recall that the CO_2 - CO gas mixture is in equilibrium with the catalyst surface. This means that the activity of the occupied active center and of the bare center remains constant during the exchange reaction. We may write the equilibrium reaction as

$$CO_2(g) + Co^{+2}|B| - Fe^{+3}|B| \underset{\leftarrow}{\rightarrow} (Co^{+3}|B| - Fe^{+3}|B|) - O^-_{ads} + CO(g) \tag{31}$$

it follows

$$k_1 = \frac{[(Co^{+3}|B| - Fe^{+3}|B|) - O^-_{ads}]}{[Co^{+2}|B| - Fe^{+3}|B|]} \left(\frac{p_{CO_2}}{p_{CO}}\right)^{-1} \tag{32}$$

where $[(Co^{+3}|B| - Fe^{+3}|B| - O^{-}_{ads}]$ is the activity of the occupied center. Ratterman (49) has found that the conductivity of cobalt ferrite catalyst is nearly independant of the ratio of CO_2 and CO in a flow reactor. From the material balance of free electrons,

$$[e^{-}]_{total} = [e^{-}]_{solid} + c_1[e^{-}]_{trans} \tag{33}$$

where $[e^{-}]$ is concentration of the free electron. The subscripts "total" refers to the total amount, "solid" refers to the solid phase and "trans" refers to transfer to catalytic intermediate. c_1 is a proportional constant.

In order to find the effect of changing a_o on the free electron concentration, differentiate equation (33) with respect to a_o

$$\frac{d\,[e^{-}]total}{d\,a_o} = \frac{d\,[e^{-}]solid}{d\,a_o} + c_1 \frac{d\,[e^{-}]\,tran}{d\,a_o} \tag{34}$$

The left hand side of equation (34) is zero, because $[e^{-}]$total is a constant. The first term of right hand side of equation (34) is zero, which was experimentally found by Ratterman. Therefore $[e^{-}]$trans is a constant independent of a_o. Since $[e^{-}]$trans $= [(Co^{+3}|B| - Fe^{+3}|B|) - O^{-}_{ads}]$ we may rearrange equation (32) and yield

$$[Co^{+2}|B| - Fe^{+3}|B|] = c_2\ a_o^{-1} \tag{35}$$

where c_2 is a constant independent of a_o.

The next task is to compare the different expressions of the forward reaction of equation (14). From equations (16), (25), (30) and (35), we have

$$\frac{d\ n14_{CO}}{A\ d\ t} = k(a_o)\ p_{14_{CO_2}} = \alpha\ a_o^{-m}\ p_{14_{CO_2}}$$

$$= k_f[Co^{+2}|B| - Fe^{+3}|B|]\ p_{14_{CO_2}}$$

$$= c_2 \times k_f \left(\frac{p_{CO_2}}{p_{CO}}\right)^{-1} p_{14_{CO_2}} \qquad (36)$$

Since by definition $a_o = p_{CO_2}/p_{CO}$, so it is concluded from equation (36) that m=1, if the state of oxygen on the active center is O^{-1}_{ads}. By the same analysis, if we have the state of oxygen O^{-2}_{ads}. instead of O^{-1}_{ads}. on the catalyst surface, we would have the equilibrium reaction

$$CO_2(g) + 2\ Co^{+2}|B| - Fe^{+3}|B| \rightleftarrows (Co^{+3}|B| - Fe^{+3}|B|)_2 - O^{-2}_{ads} + CO(g) \qquad (37)$$

and

$$[Co^{+3}|B| - Fe^{+3}|B| = \text{constant} \times \left(\frac{p_{CO_2}}{p_{CO}}\right)^{-0.5} \qquad (38)$$

The value of m would be 0.5.

C. Chemisorption and Desorption of Oxygen

Chemisorption of oxygen on cobalt ferrite occurs when an electron prossessing the necessary activation to pass through the potential barrier, reacts with the colliding oxygen molecule on the ferrite surface. Therefore, the rate of adsorption is strongly effected by the number of oxygen molecules colliding with a unit area of the surface per unit time, by the type and number of active centers which donate electrons and by the activation energy for each type of active center.

The number of collisions between oxygen molecules and the surface can be obtained from the kinetic theory of gases. It is directly proportional to the pressure of oxygen of the system and inversely proportional to the product of one-half power of the temperature and the molecular weight of oxygen. The activation energy of chemisorption is a function of the electron affinity of the oxygen molecule, the activation energy needed for the jump of an electron from the active center and the work function to transfer an electron to the oxygen molecule. If the surface coverage of the adsorbed ions is high, the interaction of the adsorbed ions is also important. Hill [31] has treated models with nearest neighbor interactions from the viewpoint of lattice statistics.

The last and the most important factor which effects the rate of adsorption is the type and number of active centers to be considered in the chemisorption of oxygen on cobalt ferrite. It has been postulated by numerous authors that the electronic defects on the surface of the semiconductor are the active centers for chemisorption. If a semiconductor has defects to the extent of 0.1% to 1% of defects of the normal lattice ions than the surface coverage will be between 0.1% and 1%. But experiments [3] [32] show that the percentage of the surface coverage is far more than 1%. In the chemisorption of oxygen on cobalt ferrite, it is postulated that two types of active centers are available. Type one is the "strong" chemisorption center which is composed of the characteristic defects of $Fe^{+2}|B|$. Type two is the "weak" chemisorption center which is composed of the normal lattice cation pair $Co^{+2}|B| - Fe^{+3}|B|$.

Both types have the ability to donate free electrons. As is discussed in the Section B (c), $Fe^{+2}|B|$ is completely ionized with the activation energy of ionization equal zero. The $Co^{+2}|B|$ of the weak chemisorption center $Co^{+2}|B| - Fe^{+3}|B|$ is partially ionized with the activation energy of ionization from 4.4 to 4.73 Kcal. The oxygen molecule is adsorbed more strongly on the strong chemisorption center than on the weak chemisorption center, because the latter has the ability to generate a free hole.

Since the cobalt ferrite was prepared by firing under the oxygen in the atmosphere and was exposed to the air for more than one year, it is appropriate to assume that all the strong chemisorption centers are covered by oxygen molecules and that the weak chemisorption centers are the ones which participates in the adsorption and desorption of oxygen in this study.

After hypothesizing the active centers, namely $Co^{+2}|B| - Fe^{+3}|B|$ pairs, for the adsorption and desorption study, it is necessary to choose a reference state for the surface, this state must have a constant number of bare active centers per unit surface area before adsorption experiment.

III. SURVEY OF LITERATURE

In this chapter, a brief review of the recent literature related to the catalytic activity of cobalt ferrite is reported. The literature is divided into three sections, the first of which is concerned with the study of the catalyst, cobalt ferrite. The second section emphasizes the catalyzed exchange reaction between CO_2 and CO . The third concerns the adsorption and desorption of oxygen on semiconductors.

A. Study of Cobalt Ferrite

The crystal structure of spinel was determined to be face-centered cubic by Bragg [9] for $MgAl_2O_4$. Barth and Posnjak [4] pointed out the two possibilities of distributing the cations while retaining the cubic symmetry of spinel. The electronic conductivity and cation arrangement of a large number of spinel oxides were studied by Verwey and co-workers [72] [73]. The relations between the electronic conductivity of certain spinels and the arrangement of the cations in the crystal structure were studied. Gorter [25] summarized the experimental and theoretical data from literature on cation distribution of spinels and carried out measurements of the saturation magnetization against temperature for a number of mixed crystal oxides with spinel structure.

The phase diagram for the Fe-Co-O system was constructed by Robin and Benard [54] based on X-ray diffraction data at temperatures up to 1000°C. Smiltens [62] studied the isotherms of the same system at 1200°C, 1400°C and 1626°C. He also reported that the non-stoichimetric cobalt ferrite with a spinel structure has the metal to oxygen ratio of

Let the activity of the occupied centers at the reference state be

$$[Co^{+3}|B| - Fe^{+3}|B|] \text{ or}$$

and integrate the above equation to obtain

$$[Co^{+3}|B| - Fe^{+3}|B|]_o - [Co^{+3}|B| - Fe^{+3}|B|] \text{ or}$$

$$= \frac{Va\ N}{A\beta RT} \left(p_{ai} - p_a \right) \tag{43}$$

where p_{ai} is the initial pressure of oxygen before the adsorption

Rearrange the above equation and combine with equation (41):

$$[Co^{+2}|B| - Fe^{+3}|B|]_b = [Co^{+2}|B| - Fe^{+3}|B|]_t$$

$$- [Co^{+3}|B| - Fe^{+3}|B|]_{or} - \frac{Va\ N}{A\beta RT} (p_{ai} - p_a) \tag{44}$$

Put equations (42) and (44) into the rate equation (40):

$$-\frac{Va}{ART}\frac{d\ pa}{dt} = k_{ads.} \{[Co^{+2}|B| - Fe^{+3}|B|]_t - [Co^{+3}|B|-Fe^{+3}|B|]_{or}$$

$$-\frac{Va\ N}{A\beta RT} (p_{ai} - p_a)\} p_a \tag{45}$$

The above equation can be simplified by defining

$$[Co^{+2}|B| - Fe^{+3}|B|]_{br} = [Co^{+2}|B| - Fe^{+3}|B|]_t - [Co^{+3}|B|-Fe^{+3}|B|]_{or} \tag{46}$$

which is the activity of the bare centers at the reference state of the surface and

$$\gamma = \frac{Va\ N}{A\beta RT} \tag{47}$$

$$-\frac{Va}{ART}\frac{dpa}{dt} = k_{ads}\{[Co^{+2}|B| - Fe^{+3}|B|]_{br} - \gamma (p_{ai} - p_a)\} p_a \tag{48}$$

oxidation of CO proceeded on transition metal oxides by means of oxygen extraction reactions, the oxide surface being alternately reduced by CO and oxidized by O_2. Wolkenstein [81] [82] [83] [84] treated the electronic phenomena in catalysis by quantum mechanics. He defined "weak" or "strong" chemisorption by the formation of covalent bond or ionic bond between the adsorbed species and the conduction electrons or electron holes of the semiconductor catalyst. Dowden [14] [15] approached the catalytic activity from the 3d-electrons of the metal ions of the transition metal oxide catalysts. The boundary-layer theory, developed by Hauffe [29] and Weisz [77] [78], emphasized the electron transfer at the interface and the electron density at the boundary layer. When the interaction between the adsorbate molecules and a solid surface involves transfer of electron, it varies the boundary layer depth and the electrical potential on the surface. The change in the surface electrical potential caused corresponding changes in the catalytic activity of the absorbate molecules. Boudart [8] outlined a qualitative picture involving changes of Fermi level of the surface, which he considered as a quasi-isolated entity, with chemisorbed species equivalent to added impurities and applying analogies with behavior of bulk Fermi level in semiconductors. Wagner [74], followed by Schwab [60] [61] and Parravano [44], studied the catalytic activity by doping the semiconductor catalyst with impurity.

The use of isotopes as tracers has been demonstrated as a powerful tool to study reaction kinetics. The most commonly used isotopes are ^{18}O, ^{13}C and ^{14}C. The exchange reaction between CO and CO_2 using ^{13}C was studied by Hayakawa [30]. The CO - CO_2 exchange reaction was investigated

by Garner [22], Winter [79] and Hauffe [18] on zinc oxides, cuprous oxides and nickel oxide. Recently, Wagner [75] [76] postulated a mechanism for the CO_2 - CO exchange reaction on Wustite. Grabke [26] [27] followed Wagner's treatment to study the CO_2 - CO exchange reaction on different oxides.

C. Chemisorption and Desorption of Oxygen

Excellent reviews of chemisorption have been provided by Low [43], Trapnell [32], Wolkenstein [82] [83], Winter [80], Parravano and Boudart [50], Hauffe [28] and Morrison [45]. The quantitative treatment of chemisorption can be divided into the following approaches.

The approach of chemisorption from the kinetic theory of gases [32] emphasizes the sticking probability of a collision between the gas molecule and the unoccupied site. The lack of direct application of this approach is due to the difficulty of expressing the sticking probability analytically and to the neglect of reactions at the gas-solid interface and in the solid phase.

The absolute rate theory was developed by Glasstone, Laidler and Eyring [24] [37]. The theory is based on the assumption that the gas molecule, moving from the gas phase to the adsorbed phase, passes over a potential energy barrier. An activated complex is formed when the molecule is at the top of the barrier. The activated complex is in statistical equilibrium with the molecules in the gas phase and with the vacant surface sites. If the activated complex is immobile, the rate of adsorption is

$$u = C_g C_s \left(\frac{kT}{h}\right) \frac{f^{\ddagger}}{Fg \cdot fs} e^{-E_a/RT} \qquad (56)$$

where Cg is the number of gas molecules per cm^3, Cs is the number of bare sites per cm^2, Fg is the partition function of the gas per cm^3, $f^{\ddagger}$ is the partition function of the activated complex, fs is the partition function of the sites, h is the Planck's constant, k is the Baltzmann's constant, and u is the rate of adsorption. The rate of desorption is given by

$$v = C_a \left(\frac{kT}{h} \right) \left(\frac{f^{\ddagger}}{f_a} \right) e^{-E_a/RT} \qquad (57)$$

where C_a is the surface concentration of the adsorbed molecule, f_a is the partition function of the adsorbed molecule, and v is the rate of desorption. The adsorption of oxygen on cuprous oxides was studied by Stone [34] [56]. The experimental results were interpretated by the absolute rate theory. For the initial stage of adsorption, the rate follows the simple theoretical equation for dissociative adsorption. The activation energy of adsorption is constant at 7 Kcal/mole. But by and large the absolute rate theory does not usually hold for chemisorption.

For a wide variety of chemisorption systems, the rate of adsorption obeys the Elovich equation [17] which maintains that the rate of adsorption decreases exponentially with increase in the amount absorbed on the solid surface. The Elovich equation can be derived for a uniform or a non-uniform surface on the basis of a variation of activation energy with the amount of absorbate on the surface [11]. Taylar and the Thon [67] have shown that, for a large number of systems, plotting the volume adsorbed against time in a semilog paper gives a straight line. The systems included the adsorption of H_2 on Cr_2O_3 gel [12], on $2MnO \cdot Cr_2O_3$ [70], on

$ZnO \cdot MoO_3$ [71] and others. The Elovich equation has found wide application in chemisorption kinetics, the following being just a few studies concerning chemisorption of oxygen: O_2 on CoO [65], O_2 on V_2O_5 [16], O_2 on Si [41], O_2 on Ge [42], O_2 on $CoO \cdot Cr_2O_3$ [67] and O_2 on NiO_2 [18].

The recent approach to the mechanism of chemisorption on semiconductors emphasizes the electronic defect of the semiconductor. The electronic defect is strongly effected by chemical stoichiometry. Defects, which act as electron donors or as electron acceptors, are generated by the metal - excess or the oxygen - excess in these oxides. Chemisorption was treated quantitatively by the boundary layer theory [1] [29] [77] [78]. It is assumed that the electron transfer is taking place across the interface during chemisorption until the potential energy of the electrons is the same in the semiconductor and on the other side of the interface Wolkenstein [83] [84] has suggested that weak chemisorption occurs on the normal lattice ions and does not involve defects. He regards as strong chemisorptions those which involve interactions between absorbates and defects, and which may involve electron transfer to the absorbate. His idea of weak chemisorption, which does not involve transfer to electrons falls outside the boundary layer theory receives further from the work of Dowden, Mackenzie and Trapnell [15], who found no correlation between the conductivity of an oxide and its activity in H_2/D_2 exchange.

Desorption may take place from the occupied sites, provided the absorbed particle possesses the necessary activation energy. Thus the rate of desorption is a function of surface coverage and activation energy. Langmuir [39] has found that the rate of thorium evaporation from tungsten increases exponentially with increase in adsorbed amount. The desorption of nitrogen from iron has been investigated by Scholten [59]

and co-workers, who found a linear dependence of activation energy on absorbed amount. There are several theoretical treatments on the rate of desorption. A simple rate equation, the Polanyi - Wigner [22] equation, was obtained by assuming that any particle possessing the requisite activation energy desorbs within the period of one vibration perpendicular to the surface. Langmuir [40] has derived the lifetime of an adsorbed particle on the surface using an empirical vapor pressure equation. The rate of desorption is inversely proportional to the lifetime and is proportional to the number of absorbed particles per unit area. Lennard-Jones and Devonshire [23] have calculated the lifetime of an absorbed particle by quantum mechanics using the probability of transfer of a single quantum of energy from the solid to the adsorbed particle. It may be valid only for physically adsorbed particles however. Desorption rate according to absolute rate theory [24] [37] is proportional to the frequency of vibration of the activated complexes perpendicular to the surface. Both theoretical and experimental investigations of desorption kinetics are much less numerous than those of adsorption kinetics.

IV. EXPERIMENTAL APPARATUS AND PROCEDURE

A. Preparation of Cobalt Ferrite

The unsupported cobalt ferrite samples were prepared by Pietrzak and Gates [52] at the University of Michigan. Reagent Grade cobalt carbonate and iron oxide were weighed and mixed. The mixture was ball milled in acetone for twenty-four hours in a stainless-steel ball mill. The slurry was then dried in a large beaker. The dried cake was crushed into powder, loaded into a crucible and fired in air at 1950°F in a furnace for twelve and one half hours. The resulting cobalt ferrite was in the form of a black powder.

Five samples with different Fe/Co ratios were prepared. The ratio of iron and cobalt in the cobalt ferrite samples was determined by a Norelco X-ray Fluorescent Spectrometer. The composition shown from the spectrometer was slightly different from the composition calculated from the original weighed amounts of reactants. This difference can be explained by the loss of cobalt in the sample during the firing process.

The specific surface area of the samples was determined by the B.E.T. method. The amount of nitrogen adsorbed on the sample at liquid nitrogen temperature was measured as a function of pressure. The detailed apparatus and calculations for this determination are in a Technical Bulletin [19] of the Mellon Institute of Industrial Research. Two samples, with $x = 1.903$ and $x = 2.099$, were measured. The measured specific surface area of the two is 2.422 and 2.545 square meters per gram respectively. The specific surface area of samples was taken as the average value 2.48 square meters per gram.

B. The CO_2 - CO Exchange Reaction

A diagram of the apparatus for the exchange reaction of CO_2 and CO is shown in Figure 1 , in which all the major components are identified. A Geiger Counter (Model No. FD-1 Gas Flow Counter by Tracerlab Inc.) was used for the measurement of soft beta radiation from ^{14}C in the gas mixture. A SC-90 Utility Scaler with a SC-42A Dual Timer also by Tracerlab was employed to amplify and register the radiation (Figure 12).

The carbon dioxide and carbon monoxide in the cylinders (by Matheson Company Inc.) were introduced into the storage bulbs after removing the moisture by passing the gases through a drying column packed with Drierite (W. A. Hammond Drierite Company). The gas samples were analyzed on the mass spectrometer (Type 21-013B, Modified to Type 21-103C specifications by Consolidated Engineering Corporation). The oxygen content was beyond the limits of detection of the mass spectrometer. The radioactive $^{14}CO_2$ with 1.0 mc radiation was supplied in a sealed glass tube by New England Nuclear Corporation.

The sealed glass tube was placed next to an iron rod inside a 10 mmOD glass tubing closed at one end. The other end of the tubing was connected to the apparatus for the exchange reaction. After evacuating the system to 1×10^{-5} mm of Hg, a magnet was used outside the tubing to move the iron rod which broke the tip of the sealed glass tube which released the $^{14}CO_2$ gas into a Toepler pump. The $^{14}CO_2$ was mixed with CO_2 - CO gas mixture in the Toepler pump and stored.

A weighed amount of 1.0000 gram of cobalt ferrite catalyst was loaded into a ceramic boat and placed in the center of the reactor. The catalyst was outgassed at 400°C for twenty-four hours under a pressure of 1×10^{-5} mm Hg. The temperature of reactor was controlled by a Model JP

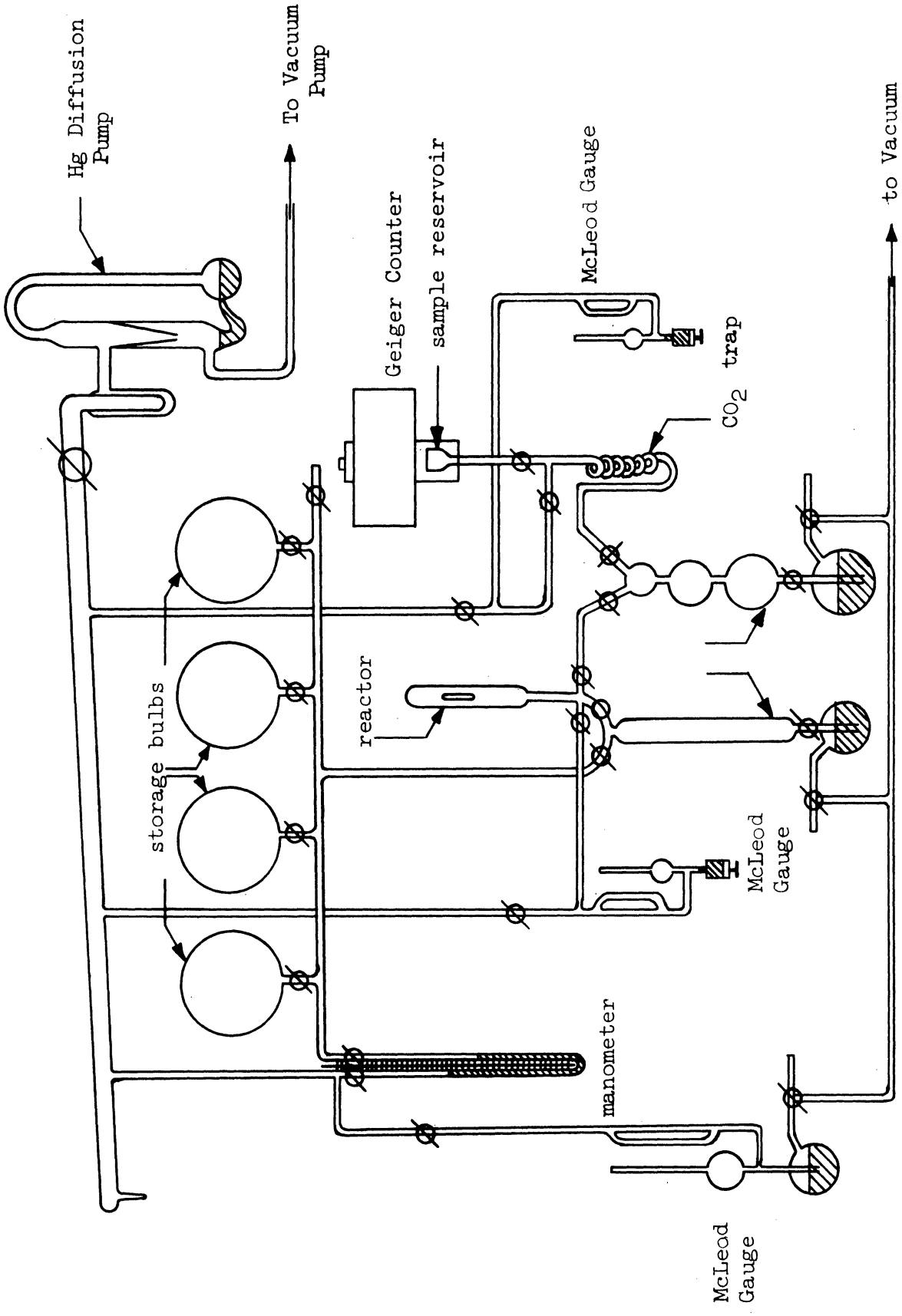

Figure 1. Apparatus For The Exchange Reactor of CO_2 and CO .

Temperature Controller by West Instrument Corporation with a Iron-Constantan thermocouple. After outgassing the temperature was lowered to the temperature of the next experiment. A gas mixture of CO_2 and CO without the radioactive CO_2 was introduced to the reactor to treat the catalyst surface. The time of the pretreatment was twenty-four hours. The surface pretreatment was repeated to make sure the gas mixture was in equilibrium with the solid surface. Then the reactor was evacuated at 1×10^{-5} mm Hg for three minutes, and the experiment started by introducing the gas mixture having the same CO_2/CO ratio as the pretreatment but with the tracer $^{14}CO_2$ in it. A gas sample was withdrawn to the Sampling Toepler Pump for analysis after a certain time. The time interval depended on the rate of the exchange reaction. The sample gas was pumped to a reservoir with a mica window below the Geiger Counter to count the total $^{14}CO_2$ and ^{14}CO in the gas.

The sample reservoir (see Figure 2) with a glass flange on the top end was made of a piece of 30 mm OD glass tubing about 1.5in. long rounded at the bottom end. The top end was sealed by a mica window with density of 6.0 mg/cm^2. The sealand was an expoxy cement supplied by Sears, Roebuck and Co. The sample gas was pumped back and forth three times through the CO_2 trap at liquid nitrogen temperature to condense the CO_2 and $^{14}CO_2$ from the gas mixture. Then the ^{14}CO was counted in the reservoir. The total count of $^{14}CO_2$ and ^{14}CO was corrected from the background count. The ^{14}CO count was corrected from both the background count and the residue $^{14}CO_2$ count which were obtained before the experiment. The sample gas was put back to the reactor after the analysis.

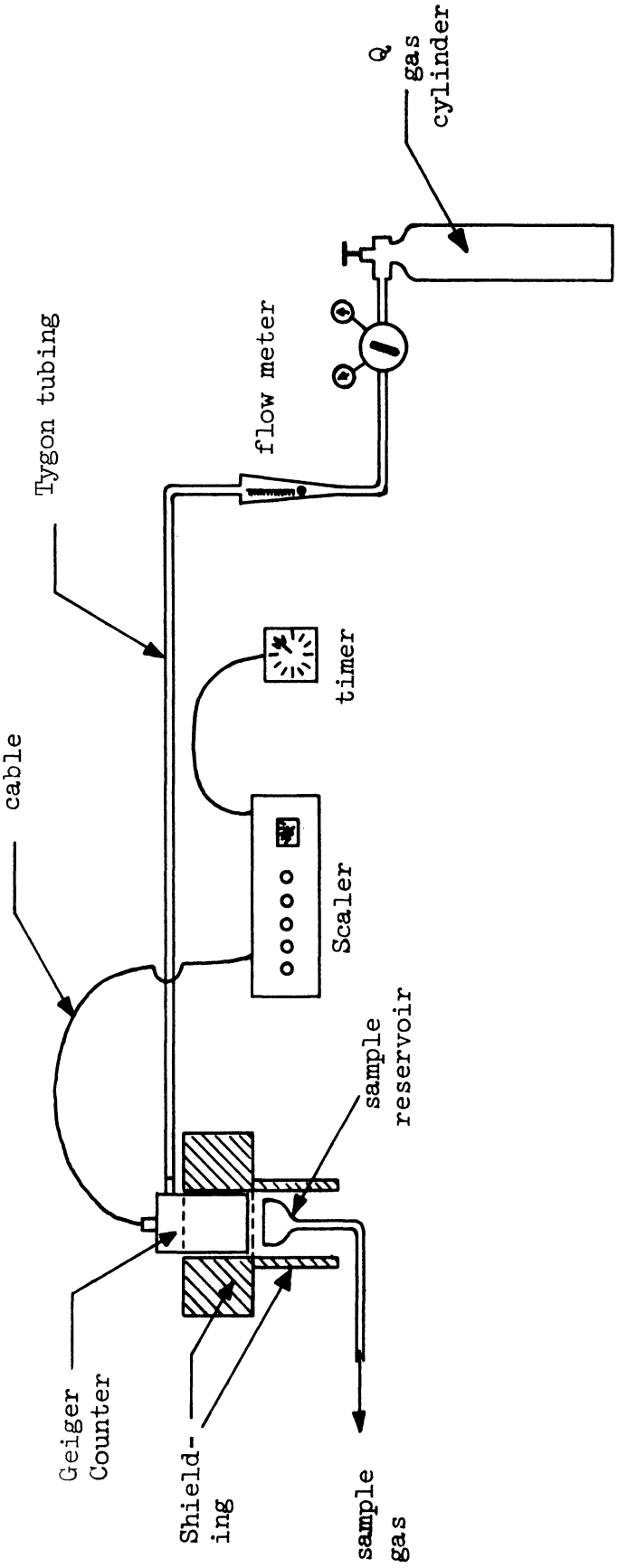

Figure 2. Geiger Counter and Accesoaries.

The initial amount of radioactive $^{14}CO_2$ was the same for each run. The total pressure of the reactor which was constant in each run, varied from 3 to 7 cm of Hg between runs depending on the ratio of CO_2 and CO. The rate constant was found experimentally independent upon the total pressure in this range. The temperature ranged from 250° to 390°C. The volume of the reactor was 507 cc. Approximately 55 cc of the gas sample was taken from the reactor for analysis.

C. Adsorption - Desorption of Oxygen

A sketch of the apparatus for the adsorption and desorption study is presented in Figure 3. The rate of adsorption was obtained from the pressure drop of the oxygen reservoir versus time. The rate of desorption was obtained from the pressure increase of the oxygen collecting reservoir versus time. The pressure was measured by two calibrated thermocouple gauges attached to the reservoirs and was checked occasionally with Mcleod Gauge. The thermocouple gauges (Televac, Model II), supplied by The Fredericks Company, can measure the range of pressure between 0.001 to 0.500 mm of Hg. The calibration of the sample container, adsorption oxygen reservoir and the desorption oxygen collecting reservoir was carried out at room temperature via the expansion method assuming ideal gas behavior. The attached gas burette and the mercury manometer were used for the calibration. The volume of the dead-space of the sample container, of the adsorption reservoir plus the manifold and of the desorption reservoir was 158.6 cc, 5302 cc and 5205 cc respectively.

A 30 mm diameter Vycor tubing closed at the bottom was used as the sample container. A weighed sample of 50.000 grams of cobalt ferrite was placed in the sample container which was then connected via a gradient

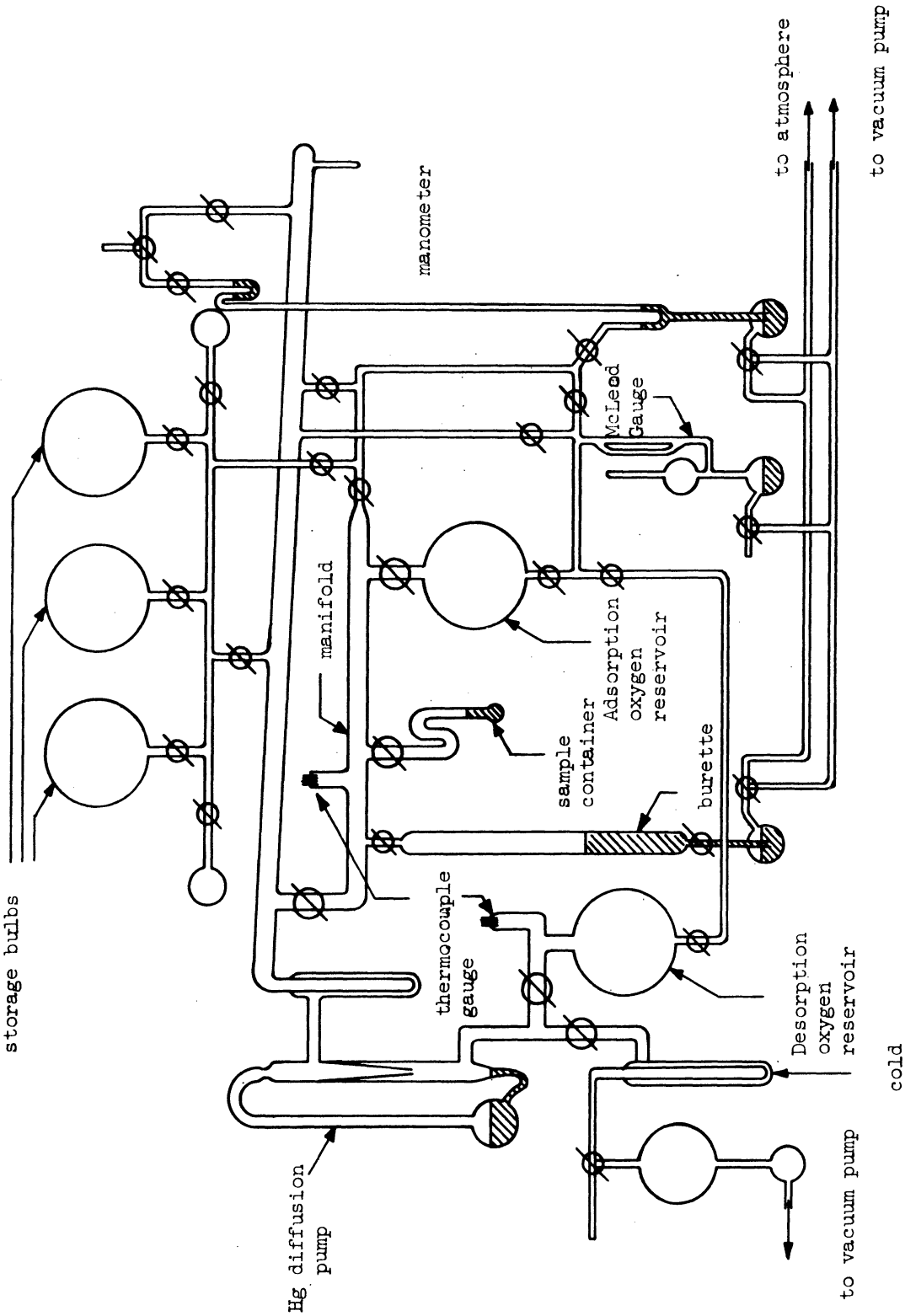

Figure 3. Apparatus for the Adsorption and Desorption of Oxygen

seal to the 15 mm Pyrex tubing of the system. After elimination of all leaks, the system could consistently be evacuated to a dynamic vacuum of 1×10^{-5} mm of Hg by the mercury diffusion pump and the mechanical pump connected in series. The system was frequently tested under static vacuum for leaks and the leak rate was less than 1 micron per day. The arbitrary reference state of the catalyst surface was chosen by evacuating the catalyst for twenty-four hours under 1×10^{-5} mm Hg pressure at 400°C. The temperature of the sample container was controlled by a Model JP Temperature Controller (West Instrument Corporation) with a Iron-Constantan thermocouple attached to the outer wall of the container. Oxygen for the adsorption studies was generated by the thermal decomposition of potassium permanganate. The gas was first passed through a trap packed with glass beads and cooled by dry ice and isopropyl alcohol before storage. Oxygen was introduced to the adsorption reservior and the sample manifold after the system was evacuated to 1×10^{-5} mm Hg and the samples was in its reference state. Adsorption began when the 15 mm stop-cock connecting the sample container and the sample manifold was opened. The normal duration of an adsorption run was two days. After the completion of an adsorption run, the stopcock to the sample container was closed, and the sample manifold and adsorption and desorption reservoirs were evacuated. Desorption was always followed at the temperature at which oxygen was adsorbed and hence the sample temperature was not changed. At zero-time, the stopcock to the sample container would be opened, and the subsequent pressure increase in the desorption reservoir with time followed. The amount of oxygen retained in the sample container at the end of adsorption would be subtracted from the oxygen desorbed. The sample manifold was maintained at pressure 1×10^{-5} mm Hg. The desorbed oxygen was pumped to the desorption reservior by the

mercury diffusion pump. The amount of oxygen desorbed was smaller than the amount adsorbed at the same temperature (see Table 4). After the completion of a desorption run, the temperature of the sample container would be raised to 400°C or even 450°C for outgassing till the amount of oxygen adsorbed was outgassed as determined by a material balance. The surface of the sample would return to its reference state and the next adsorption run might be followed.

The error of the Geiger Counter was within 1 per cent for 1,000 counts/min. The errors for both temperature controllers for the reactors were within $\pm$ 3°C at 350°C. The ionization gauge had an error less than 1 micron at 100 microns. Thus, the maximum percentage error of rate constants is $\pm$ 9 per cent.

V. EXPERIMENTAL RESULTS

A. CO_2 - CO Exchange Reaction

The CO_2 - CO exchange reaction was catalyzed by four cobalt ferrite samples, $Co_{3-x}Fe_x O_4$, having compositions $x = 1.903$, 1.954, 2.006 and 2.009. Table 1 summarizes results of experiments performed at different CO_2 - CO ratios and different temperatures on each sample.

All the results were obtained on 1.000 gm of cobalt ferrite catalyst with surface area 2.48 square meter which had been outgassed for one day at 400°C and at a pressure of 1×10^{-5} mm Hg and pretreated twice with the CO_2 - CO gas mixture before each run. The percentage of $^{14}CO_2$ in CO_2 was 0.00266%. Two or three runs were performed under the same experimental condition to insure the reproducibility of results within 1.5% of ^{14}CO formation.

Experimental data are tabulated in Appendix I. The results of the percentage formation of ^{14}CO versus time for $Co_{0.901}Fe_{2.099}O_4$ at 350°C with different CO_2/CO ratios are plotted in Figure 4 as an example plot of raw data. The rate constant $k(a_o)$ was obtained from the rate of formation of ^{14}CO by applying Equation (21),

$$\frac{V}{ART}\frac{dp_{^{14}CO}}{dt} = k(a_o)[p^i_{^{14}CO_2} - (1 + a_o)p_{^{14}CO}] \qquad (21)$$

Two methods were employed to calculate the value of $k(a_o)$, the initial rate method and the digital computer simulating method. The detailed calculation is in Appendix II. The values of $k(a_o)$ are presented in Table 1.

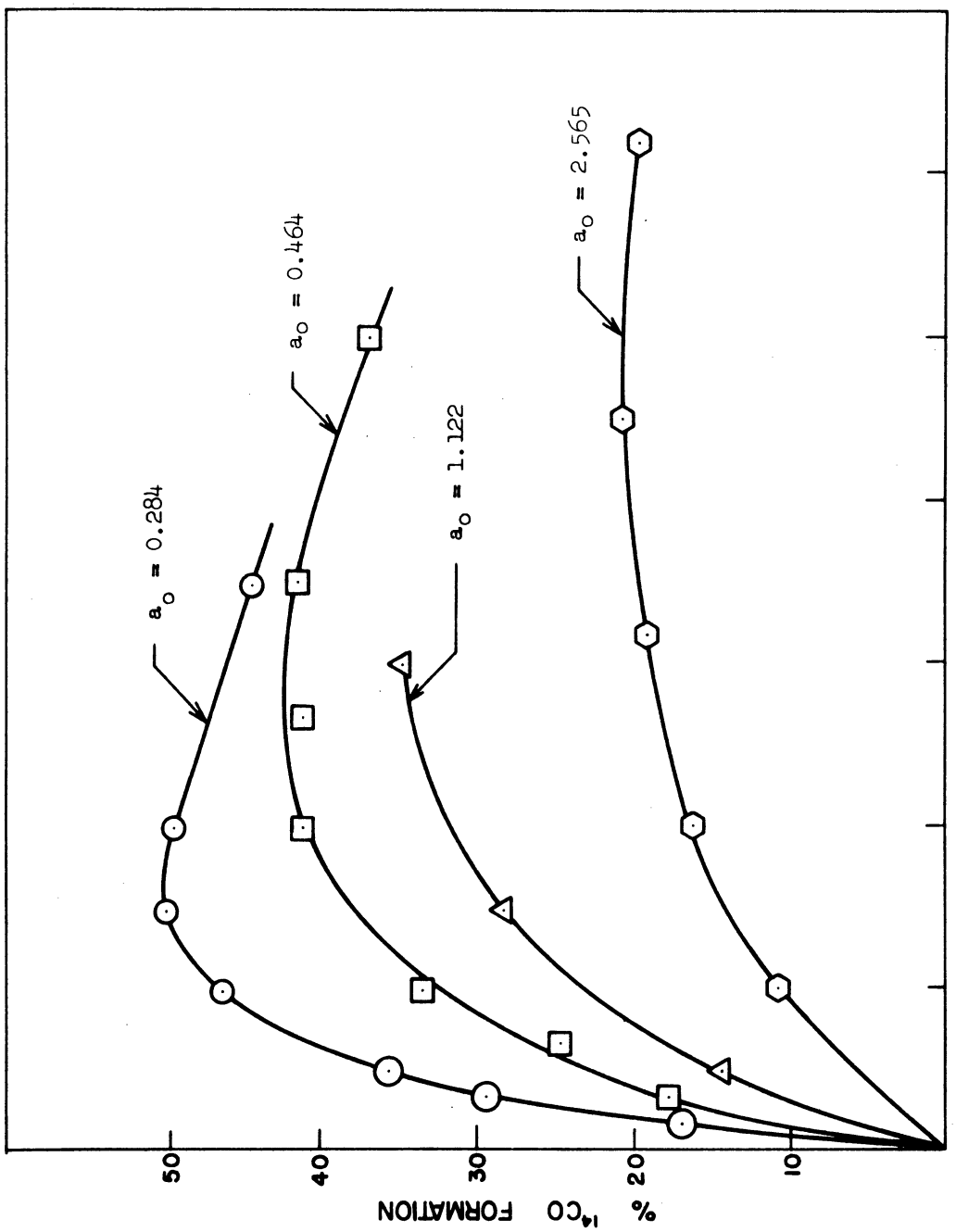

Figure 4. Formulation of ^{14}CO Versus Time on $CO_{0.901}Fe_{2.099}O_4$ With A = 2.48 x 10^4 cm^2 and T = 350°C.

TABLE 1

SUMMARY OF EXPERIMENTAL RESULTS OF THE EXCHANGE REACTION OF CO_2 AND CO ON $Co_{3-x}Fe_xO_4$

x	p_{CO_2}/p_{CO} Ratio	Temp. (°C)	$k(a_o) \times 10^7$ $[\frac{\text{mole}}{\text{hr.atm.cm}^2}]$
1.903	0.464	350°C	0.064
	0.464	380°C	0.735
	0.464	410°C	3.030
1.954	0.464	310°C	0.094
	0.464	350°C	0.760
	0.464	390°C	2.670
2.006	0.464	250°C	0.0524
	0.464	300°C	0.500
	0.464	350°C	3.920
2.099	0.464	310°C	0.299
	0.464	350°C	2.55
	0.464	390°C	6.37
1.903	0.218	350°C	0.122
	0.464	350°C	0.064
	1.442	350°C	0.0184
	2.190	350°C	0.0132
2.006	0.218	250°C	0.100
	0.464	250°C	0.0524
	1.442	250°C	0.0145
2.099	0.284	350°C	4.560
	0.464	350°C	2.550
	1.122	350°C	1.140
	2.565	350°C	0.464

TABLE 2

ACTIVATION ENERGY OF THE EXCHANGE REACTION OF CO_2 AND CO ON $Co_{3-x}Fe_xO_4$

x	1.903	1.954	2.006	2.009
$E_a[\frac{\text{kcal}}{\text{mole}}]$	54.8	32.4	27.7	30.4

Knowing the values of $k(a_o)$, the constant m which characterizes the catalytic intermediate on the catalyst surface was obtained from Equation (27),

$$\left(\frac{\partial \ell n[k(a_o)]}{\partial \ell n\, a_o}\right)_T = -m \qquad (27)$$

Figure 5 is the plot of $k(a_o)$ versus a_o for $x = 1.903$, 2.006 and 2.099. The results show that $m = 1$ for all three samples.

The activation energy E_a of four samples with $a_o = 0.464$ was calculated from Equation (29),

$$\left(\frac{\partial \ell n[k(a_o)]}{\partial(\frac{1}{T})}\right)_{a_o} = -\frac{E_a}{R} \qquad (29)$$

Figure 6 presents the plot of $k(a_o)$ versus $\frac{1}{T}$ for four samples. The values of E_a are tabulated in Table 2.

B. Adsorption and Desorption of Oxygen

The generalized rate expression of oxygen adsorption can be written as

$$-\frac{d\, n_a}{A\, d\, t} = K_{ads}\, p_a = \sum_i k_{ads}^i\, [\text{active center } i]_b\, p_a \qquad (39)$$

where k_{ads}^i = the rate constant for i type active center

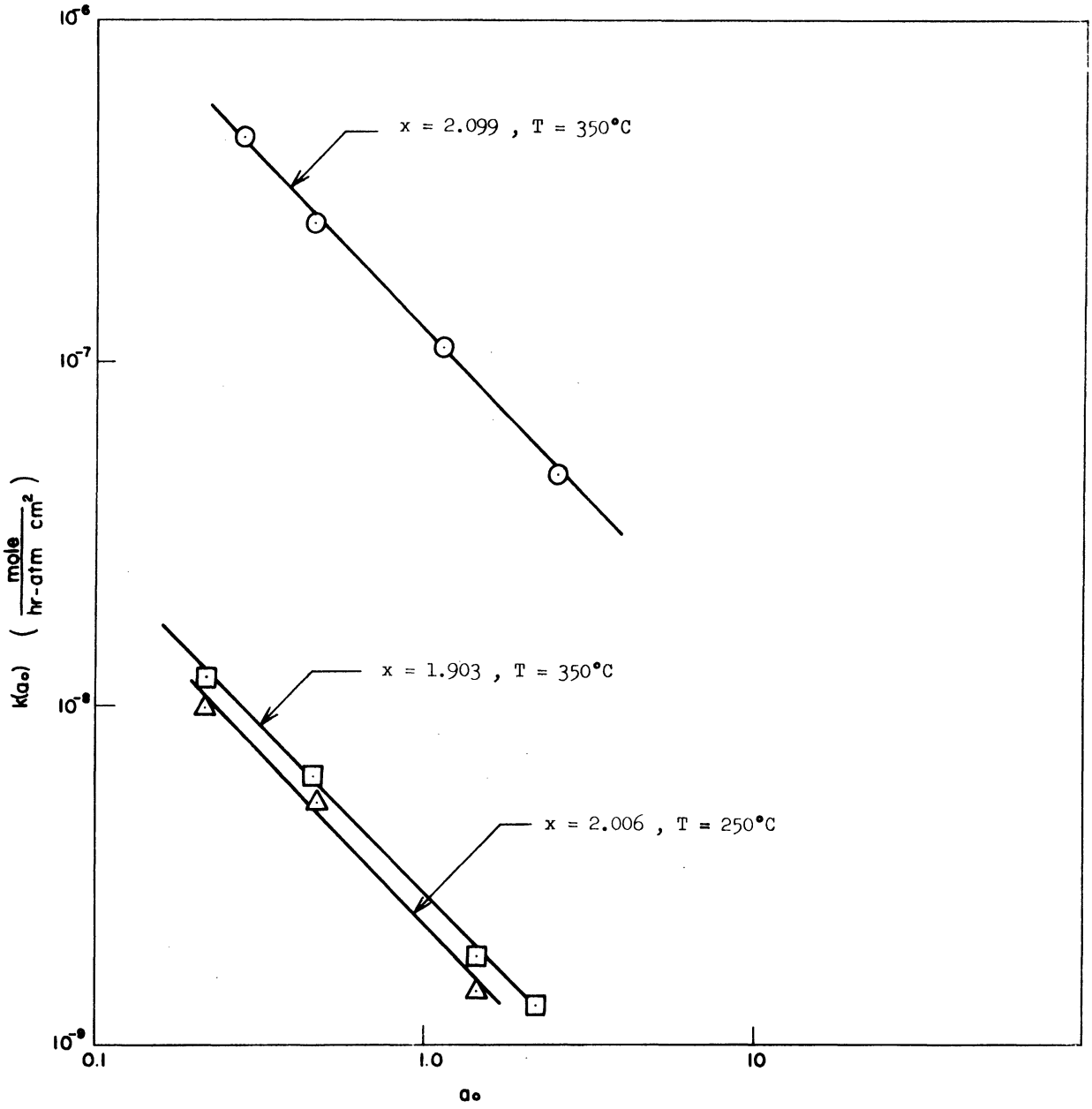

Figure 5. The Value m From $k(a_o)$ Versus a_o .

$[\text{active center i}]_b$ = the activity of the bare i type active center

n_a = moles of O_2 in the gas phase during the adsorption

p_a = pressure of O_2 in the reactor during the adsorption and

K_{ads} is the overall rate constant which is a function of catalyst composition, temperature and surface coverage

Based on the model described in the previous section, the rate of adsorption of oxygen on cobalt ferrite, provided the desorption rate is small, can be written as

$$-\frac{d\, n_a}{A\, d\, t} = k_{ads}\, [Co^{+2}|B| - Fe^{+3}|B|]_b\, p_a \qquad (40)$$

where

$[Co^{+2}|B| - Fe^{+3}|B|]_b$ = activity of the bare active center $Co^{+2}|B|.\ Fe^{+3}|B|$

Since the total number of bare and occupied active centers is constant for a catalyst, we have

$$[Co^{+2}|B| - Fe^{+3}|B|]_b + [Co^{+3}|B| - Fe^{+3}|B|]_o = [Co^{+2}|B| - Fe^{+3}|B|]_t \qquad (41)$$

where the subscripts o and t stand for occupied and total respectively. From the material balance of oxygen, we have

$$\frac{A\,\beta}{N}\, d[Co^{+3}|B| - Fe^{+3}|B|]_o = -\frac{Va}{RT}\, d\, p_a = -\, dn_a \qquad (42)$$

where A = surface area of cobalt ferrite

β = number of active centers per unit area

N = Avogadro number

V_a = volume of the adsorption oxygen reservoir

Let the activity of the occupied centers at the reference state be

$$[Co^{+3}|B| - Fe^{+3}|B|] \text{ or}$$

and integrate the above equation to obtain

$$[Co^{+3}|B| - Fe^{+3}|B|]_o - [Co^{+3}|B| - Fe^{+3}|B|] \text{ or}$$

$$= \frac{Va\ N}{A\beta RT} \left(p_{ai} - p_a \right) \tag{43}$$

where p_{ai} is the initial pressure of oxygen before the adsorption

Rearrange the above equation and combine with equation (41):

$$[Co^{+2}|B| - Fe^{+3}|B|]_b = [Co^{+2}|B| - Fe^{+3}|B|]_t$$

$$- [Co^{+3}|B| - Fe^{+3}|B|]_{or} - \frac{Va\ N}{A\beta RT} (p_{ai} - p_a) \tag{44}$$

Put equations (42) and (44) into the rate equation (40):

$$-\frac{Va}{ART}\frac{d\ pa}{dt} = k_{ads.} \{[Co^{+2}|B| - Fe^{+3}|B|]_t - [Co^{+3}|B| - Fe^{+3}|B|]_{or}$$

$$-\frac{Va\ N}{A\beta RT} (p_{ai} - p_a)\} p_a \tag{45}$$

The above equation can be simplified by defining

$$[Co^{+2}|B| - Fe^{+3}|B|]_{br} = [Co^{+2}|B| - Fe^{+3}|B|]_t - [Co^{+3}|B| - Fe^{+3}|B|]_{or} \tag{46}$$

which is the activity of the bare centers at the reference state of the surface and

$$\gamma = \frac{Va\ N}{A\beta RT} \tag{47}$$

$$-\frac{Va}{ART}\frac{dpa}{dt} = k_{ads}\{[Co^{+2}|B| - Fe^{+3}|B|]_{br} - \gamma (p_{ai} - pa)\} p_a \tag{48}$$

By knowing the rate of pressure drop in the system, the rate constant can be calculated from equation (48).

The rate of desorption can be expressed by

$$\frac{dn_d}{Adt} = k_{des.} \quad [Co^{+3}|B| - Fe^{+3}|B|]_o \tag{49}$$

where n_d = moles of O_2 desorbed

Since the desorption experiment starts right after an adsorption experiment, the activity of the occupied center at the beginning of the desorption is

$$[Co^{+3}|B| \; Fe^{+3}|B|]_{or} + \gamma (p_{ai} - p_{af})$$

where p_{af} is the final pressure or equilibrium pressure of adsorption. The material balance of oxygen during the desorption becomes

$$\frac{A\beta}{N} \; d[Co^{+3}|B| - Fe^{+3}|B|]_o = - \frac{Vd}{RT} \; d\, p_d = - dn_d \tag{50}$$

where p_d = the pressure of the bulb collecting the desorbed oxygen

n_d = moles of O_2 desorbed

V_d = the volume of the oxygen collecting reservoir

The integrated form of the above equation is

$$[Co^{+3}|B| - Fe^{+3}|B|]_{or} + \gamma (p_{ai} - p_{af}) - [Co^{+3}|B| - Fe^{+3}|B|]_o$$

$$= \frac{Vd \; N}{A\beta RT} \quad (p_d - p_{di}) \tag{51}$$

where p_{di} = the initial pressure of the bulb collecting the desorbed oxygen

Put equations (50) and (52) into equation (49),

$$\frac{Vd}{ART}\frac{dP_d}{dt} = k_{des.}\left\{[Co^{+3}|B| - Fe^{+3}|B|]_{or} + \gamma\,(p_{ai} - p_{af}) - \frac{Vd\ N}{A\beta RT}(p_d - p_{di})\right\} \quad (52)$$

Define $[Co^{+3}|B| - Fe^{+3}|B|]_{oid} = [Co^{+3}|B| - Fe^{+3}|B|]_{or} + \gamma(p_{ai} - p_{af})$ (53)

= the initial activity of occupied center at the beginning of the desorption and

$$\xi = \frac{Vd\ N}{A\beta RT} \quad (54)$$

The desorption rate equation (52) becomes

$$\frac{V\ d}{ART}\frac{dpd}{dt} = k_{des.}\left\{[Co^{+3}|B| - Fe^{+3}|B|]_{oid} - \xi\,(pd - pi)\right\} \quad (55)$$

By measuring the rate of pressure increase in the collecting bulb, the desorption rate constant is obtained from equation (55).

The adsorption and desorption of oxygen were performed on five cobalt ferrite samples with $x = 1.903$, 1.954, 2.006, 2.058 and 2.099. All the experiments were obtained on 50.000 gram of samples, corresponding to $1.24 \times 10^6 cm^2$ surface area, placed in the sample container. The reproducibility of results of adsorption runs was within 2 microns for p_a after the surface was brought back to its reference state by checking the material balance of oxygen. Without checking the material balance of oxygen, the reproducibility of p_a was as poor as 20 to 30 microns. Table 3 summarizes the results of the adsorption runs.

Experimental data of adsorption are tabulated in Appendix I. Figure 7 is a sample plot of the pressure of oxygen p_a versus time t at 300°C, 200°C and 100°C on cobalt ferrite with $x = 2.006$.

TABLE 3

SUMMARY OF EXPERIMENTAL RESULTS OF ADSORPTION OF OXYGEN ON $Co_{3-x}Fe_xO_4$

x	Temp. (°C)	P_{ai} (microns)	P_{af} (microns)	$\frac{\Delta n_a}{A} \times 10^{11}$ $(\frac{mole}{cm^2})$	$-(\frac{dn_a}{Adt})_{t=o} \times 10^{10}$ $(\frac{mole}{hr.cm^2})$	Initial rate const. $K_{ads.} \times 10^4$ $(\frac{mole}{hr.cm^2.atm})$	$E_a(\frac{kcal}{mole})$
	300	101.7	54.0	1.09	1.01	0.755	
1.903	200	104.1	62.5	0.952	0.64	0.468	2.81
	100	100.0	70.1	0.684	0.273	0.204	
	500	103.3	39.0	1.47	0.95	0.70	
1.954	400	105.7	55.0	1.16	0.54	0.394	7.32
	300	102.0	85.6	0.376	0.174	0.131	
	300	102.3	2.15	2.29	4.66	3.46	
2.006	200	101.2	6.2	2.18	2.96	2.22	2.18
	100	100.0	19.1	1.85	1.58	1.20	
	400	100.9	28.0	1.67	0.66	0.514	
2.058	350	99.4	44.5	1.23	0.342	0.262	9.83
	300	103.2	69.0	0.794	0.163	0.120	
	400	103.3	21.0	1.88	0.507	0.373	
2.099	300	102.5	52.0	1.06	0.203	0.151	7.59
	200	105.2	99.2	0.137	0.0538	0.039	

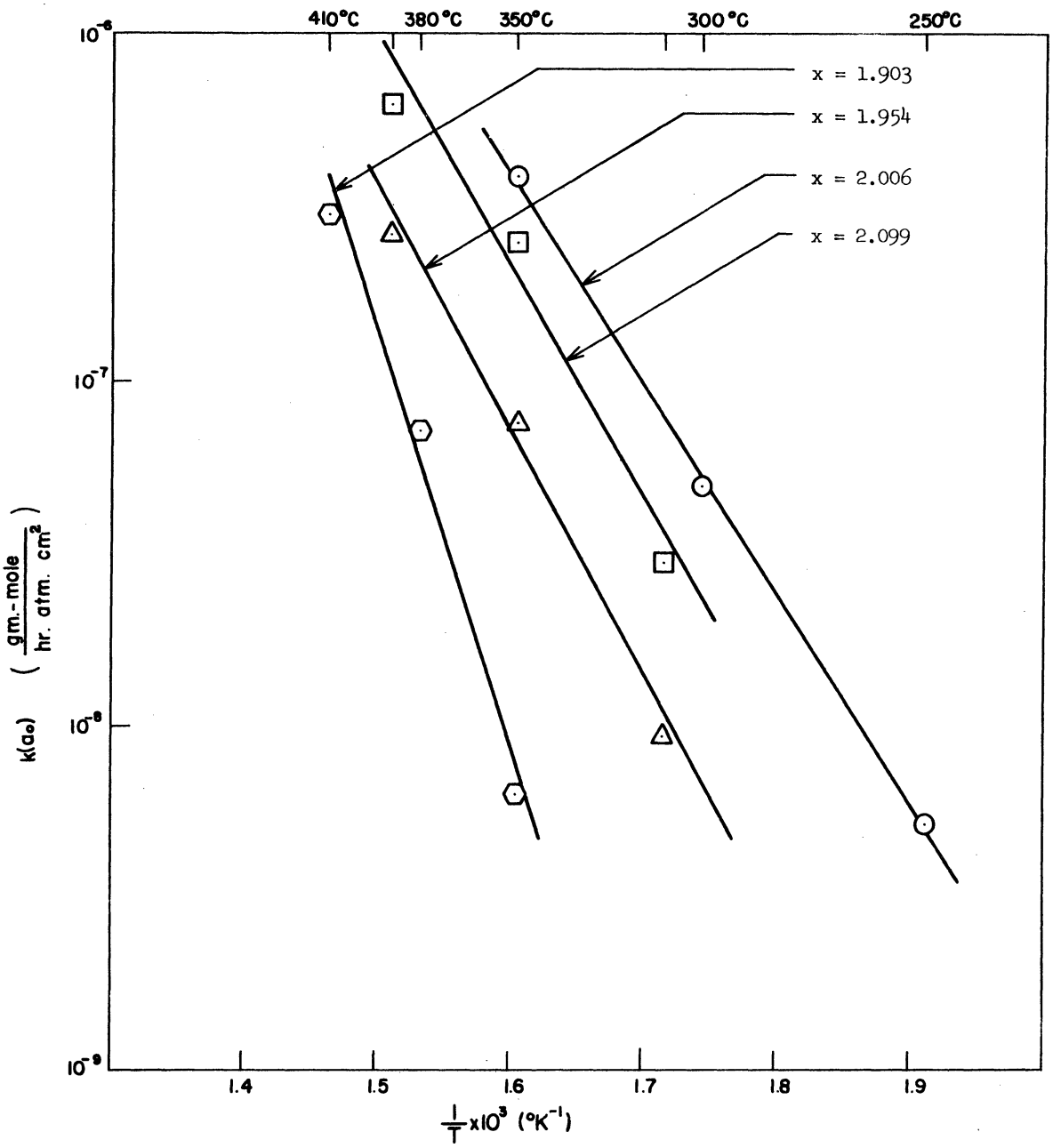

Figure 6. Activation Energy of the Exchange Reaction From $k(a_o)$ Versus $\frac{1}{T}$, $a_o = 0.464$.

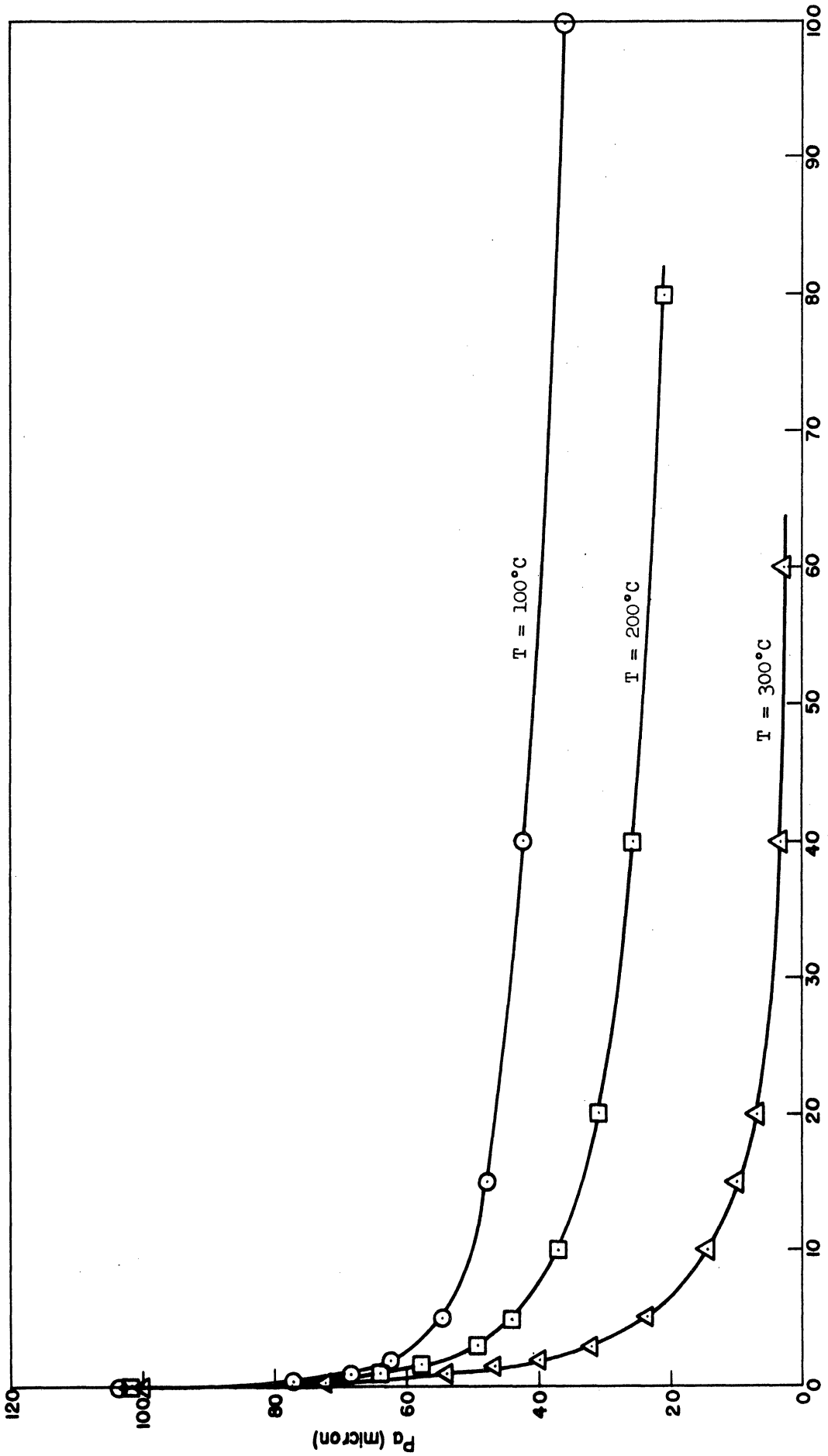

Figure 7. Adsorption of Oxygen on $Co_{0.994}Fe_{2.006}O_4$.

From Figure 7, it shows that p_a changes very little after the first hour of adsorption. The final pressure of adsorption p_{a_f} is then arbitrarily chosen as the pressure at twenty-four hours of adsorption. The amount of oxygen adsorbed per square centimeter surface was calculated from the integrated form of Equation (42),

$$\frac{\Delta n_a}{A} = \frac{V_a}{ART} (p_{ai} - p_{af}) \tag{58}$$

The experimental data follow very well to the theoretical rate expression of Equation (48),

$$- \frac{V_a}{ART} \frac{dp_a}{dt} = k_{ads} \left\{ [Co^{+2}|B- - Fe^{+3}|B|]_{br} - \gamma(p_{ai} - p_a) \right\} p_a \tag{48}$$

The constants k_{ads} and $[Co^{+2}|B| - Fe^{+3}|B|]_{br}$ were calculated by simulating method with digital computer. The detailed procedure is in Appendix II. The values of initial rate of adsorption and initial rate constant K_{ads} were obtained from Equation (40) at $t = 0$,

$$\left(\frac{d\ n_a}{A\ dt}\right)_{t\ =\ 0} = K_{ads} p_{ai} = k_{ads} [Co^{+2}|B| - Fe^{+3}|B|]_{br}\ p_{ai} \tag{59}$$

The activation energy of adsorption of initial rates was calculated from

$$\left[\frac{\partial \ell n K_{ads}}{\partial(\frac{1}{T})}\right]_{ref.state} = - \frac{Ea}{R} \tag{60}$$

by knowing the K_{ads} at reference state for three different temperatures. Figure 8 is the plot of $\log K_{ads}$ versus $\frac{1}{T}$ for five samples.

The experimental data on desorption were poor. The derivation of p_d for runs under the same condition was as high as 50% because of the following reasons: (i) The rate of desorption was so slow that the pressure change with respect to time could not be read accurately from

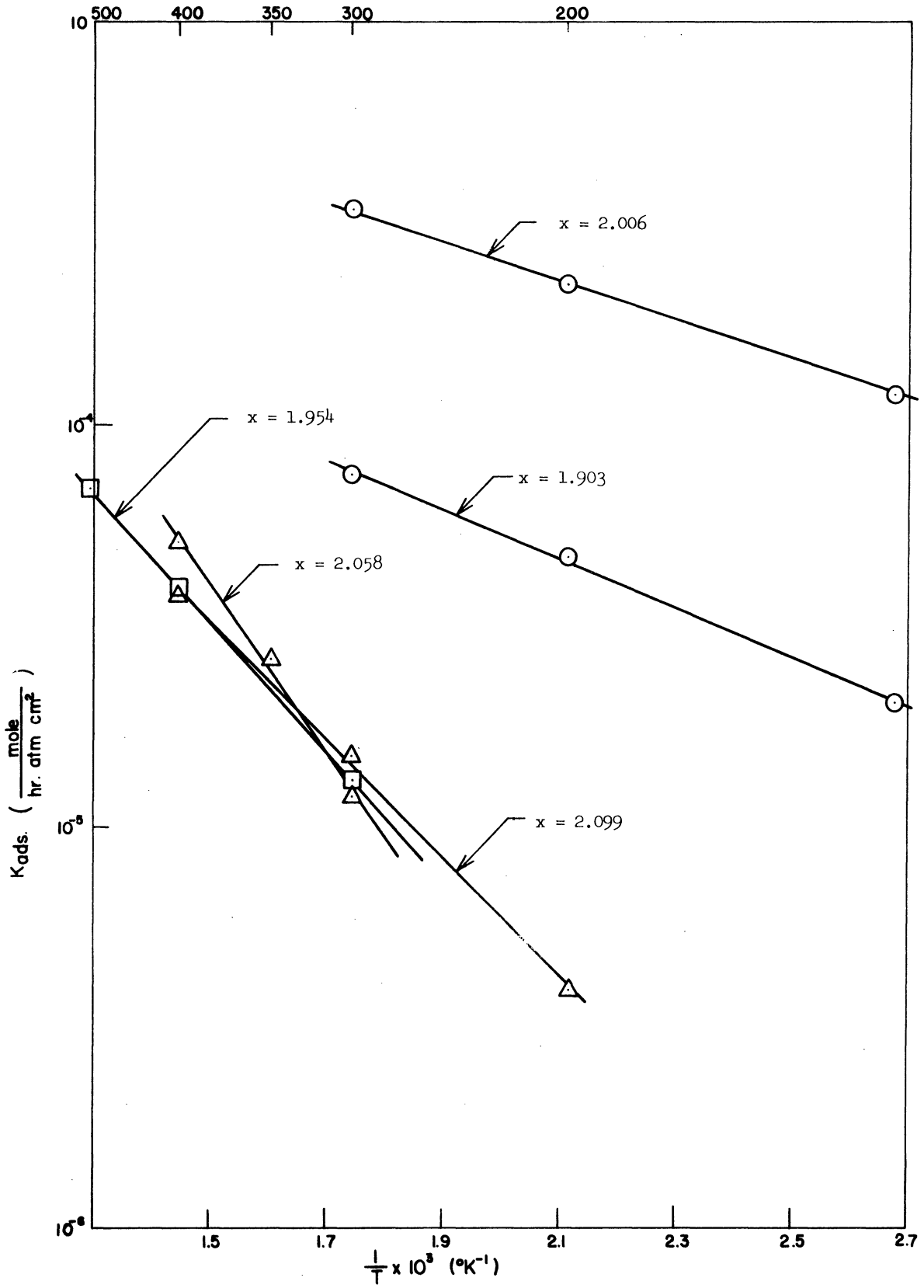

Figure 8. Activation Energy of Oxygen Adsorption From $K_{ads.}$ Versus $\frac{1}{T}$.

the thermocouple gauge. (ii) The desorbed oxygen was collected by the mercury diffusion pump into the desorption reservoir. The efficiency, the percentage of the desorbed oxygen collected by the pump at the same short period of time, could not be very high because of the extremely low pressure of the sample container. (iii) There was a certain amount of oxygen trapped in the dead-space of the sample container. The trapped oxygen may also contribute to the error of the desorption data.

The results presented for the discussion were the amount of oxygen desorbed per unit surface area in twenty-four hours and the initial rate of desorption. The former was obtain by integrating Equation (50), which gave

$$\frac{\Delta n_d}{A} = \frac{Vd}{ART} (p_{df} - p_{di}) \qquad (61)$$

The latter was obtained by taking the average rate of desorption in the first five minutes. Table 4 summarizes the results of desorption.

C. Summary of Results in Terms of Catalyst Composition

The purpose of this research was to investigate the catalytic activity of cobalt ferrite in terms of its composition. The following figures summarize the results plotted against the composition of the catalyst so that it is convenient for the discussion.

Figure 9 is the plot of the rate constant of the exchange reaction versus the composition x at 350°C and with CO_2/CO ratio of 0.464.

Figure 10 was plotted with the activation energy Ea of the exchange reaction versus the composition x, CO_2/CO ratio = 0.464 and the temperature ranging from 250 to 410°C.

Figure 11 shows the plot of the amount of oxygen adsorbed per unit surface area versus the composition x at 300°C.

TABLE 4

SUMMARY OF EXPERIMENTAL RESULTS OF THE DESORPTION OF OXYGEN ON $CO_{3-x}Fe_xO_4$

x	Temperature(°C)	$P_{df} - P_{di}$ (microns)	$\frac{\Delta n_a}{A} \times 10^{11}$ $\frac{mole}{cm^2}$	$\frac{\Delta n_d}{A} \times 10^{12}$ $\frac{mole}{cm^2}$	$\frac{dn_d}{Adt} \times 10^{12}$ $\frac{mole}{hr \cdot cm^2}$
1.093	300	6.80	1.09	1.59	1.25
	200	2.1	0.952	0.49	1.05
	100	0.31	0.684	0.072	0.122
1.954	500	4.72	1.47	11.3	9.8
	400	14.5	1.16	3.38	3.5
	300	7.3	0.376	1.70	1.4
2.006	300	6.60	2.29	1.55	0.725
	200	1.20	2.18	0.28	0.312
	100	2.05	1.85	0.47	0.221
2.058	400	81.5	1.67	19.0	11.6
	350	38.3	1.23	8.94	2.80
	300	16.0	0.794	3.74	1.68
2.099	400	31.1	1.88	7.3	2.80
	300	13.5	1.06	3.16	1.40
	200	0.2	0.137	0.047	0.056

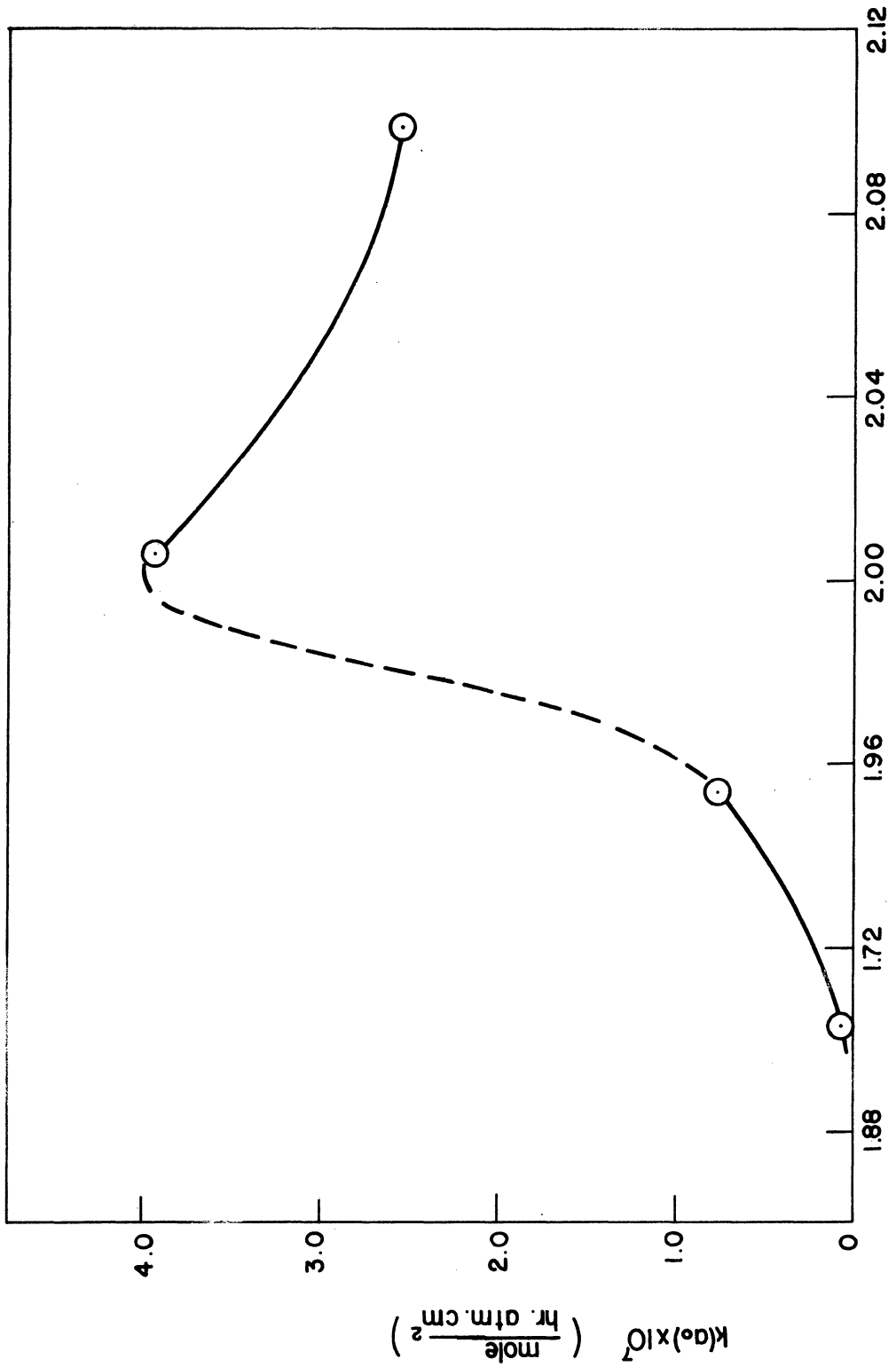

Figure 9. The Rate Constant $k(a_o)$ of the Exchange Reaction Versus Composition x , T = 350°C , a_o = 0.464.

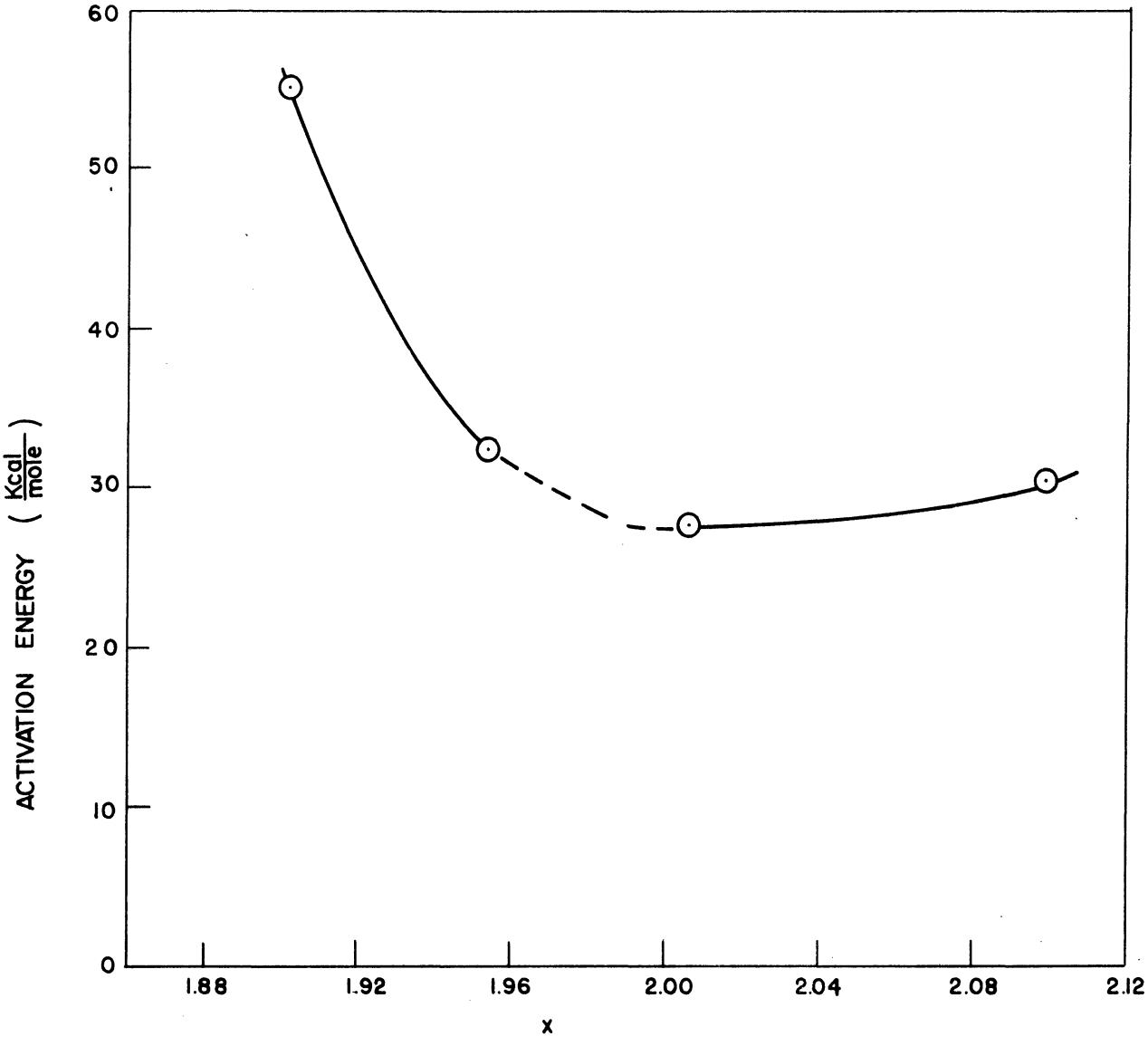

Figure 10. Activation Energy of the Exchange Reaction Versus Composition x , $a_o = 0.464$.

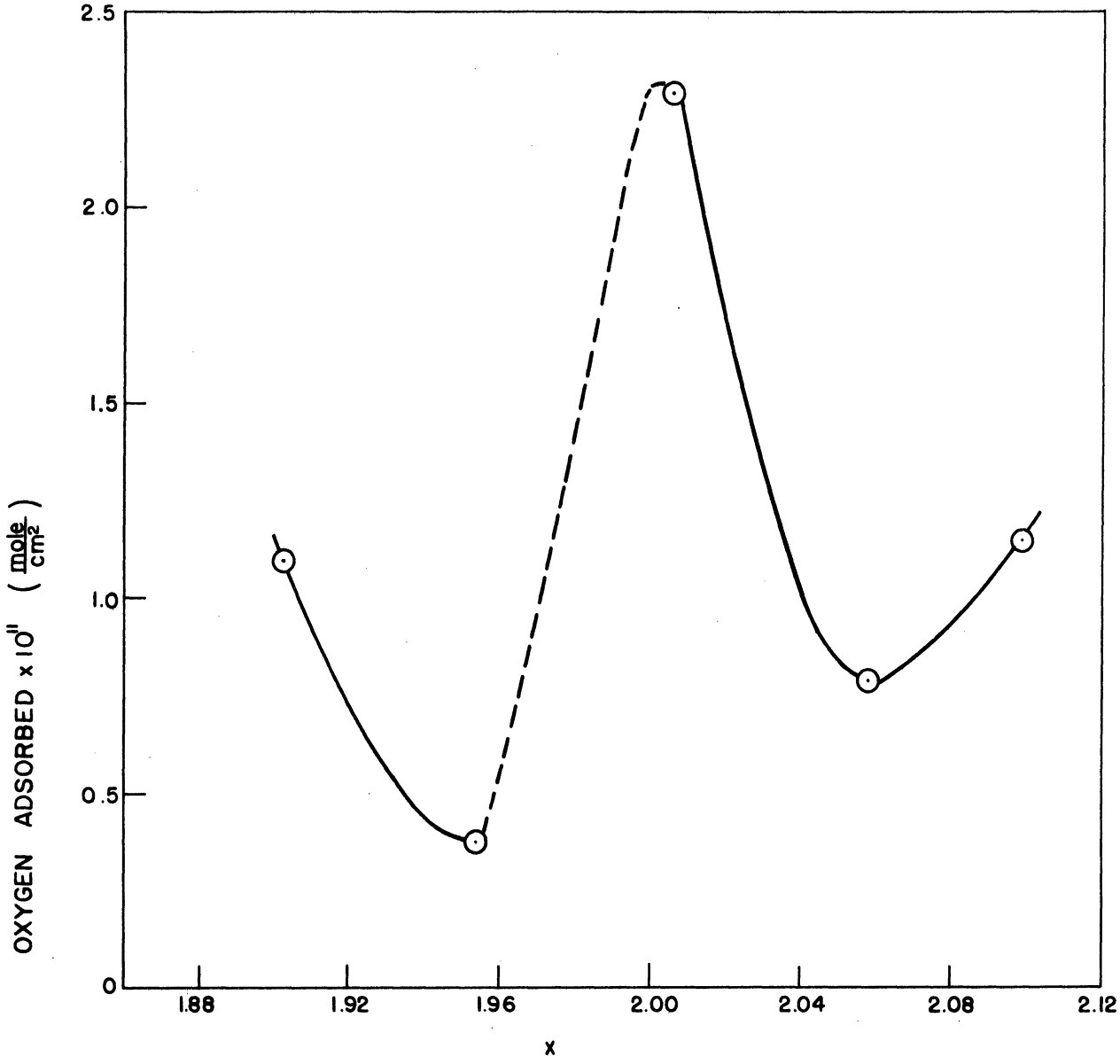

Figure 11. Amount of Oxygen Adsorbed in 24 Hours Versus Composition x , T = 300°C.

Figure 12 shows the initial rate of adsorption versus the composition x at 300°C.

Figure 14 represents the initial adsorption rate constant k_{ads} versus the composition x at 300°C.

Figure 14 indicates the initial rate of desorption versus the composition x at 300°C.

Figure 15 presents the amount of oxygen desorbed per unit area versus the composition x at 300°C.

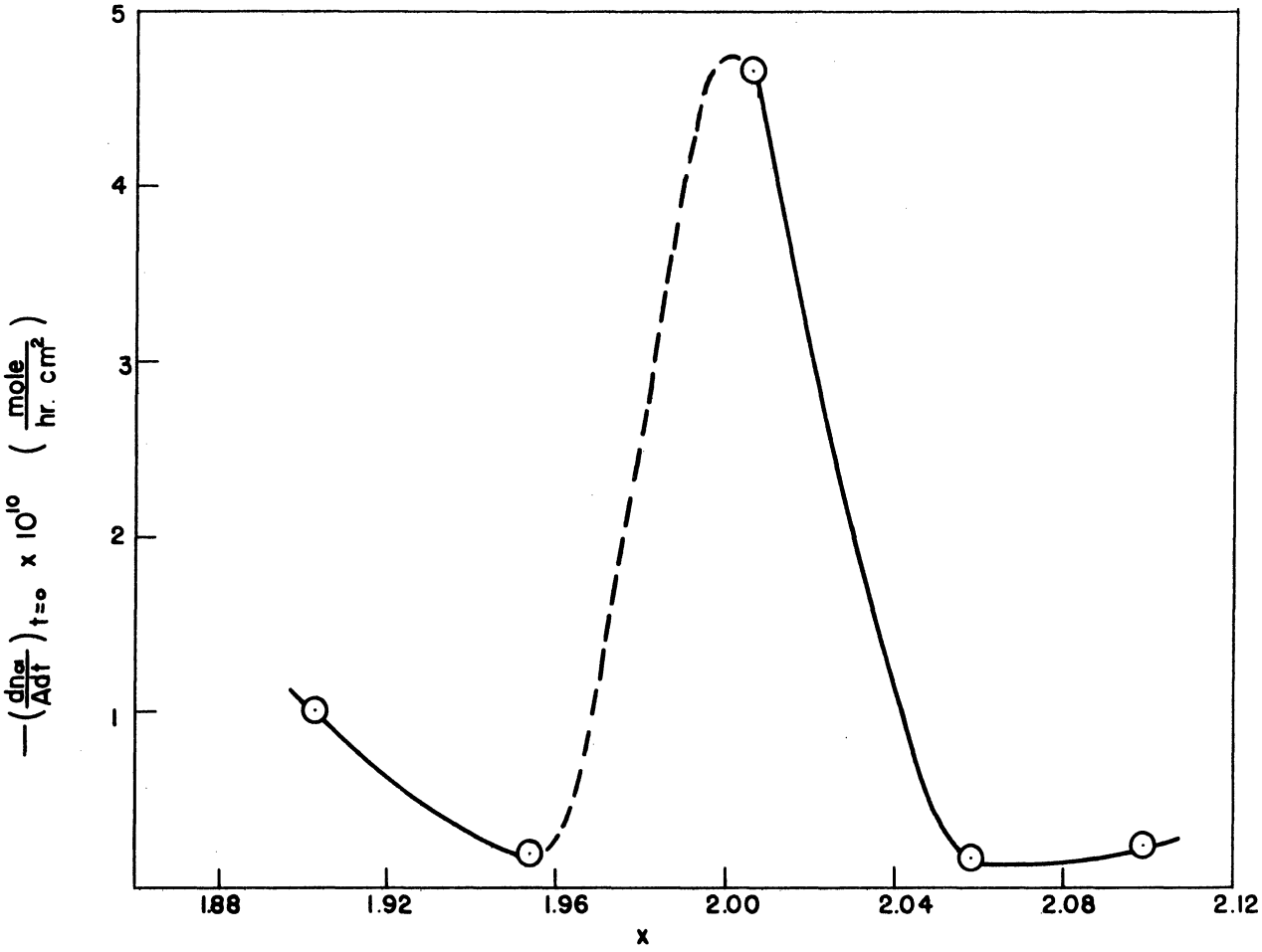

Figure 12. Initial Rate of Oxygen Adsorption on $CO_{3-x}Fe_xO_4$ Versus Composition x , T = 300°C $P_{ai} \cong$ 100 Micron of Hg.

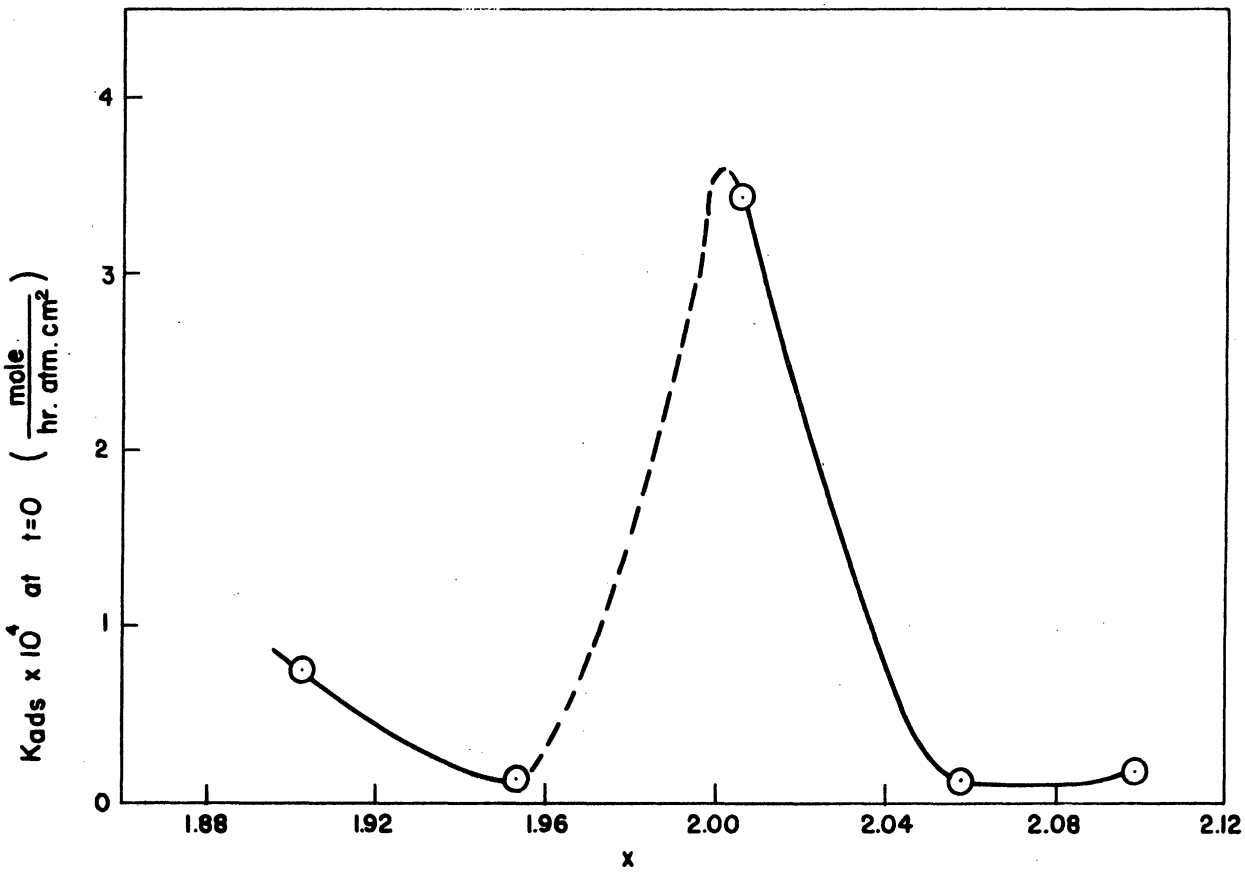

Figure 13. Initial Rate Constant of Adsorption K_{ads}. Versus Composition x on $Co_{3-x}Fe_xO_4$, T = 300°C

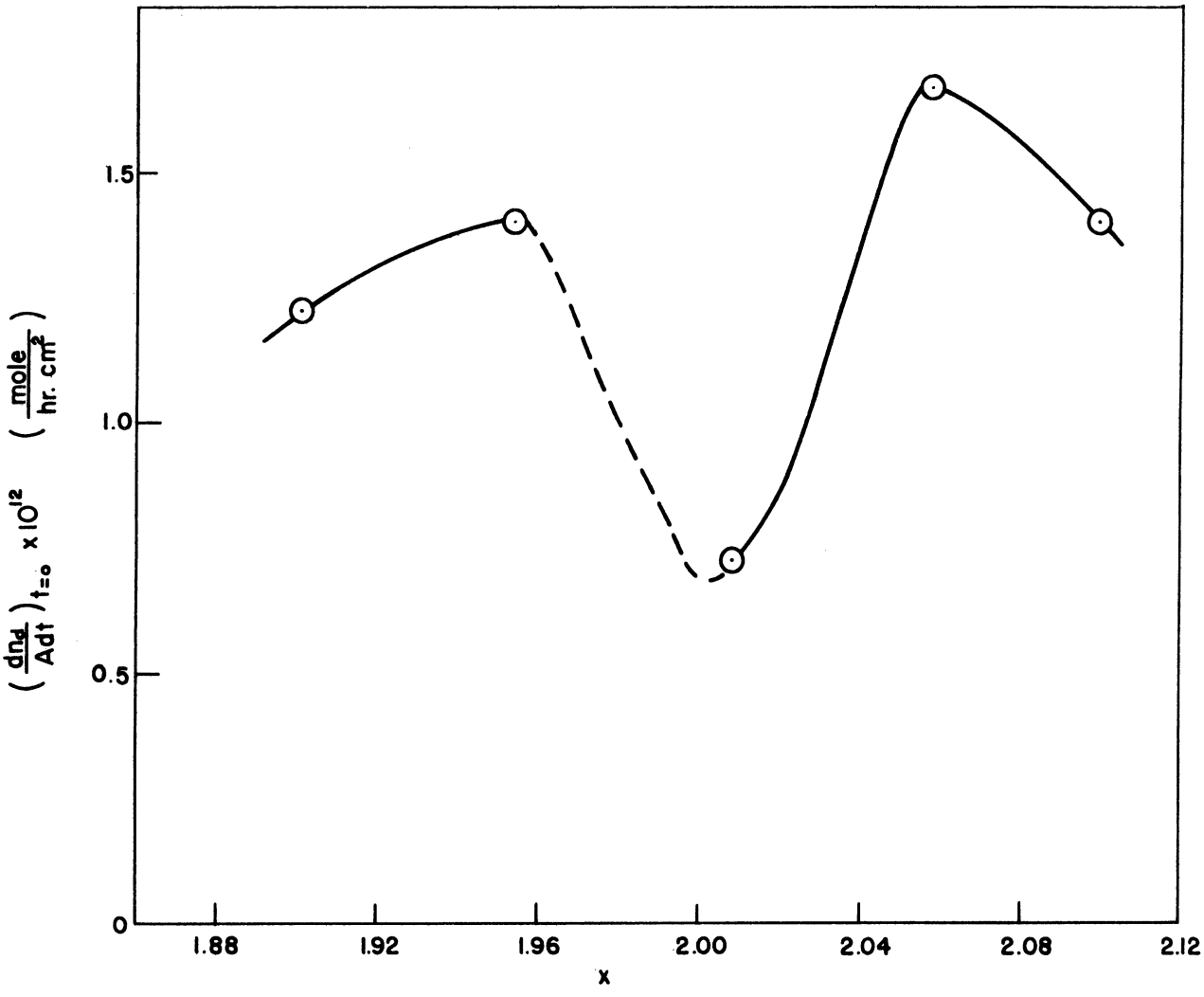

Figure 14. Initial Rate of Desorption from $CO_{3-x}\ Fe_x\ O_4$ Versus Composition x , T = 300°C.

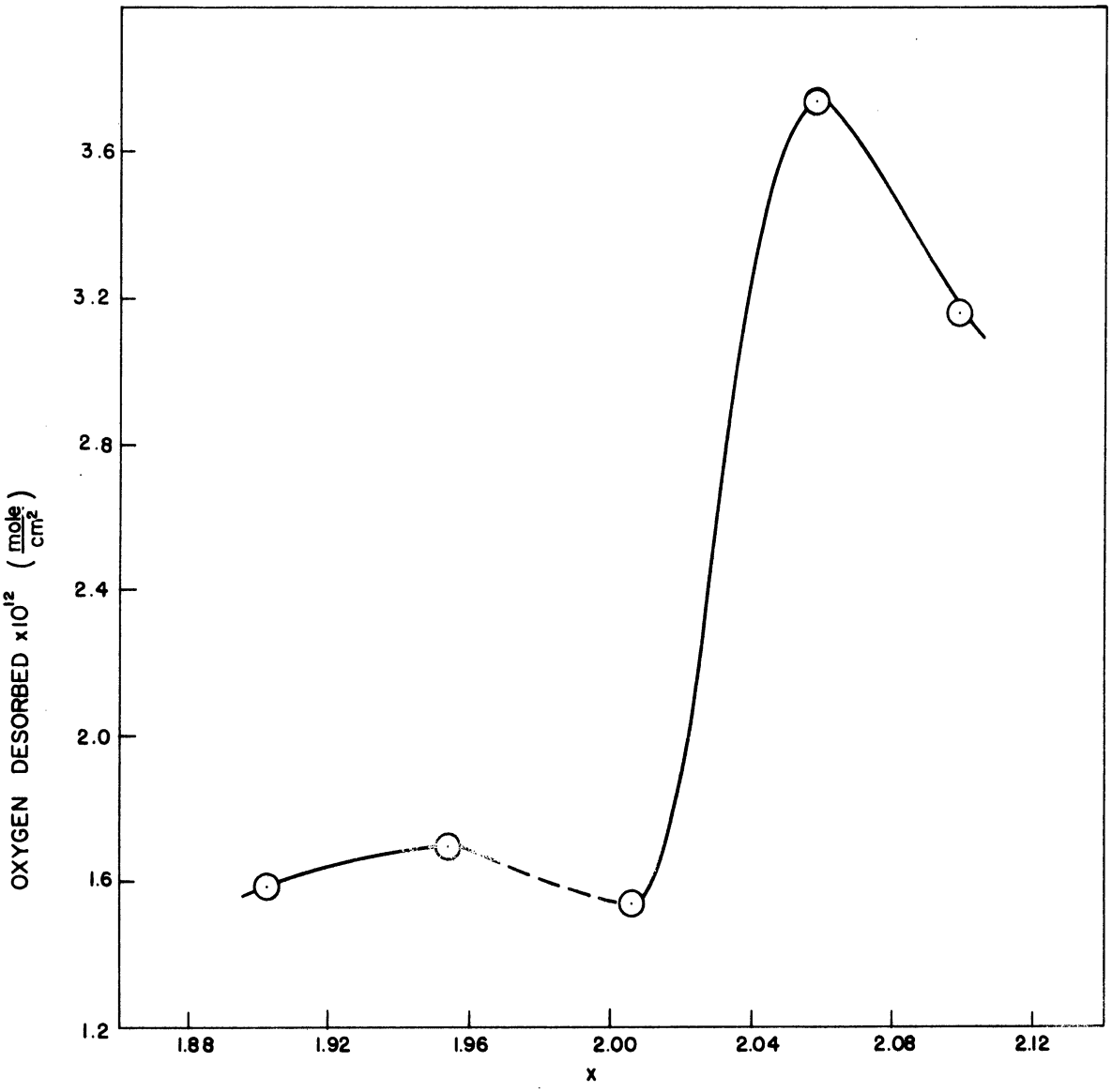

Figure 15. Amount of Oxygen Desorbed From CO_{3-x} Fe_x O_4 in 24 Hours Versus Composition x , T = 300°C.

VI. DISCUSSION OF RESULTS

The results shown in Figures 9, 12 and 13 give a uniform pattern of curves which has a maximum when x is in the vicinity of two. These extremes indicate that the rate constant of the CO_2 - CO exchange reaction, the rate constant of adsorption of oxygen, and the initial rate of adsorption for the intrinsic sample, which is an insulator at $x = 2$, are higher than the extrinsic samples with $x \neq 2$. The same conclusion was obtained in some other works [51] [33]. The conclusion is, however, contrary to other statements in the literature [13] [66]. These claim that the catalytic activity of oxides is according to the order

p-type oxides > insulator > n-types.

The reason for the claim is from a specific experimental result. That is, the p-type oxides, the oxides of copper, nickel, cobalt and iron have higher catalytic activity in the decomposition of N_2O than the n-type oxides, the oxide of zinc, chromium and gallium. These two contradictory orders of activity are discussed in the following paragraphs.

The catalytic activity, as well as other properties, of a metal oxide is determined by the metallic element of the oxide, the crystal structure and the defects. The metallic element and its electronic structure determine the valence of the cation. The crystal structure and the metallic element determine the type of chemical bonds between the metallic element and the oxygen of the oxide. The metallic element of the oxide is undoubtedly the predominant factor in effecting the chemical properties of the oxide. Defects of the metallic oxide may act as electron donors or electron acceptors which effect predominately the electronic properties of the oxide.

The results in this research are obtained in which the metallic cations and the crystal structure of the oxide catalyst are invariant. The only parameter is the defect of the oxide with which the oxide is made into n-type, intrinsic or p-type by varying the composition of the cations. The other statement is based on the comparison of oxides with different metallic cations and with different crystal structures. It may well be that copper oxide has higher catalytic activity than zinc oxide, not because they are p- or n-type but because they are different materials.

In order to understand the mechanism of a catalytic reaction, it is necessary to know the active center and the catalytic intermediate of a reacting system. In the exchange reaction of CO_2 and CO, the result in Figure 5 gives the value of $m = 1$ for three samples with $x = 1.903$, 2.006 and 2.099. This result indicates that the catalytic intermediate on all three types -- n-type, p-type and intrinsic -- of cobalt ferrite is O^-_{ads} (see Chapter 2, Section C). The extra electron of the catalytic intermediate O^-_{ads} is obtained from the active center on the catalyst surface. The proposed active center is the cation pairs $Co^{+2}|B| - Fe^{+3}|B|$ -- the normal lattice cation pairs. Electronic defects have been considered as the active centers for catalytic reactions in the literature [10][62]. If the active center for the exchange reaction of CO_2 and CO are defects, the catalytic activity, which may be represented by the rate constant, for n-type or p-type cobalt ferrite would be higher than the intrinsic cobalt ferrite. But the results in Figures 9 and 13 show that it is not so. This indicates that the active center for the exchange reaction is not the characteristic defect. Experimental results have verified that $Co^{+2}|B| - Fe^{+3}|B|$ is the active center. For the intrinsic cobalt ferrite

catalyst, the concentration of the active center $Co^{+2}|B| - Fe^{+3}|B|$ is higher than in either the n-type or the p-type cobalt ferrite, as is the catalytic activity.

The next item to be discussed is the dependence of the magnitude of the rate constants $k(a_o)$ and K_{ads} on catalyst compositions. The theory which is employed to explain the catalytic activity difference among catalysts with different composition is based on the activity of the active center $Co^{+2}|B| - Fe^{+3}|B|$. For n-type cobalt ferrite, which has a certain amount $Co^{+2}|B|$ replaced by $Fe^{+2}|B|$, and also for the p-type which has a certain amount of $Fe^{+3}|B|$ replaced by $Co^{+2}|B|$; so that the surface concentration of the active center $Co^{+2}|B| - Fe^{+3}|B|$ for the n-type or the p-type is lower than the activity of the intrinsic. The catalytic activity difference is in the order of magnitude of eighty, but the concentration difference among samples is within 10% in the value of x. This can be explained by the distribution of defects in a single crystal and by the activation energy. The sample was prepared by firing cobalt carbonate and iron oxide at 1950°C. At this high temperature, the defects are ionized to form free electrons or electron holes depending on whether the sample is iron-excess or cobalt-excess in its composition. We may expect that the defect concentration on the surface layer is higher than the defect concentration in the bulk. The activation energy difference (cf. Tables 2 and 3) also contribute to the difference of the catalytic activity.

It is worth noting that the plot of $k(a_o)$ or K_{ads} versus x in Figure 9 or 13 would pass through a maxi um at $x = 2$ if the curve is continuous. Unfortunately there is no way of knowing experimentally what the exact maximum value of $k(a_o)$ or K_{ads}. is, since the stoichiometric cobalt ferrite, $COFe_2O_4$ is seldom obtained.

With the catalytic intermediate and the active center defined, it is possible to postulate the reaction mechanism of the exchange reaction as following:

$$\text{(i)}\quad CO_2(g) + Co^{+2}|B| - Fe^{+3}|B| \rightarrow \overset{O^-}{|}Co^{+3}|B| - Fe^{+3}|B| + CO(g) \qquad (62)$$

$$\text{(ii)}\quad \overset{O^-}{|}Co^{+3}|B| - Fe^{+3}|B| \rightarrow Co^{+3}|B| - \overset{O^-}{|}Fe^{+3}|B| \qquad (63)$$

$$\text{(iii)}\quad Co^{+3}|B| - \overset{O^-}{|}Fe^{+3}|B| + CO(g) \rightarrow Co^{+3}|B| - Fe^{+2}|B| + CO_2(g) \qquad (64)$$

$$\text{(iv)}\quad Co^{+3}|B| - Fe^{+2}|B| \rightarrow Co^{+2}|B| - Fe^{+3}|B| \qquad (65)$$

Because of lack of thermodynamic data for surface reactions on cobalt ferrite, it is rather difficult to discuss each step quantitatively. But we can discuss the steps in a qualitative manner. Step (i) is the reduction reaction of CO_2 which has a possible positive ΔH and ΔF. So the activity of the products CO and $\overset{O^-}{|}Co^{+3}|B| - Fe^{+2}|B|$ is smaller than the activity of the reactants CO_2 and $Co^{+2}|B| - Fe^{+3}|B|$ in an equilibrium system. Since a_{CO} and a_{CO_2} are fixed by the partial pressure of CO and CO_2, we may expect to have $[Co^{+2}|B| - Fe^{+3}|B|] \gg [\overset{O^-}{|}Co^{+3}|B| - Fe^{+3}|B|]$. This was verified by the conductivity measurement by Ratterman [49]. Step (ii) involves a change of bonds from $O^- - Co^{+3}|B|$ to $O^- - Fe^{+3}|B|$. Because of the same charge and almost the same ionic radius ($r_{Fe^{+3}} = 0.67$ A, $r_{Co^{+3}} = 0.65$ A) of $Co^{+3}|B|$ and $Fe^{+3}|B|$, we may expect very little change in the vibration frequency, and likewise in the vibration partition function and in the free energy. Therefore the activities of $\overset{O^-}{|}Co^{+3}|B| - Fe^{+3}|B|$ and $Co^{+3}|B| - \overset{O^-}{|}Fe^{+3}|B|$ are almost the same. Step (iii) is a possible exothermic reaction of the oxidation of CO, so the ΔH and ΔF are negative. We may expect $[Co^{+3}|B| - Fe^{+2}|B|] \gg \overset{O^-}{|}Co^{+3}|B| - Fe^{+3}|B|$. Step (v) involves

an electron transfer between the ion pair. In cobalt ferrite, the $Co^{+2}|B| - Fe^{+3}|B|$ with lower potential energy is more stable than $Co^{+3}|B| - Fe^{+2}|B|$. Jonker [35] has shown that the potential energy of $Fe^{+3}|B|$ is 0.025 eV lower than $Fe^{+2}|B|$ and the potential energy of $Co^{+2}|B|$ is 0.15 eV lower than $Co^{+3}|B|$. Therefore $[Co^{+2}|B| \cdot Fe^{+3}|B|]$ is higher than $[Co^{+3}|B| - Fe^{+2}|B|]$. We may conclude that the activity of the bare and covered active center is in the order of $[Co^{+2}|B| - Fe^{+3}|B|] > [Co^{+3}|B| - Fe^{+2}|B|] \gg [Co^{+3}|B| - \overset{O^-}{Fe^{+3}}|B|] = [\overset{O^-}{Co^{+3}}|B| - Fe^{+3}|B|]$.

The experimental result of the oxygen adsorption in Figures 11, 12 and 13 also show that the intrinsic cobalt ferrite has a higher activity than both the n-type and the p-type. With the same proposed active center as the exchange reaction it is postulated that the mechanism of oxygen adsorption and desorption follows the steps:

$$\text{(i)}\quad O_2(g) + Co^{+2}|B| - Fe^{+3}|B| \rightarrow \overset{O}{\underset{O^-}{Co^{+3}}}|B| - Fe^{+3}|B| \qquad (66)$$

$$\text{(ii)}\quad \overset{O}{\underset{O^-}{Co^{+3}}}|B| - Fe^{+3}|B| \rightarrow \overset{O^-}{\underset{O}{Co^{+3}}}|B| - Fe^{+3}|B| \qquad (67)$$

$$\text{(iii)}\quad \overset{O^-}{\underset{O}{Co^{+3}}}|B| - Fe^{+3}|B| \rightarrow \overset{O \text{ - - - - } O^-}{Co^{+3}|B| \quad\quad Fe^{+3}|B|} \qquad (68)$$

$$\text{(iv)}\quad \overset{O \text{ - - - - } O^-}{Co^{+3}|B| \quad\quad Fe^{+3}|B|} \rightarrow \overset{O \text{ - - - - } O}{Co^{+3}|B| \cdot Fe^{+2}|B|} \qquad (69)$$

$$\text{(v)}\quad \overset{O \text{ - - - - } O}{Co^{+3}|B| \quad\quad Fe^{+2}|B|} \rightarrow Co^{+3}|B| \cdot Fe^{+2}|B| + O_2(g) \qquad (70)$$

$$\text{(vi)}\quad Co^{+3}|B| - Fe^{+2}|B| \rightarrow Co^{+2}|B| - Fe^{+3}|B| \qquad (71)$$

Step (i) is the step of oxygen adsorption in which an electron is transferred from the active center to the oxygen molecule. Step (ii) (iii) and (iv) are the electron transfer steps between two oxygen atoms and between the oxygen atom and $Fe^{+3}|B|$. Step (v) is the step of oxygen desorption. Step (vi) is the internal electron transfer of the active center which returns to the more stable form.

The next few paragraphs are to discuss separately the effect of the defects on the rate constant and on the activation energy of the exchange reaction, of the oxygen adsorption and of the oxygen desorption.

The rate constant $k(a_o)$ of the exchange reaction decreases with an increase of the defect concentration for both n-type and p-type samples as shown in Figure 9. There are two ways that $k(a_o)$ is effected by defects. The first and the direct way which has been discussed is that defects reduce the number of active centers. The second and the indirect way is that the defect located next to the active center (see Appendix III) may alter the polarity of the active center so that the potential field, which effects the activation energy, is changed. From quantum mechanics, it has been shown that the formation of ionic bonds and nonpolar covalent bonds represents extreme cases of the chemical bond formation. The intermediate case is the formation of polar covalent bonds. For n-type samples, it is assumed that the predominate defect $\underset{(\delta-)}{Fe^{+2}}|B|$ is covered by $\underset{(\delta+)}{O_{ads}}$. (see Section II.B, (d)) with the reaction $Fe^{+2}|B| + O_{ads} \rightarrow Fe^{+3}|B|_i + O_{ads}$. The ionized defect $Fe^{+3}|B|_i$, has a positive polarity $\delta+$ because of the donation of an electron. If the active center of the exchange reaction, $Co^{+2}|B| - Fe^{+3}|B|$, is next to the defect $Fe^{+3}|B|_i$, the positive polarity $\delta+$ will contribute a certain attraction to the outer-shell 3d electron of the $Co^{+2}|B|$ ion of the active center, to make

the 3d electron more difficult to ionize. Thus the activation energy of the exchange reaction should be higher for the n-type sample than for the intrinsic. For p-type, the predominate defect is $Co^{+3}|B|$, an electron acceptor. If the active center $Co^{+2}|B| - Fe^{+3}|B|$ is next to $Co^{+3}|B|$ with a strong positive polarity, the active center will need an even higher energy than the n-type to become ionized. Therefore the activation energy of the exchange reaction for the p-type should be higher than both the intrinsic and the n-type. The result shown in Table 2 is so.

The rate constant $K_{ads.}$ and activation energy E_a of oxygen adsorption as shown in Figure 13 and Table 3 are influenced by the defect in the same way as is the exchange reaction. The primary effect of the defect is the influence on the number of active centers from which the intrinsic sample has a larger $K_{ads.}$ than both the n-type and the p-type. The secondary effect is the alteration of the polarity of the active center from which the activation energy for the n-type or the p-type sample is higher than the intrinsic. These effects are shown in Figure 13 and Table 3. Table 3 also shows that the activation energy tends to drop for both n-type and p-type when the defect concentration goes beyond a certain value. This can be explained by the bare "strong" chemisorption center (see Sec. II.C) of defects $Fe^{+2}|B|$ and $Co^{+2}|B|_i$ participating in the oxygen adsorption. If the oxygen covered defect $Fe^{+2}|B|$ or $Co^{+2}|B|_i$ concentration on the surface is close enough to a certain value, there will be an appreciable amount of oxygen molecules desorbed from the "strong" chemisorption center when the sample is brought to its reference state by heating it at 400°C under vacuum. The bare "strong" chemisorption center has a much lower activation energy than the "weak" active center $Co^{+2}|B| - Fe^{+3}|B|$ in the adsorption of oxygen. The experimental

value of the activation energy at $x = 1.903$ and $x = 2.009$ is the overall activation energy of adsorption of the two types of active centers. It is worth noting that there is no activation energy drop of the exchange reaction at high defect concentrations because the "strong" chemisorption centers are covered by $O^-_{ads.}$ which do not participate in the exchange reaction.

The desorption of oxygen molecules involves the breaking of $O - Co^{+3}|B|$ and $O - Fe^{+2}|B|$ bonds (see page 63 Step (v)). It is not surprising that the activation energy of desorption is much higher than the activation energy of adsorption. The high activation energy of desorption results that the effect of the activation energy outweighs the effect of the surface coverage in the determination of the rate of desorption. The effect of the polarity of the defect toward the active center is the same as in the exchange reaction and in the oxygen adsorption. The positive polarity of the defects next to the active centers of the n-type and p-type samples makes it easier for the active center to take the electron back from the adsorbed oxygen molecule in the n- or p-type than in the intrinsic (see page 63 Step (iv)). Therefore the activation of desorption is lowered for both n-type and p-type samples. This results in the higher desorption rate for both n-type and p-type samples than for the intrinsic as shown in Figure 14. The desorption rate is reduced again when the defect concentration is higher than a certain value. This is due to the desorption of oxygen molecules which were adsorbed on the "strong" active centers. The explanation is the same as in the adsorption of oxygen at high defect concentrations.

It is important to investigate the possible secondary reactions which may effect the rate of formation of ^{14}CO in the exchange reaction

of CO_2 and CO. The adsorption of CO has been observed on both n-type and p-type semiconductors [32]. There is a possible exchange reaction between the ^{14}CO in the gas phase and the $CO^-_{ads.}$. The activation energy of this reaction is high because $CO^-_{ads.}$ is strongly adsorbed on oxides [23]. The second possible reaction is $^{14}CO(g) + CO(g) \rightarrow {}^{14}C + CO_2(g)$ which is thermodynamically possible when the p^2_{co}/p_{co_2} ratio is higher than 3×10^{-5} at 350°C. Brandner [10] reported the formation of carbon on gold strips used as the catalyst in the exchange reaction CO_2 and CO. These two possible secondary reactions contribute to the disappearance of ^{14}CO from the gas phase when there is an appreciable amount of ^{14}CO formed in the gas phase during the later half of an experiment. But the rate constant $k(a_o)$ which is obtained from data of the very early part of the experiment, is not effected by these secondary reactions. Figure 4 shows that these secondary reactions did occur.

Finally, it is shown that the rate of oxygen adsorption does not follow the absolute rate theory. If the adsorbed oxygen molecule is immobile on the surface, Equation (56) derived from the theory can be simplified to

$$u\, e^{E_a/RT} = C_g C_s \frac{\sigma}{\sigma^{\neq}} \frac{h^4}{8\pi I (2\pi m k T)^{3/2}} \tag{72}$$

If the adsorbed oxygen molecule is mobile, Equation (56) becomes

$$u\, e^{E_a/RT} = C_g \frac{kT}{h} \frac{h}{(2\pi m k T)^{1/2}} \tag{73}$$

For the sample with $x = 2.006$ at $T = 300°C$, the experimentally obtained value of $u\, e^{E_a/RT}$ is 1.053×10^{12} molecules per sec. From Equations (72) and (73), the calculated values of $u\, e^{E_a/RT}$ are 3.25×10^{20} and

2.61×10^{17} molecule per sec. respectively. Comparing these values, it is obvious that the absolute rate theory does not apply to our model of the rate of oxygen adsorption.

VII. CONCLUSIONS

The following conclusions have been obtained from results of the study of the catalyzed exchange reaction of CO_2 and CO, and the adsorption and desorption of oxygen on cobalt ferrite $Co_{3-x}Fe_xO_4$, with x ranging from 1.903 to 2.099.

(1) For the exchange reaction and the oxygen adsorption, the catalytic activity of the intrinsic cobalt ferrite is higher than the catalytic activity of the n-type or the p-type. This is contrary to what was claimed in literature. For the oxygen desorption, the rate of desorption of the n-type or the p-type is higher than the rate of desorption of the intrinsic sample. We may generalize the results by stating that: for reactions involving the electron transfer from cobalt ferrite to the catalytic intermediate, the catalytic activity follows

intrinsic > n-type or p-type,

for reactions involving the electron transfer from the catalytic intermediate to the solid, the catalytic activity follows

n-type or p-type > intrinsic.

(2) The catalytic intermediate for the exchange reaction is $O^-_{ads.}$. The catalytic intermediate of the oxygen adsorption and desorption is in different forms of $O^-_{2ads.}$. The active center for both reactions is the ion pair, $Co^{+2}|B| - Fe^{+3}|B|$. This is also contrary to some literature in which the defects are being considered as active centers for the catalytic reaction.

(3) The defects $Co^{+3}|B|$ and $Fe^{+2}|B|$ effect the catalytic activity of the exchange reaction in two ways. The predominant effect is that the defects reduce the number of the active center $Co^{+2}|B| - Fe^{+3}|B|$ on the catalyst surface. The second effect is that the

defects alter the polarity of the active center, so that the activation energy of the exchange reaction increases with the increase of the defect concentration.

(4) For the adsorption of oxygen, the defects effect the rate of adsorption in three ways. The first two are the same as in the exchange reaction, namely the effects of the number of the active center and the polarity. The third way is that the defect causes a decrease of the activation energy when the surface concentration of defects is higher than a certain value. This is due to the defect itself acting as the active center, at the high defect concentration.

(5) The defects give the same three effects in the desorption of oxygen as in the oxygen adsorption. Because of the high activation energy of desorption, the polarity effect outweighs the effect of the number of active centers. This results that the rate of desorption for the n-type or the p-type is higher than the intrinsic sample. The third effect at a high defect concentration results in the increase of the activation energy. This effect causes the decrease of the desorption rate at high defect concentrations.

(6) There are two possible secondary reactions occurring with the exchange reaction. They are (i) $^{14}CO(g) + CO^{-}_{ads.} \rightarrow {}^{14}CO^{-}_{ads} + CO(g)$ and (ii) $^{14}CO(g) + CO(g) \rightarrow 14C(s) + CO_2(g)$. They may cause the decrease of ^{14}CO in the gas phase.

APPENDICES

APPENDIX I EXPERIMENTAL DATA

A. Experimental Data of the Exchange Reaction of CO_2 and CO

TABLE 5

^{14}CO EXPERIMENTAL DATA ON THE FORMATION OF ^{14}CO CATALYZED BY 1.000 GRAM OF $Co_{3-x}Fe_xO_4$

Time (hours)	Total Counts per Two Minutes	Corrected Total Counts per Two Minutes	^{14}CO Counts per Two Minutes	Corrected ^{14}CO Counts per Two Minutes	$^{14}CO\%$
		Run No. 18-2, x=1.903, a_o=0.464, T=350°C			
1.5	21514	21466	705	553	2.57
10.0	20727	20699	3118	2966	14.32
22.67	20542	20494	5181	5030	24.6
34.67	20388	20324	5980	5828	28.7
47.33	19842	19794	6331	6180	31.2
59.67	19276	19228	6061	5910	30.8
70.67	18540	18492	5451	5300	28.6
95.17	17896	17858	4346	4194	23.5
108.0	17590	17542	3947	3796	21.6
143.17	16752	16704	2923	2772	16.5
		Run No. 18-3,x=1.90$\frac{1}{2}$, a_o=0.464, T=380°C			
1.0	20814	20766	3222	3070	14.8
3.0	20327	20279	5412	5260	25.9
5.0	19751	19703	6115	5964	30.2
10.17	18766	18718	5442	5390	28.8
24.67	17422	17374	3578	3426	19.7

TABLE 5 (CONT'D)

Time (hours)	Total Counts per Two Minutes	Corrected Total Counts per Two Minutes	^{14}CO Counts per Two Minutes	^{14} Corrected CO Counts per Two Minutes	$^{14}CO\%$
		Run No. 18-4, x=1.903, a_o=0.464, T=380°C			
0.5	21375	21327	2430	2278	10.67
2.0	20849	20801	4867	4716	22.6
4.0	20195	20144	5972	5820	28.8
6.0	20086	20038	6242	6092	30.4
25.5	17842	17794	3365	3214	18.1
		Run No. 18-5, x=1.903, a_o=0.464, T=410°C			
1.0	23217	23169	6349	6198	25.7
2.0	22676	22628	6931	6781	29.9
3.5	21726	21678	6543	6392	29.4
5.5	20937	20889	5289	5138	24.6
11.0	16404	16365	3620	3468	21.2
		Run No. 18-6, x=1.903, a_o=0.464, T=410°C			
0.5	21899	21851	5043	4892	22.4
1.5	20786	20728	6103	5952	28.8
2.5	19718	19670	5758	5606	28.5
		Run No. 14-6, x=1.954, a_o=0.464, T=350°C			
2.0	19568	19520	5290	5138	26.3
5.33	18302	18254	6838	6676	35.6
10.33	17581	17533	6146	5994	34.2
25.0	16187	16139	3838	3686	22.6
29.67	15582	17534	3298	3146	18.0

TABLE 5 (CONT'D)

Time (hours)	Total Counts per Two Minutes	Corrected Total Counts per Two Minutes	^{14}CO Counts per Two Minutes	Corrected ^{14}CO Counts per Two Minutes	^{14}CO%
		Run No. 14-7, x=1.954, a_o=0.464, T=350°C			
1.0	19322	18274	3183	3032	16.6
4.09	18752	18704	6462	6310	33.8
6.0	18422	18374	6673	6522	35.5
12.5	17436	17388	5431	5278	30.4
24.5	16010	15962	3545	3392	21.3
		Run No. 14-8, x=1.954, a_o=0.464, T=310°C			
2.0	19905	19857	1888	1736	8.75
4.0	19811	19763	3214	3062	15.5
8.84	19623	19575	5341	5188	26.6
23.0	18912	18864	7212	7060	37.4
		Run No. 14-9, x=1.954, a_o=0.464, T=310°C			
14.0	18959	18911	6112	5960	31.4
19.0	18608	18560	6493	6342	34.1
27.0	18530	18482	6844	6692	36.3
36.67	17568	17520	6698	6546	37.3
49.0	17286	17238	6208	6056	35.1
66.67	16552	16504	5279	5128	31.1
86.0	16068	16020	4662	4510	28.1

TABLE 5 (CONT'D)

Time (hours)	Total Counts per Two Minutes	Corrected Total Counts per Two Minutes	^{14}CO Counts per Two Minutes	Corrected ^{14}CO Counts per Two Minutes	^{14}CO%
	Run No. 14-10, x=1.954, a_o=0.464, T=390°C				
1.0	20198	20150	6710	6658	32.6
2.0	19236	19188	5859	5708	29.8
3.0	18563	18515	5048	4896	26.4
4.0	17894	17846	4245	4094	22.9
	Run No. 14-11, x=1.954, a_o=0.464, T=390°C				
0.67	20676	20628	6030	5878	28.5
1.50	20208	20160	6285	6134	30.4
5.50	17951	17903	3530	3218	18.0
	Run No. 14-12, x=1.954, a_o=0.464, T=390°C				
0.33	20848	20800	4130	3818	15.9
	Run No. 10-8, x=2.006, a_o=0.464, T=300°C				
1.0	18707	18659	1802	1650	8.85
3.5	16606	16558	3939	3788	22.8
	Run No. 10-9, x=2.006, a_o=0.464, T=300°C				
2.0	19440	19392	3211	3058	15.8
3.67	19377	19329	4441	4289	22.2
10.84	18734	18686	7046	6894	36.9
22.67	17873	17825	6642	6290	35.2
33.33	16918	16870	5772	5620	33.3
48.67	16057	16009	4658	4506	28.1

TABLE 5 (CONT'D)

Time (hours)	Total Counts per Two Minutes	Corrected Total Counts per Two Minutes	^{14}CO Counts per Two Minutes	^{14}Corrected CO Counts per Two Minutes	^{14}CO%
	Run No. 10-10, x=2.006, a_o=0.464, T=300°C				
1.5	19197	19149	2365	2213	11.6
6.25	18808	18760	6211	6059	32.3
17.92	19298	19250	7135	6983	36.3
24.84	17452	17404	6410	6249	35.9
47.84	14719	15671	4679	4527	28.9
	Run No. 10-12, x=2.006, a_o=0.464, T=250°C				
1.5	20945	20897	439	287	1.37
6.17	18610	18562	1093	941	5.07
11.5	18624	18576	1775	1623	8.75
27.0	19510	19462	3187	3035	15.6
35.0	18495	18447	3714	3562	19.3
48.17	18998	18950	4602	4450	24.0
75.17	17684	17636	5712	5560	31.5
97.17	17661	17613	6254	6102	34.7
106.67	17414	17366	6218	6066	34.9
118.67	16859	16811	6410	6258	37.2
123.0	16682	16634	6351	6199	37.3
144.0	18042	17994	6671	6520	36.2
168.67	16382	16334	6591	6440	39.4

TABLE 5 (CONT'D)

Time (hours)	Total Counts per Two Minutes	Corrected Total Counts per Two Minutes	^{14}CO Counts per Two Minutes	^{14}Corrected CO Counts per Two Minutes	$^{14}CO\%$
192.00	15885	15837	6585	6433	40.6
216.67	15667	15619	6284	6132	39.2
241.0	15845	15797	6099	5947	37.6
	Run No. 10-13, x=2.006, a_o=0.464, T=350°C				
1.0	20775	20727	7106	6954	33.6
2.5	19121	19073	7107	6955	36.5
4.5	17904	17856	5628	5476	30.7
11.5	16244	16196	3014	2862	17.7
	Run No. 10-14, x=2.006, a_o=464, T=350°C				
0.5	19518	19470	5073	4921	25.3
1.5	19373	19325	6946	6594	34.1
3.5	17598	17550	5965	5813	33.1
10.5	16344	16296	3086	2934	18.0
25.0	14502	14454	1198	1046	7.3
	Run No. 17-1, x=2.099, a_o=0.464, T=350°C				
1.0	21456	21408	5540	5388	25.2
2.0	20346	20298	6993	6841	33.7
3.5	19929	19881	7333	7181	36.1
9.5	19135	19087	5874	5722	30.0
24.5	18133	18085	3689	3537	19.5

TABLE 5 (CONT'D)

Time (hours)	Total Counts per Two Minutes	Corrected Total Counts per Two Minutes	^{14}CO Counts per Two Minutes	Corrected ^{14}CO Counts per Two Minutes	^{14}CO%
	Run No. 17-2, x=2.099,		a_o=0.464, T=350°C		
0.5	19526	19478	2969	2817	14.5
1.5	19093	19045	5630	5478	28.8
3.0	18543	18495	6712	6560	35.5
4.5	17781	17733	6450	6298	35.5
23.0	15951	15903	3060	2908	18.3
29.0	15332	15284	2533	2381	15.6
	Run No. 17-3, x=2.099,		a_o=0.464, T=310°C		
2.0	19005	18957	1828	1676	8.9
4.5	18613	18565	3321	3170	17.1
10.5	18411	18363	5780	5628	30.7
19.0	18209	18161	6981	6830	37.6
24.0	17643	17595	6692	6540	37.2
28.5	17187	17139	6566	6414	37.4
36.5	17107	17059	6273	6121	35.9
52.5	16590	16542	5548	5396	32.6
72.0	15821	15773	4811	4660	29.6
95.3	15431	15381	3898	3746	24.4
	Run No. 17-5, x=2.099,		a_o=0.464, T=390°C		
1.0	20547	20499	6944	6792	33.1
2.0	19595	19547	5768	5616	28.7

TABLE 5 (CONT'D)

Time (hours)	Total Counts per Two Minutes	Corrected Total Counts per Two Minutes	^{14}CO Counts per Two Minutes	Corrected ^{14}CO Counts per Two Minutes	^{14}CO%
3.0	18643	18595	4826	4674	25.2
4.0	17936	17888	4193	4041	22.6
5.0	17389	17341	3508	3356	19.3
	Run No. 17-6, x=2.099, a_o=0.464, T=390°C				
0.67	21749	21701	7353	7201	33.2
1.67	19673	19625	6271	6120	31.2
	Run No. 17-7, x=2.099, a_o=0.464, T=390°C				
0.33	20944	20896	6037	5885	28.2
1.33	19849	19801	6419	6267	31.7
	Run No. 18-11, x=1.903, a_o=0.464, T=350°C				
1.0	9001	8953	209	133	1.49
3.0	8952	8904	544	468	5.26
9.75	9029	8981	1352	1276	14.2
23.67	8673	8625	2617	2541	29.4
34.0	8728	8680	2866	2790	32.1
48.0	8456	8408	2835	2759	32.8
59.25	8367	8319	3858	2782	33.4
73.0	8081	8025	2438	2362	29.3
	Run No. 18-21, x=1.903, a_o=2.19, T=350°C				
2.0	8374	8326	136	60	0.72
4.0	8274	8226	185	119	1.45

TABLE 5 (CONT'D)

Time (hours)	Total Counts per Two Minutes	Corrected Total Counts per Two Minutes	^{14}CO Counts per Two Minutes	^{14}Corrected CO Counts per Two Minutes	^{14}CO%
10.5	8420	8372	370	294	3.50
24.25	8325	8277	584	508	6.14
34.25	8154	8106	711	635	7.82
48.25	8108	8060	844	768	9.51
71.25	8229	8181	877	801	9.78
	Run No. 18-33, x=1.903, a_o=0.218, T=350°C				
1.5	8287	8239	382	306	3.71
3.5	8355	8307	657	581	7.00
6.0	8221	8173	957	881	10.77
11.0	8104	8056	1634	1558	19.30
	Run No. 18-44, x=1.903, a_o=1.442, T=350°C				
1.84	9109	9061	169	93	1.02
5.5	8798	8750	344	268	3.07
20.0	8772	8724	946	870	10.10
47.5	8703	8655	1535	1459	16.82
	Run No. 10-21, x=2.006, a_o=0.218, T=250°C				
1.5	7407	7359	288	212	2.88
5.5	7465	7417	796	720	9.70
12.0	7384	7336	1627	1551	21.2
24.0	7436	7388	2343	2267	30.8

TABLE 5 (CONT'D)

Time (hours)	Total Counts per Two Minutes	Corrected Total Counts per Two Minutes	^{14}CO Counts per Two Minutes	Corrected ^{14}CO Counts per Two Minutes	$^{14}CO\%$
	Run No. 10-31, x=2.006, a_o=1.442, T=250°C				
2.0	2837	2789	92	19	0.68
6.0	8002	7954	282	206	2.59
12.0	8019	7971	482	406	5.10
25.0	7687	7639	830	754	9.85
	Run No. 17-12, x=2.099, a_o=0.464, T=350°C				
0.33	10499	10451	1954	1878	18.0
	Run No. 17-13, x=2.099, a_o=0.464, T=350°C				
0.67	9740	9692	2460	2384	24.6
2.67	9452	9404	3918	3842	40.9
5.0	9087	9039	3615	3539	39.2
	Run No. 17-14, x=2.099, a_o=0.464, T=350°C				
1.0	9910	9862	3397	3321	33.7
2.0	9506	9458	3969	3893	41.2
3.5	9114	9066	3843	3767	41.5
	Run No. 17-21, x=2.099, a_o=2.565, T=350°C				
1.0	8300	8252	975	899	10.9
2.0	8189	8141	1401	1325	16.3
3.17	7982	7934	1605	1529	19.3
6.17	7818	7770	1603	1527	19.7

TABLE 5 (CONT'D)

Time (hours)	Total Counts per Two Minutes	Corrected Total Counts per Two Minutes	^{14}CO Counts per Two Minutes	Corrected ^{14}CO Counts per Two Minutes	$^{14}CO\%$
	Run No. 17-22, x=2.099, a_o=2.565, T=350°C				
4.5	8136	8088	1750	1674	20.7
	Run No. 17-31, x=2.099, a_o=0.284, T=350°C				
0.17	7580	7532	1356	1280	17.0
1.0	7366	7318	3458	3382	46.3
	Run No. 17-32, x=2.099, a_o=0.284, T=350°C				
0.33	7739	7691	2347	2271	29.6
1.5	7374	7325	3720	3644	49.8
	Run No. 17-33, x=2.099, a_o=0.284, T=350°C				
0.5	7553	7505	2758	2682	35.8
2.0	7083	7035	3551	3475	49.2
3.5	7684	6736	3065	2989	44.6
	Run No. 17-41, x=2.099, a_o=1.122, T=350°C				
0.5	9108	9060	1372	1296	14.3
1.5	8462	8418	2455	2379	28.3
3.0	8701	8653	3050	2974	34.4

B. Adsorption Rate Data

TABLE 6

EXPERIMENTAL DATA ON THE ADSORPTION OF OXYGEN BY 50.000 GRAM OF COBALT FERRITE

Time(minutes)	p_a(microns)	Time(minutes)	p_a(microns)
Run No. 10-14, x = 2.006, T = 300°C, Room Temperature = 26.1°C			
0	102.3	10	14.2
0.25	85.2	15	9.8
1.00	54.3	40	3.0
1.50	47.0	60	2.2
2.0	40.2	1150	1.7
3.0	32.2	2710	1.5
5.0	23.5		
Run No. 10-15, x = 2.006, T = 300°C, Room Temperature = 29.1°C			
0	103.5	5	23.8
0.25	87.4	10	13.3
0.50	74.1	15	10.2
1.00	56.5	20	6.9
1.50	47	50	3.4
2.0	40.5	1325	2.7
3.0	32.5	2470	1.9

TABLE 6 (CONT'D)

Time(minutes)	p_a(microns)	Time(minutes)	p_a(microns)
Run No. 10-19, x = 2.006, T = 200°C, Room Temperature = 25.7°C			
0	101.2	10	37
0.25	88.5	20	31
0.50	76.8	40	25.7
1.0	64.0	80	20.9
1.5	58.1	190	12.9
3.0	49.0	1190	6.2
5.0	44.2		
Run No. 10-20, x = 2.006, T = 200°C, Room Temperature = 25.3°C			
0	102.2	10	38.1
0.25	87.4	20	31.9
0.50	77.9	40	26.6
1.0	66.0	80	20.9
1.5	59.7	170	15.6
3.0	51.1	1180	6.0
5.0	45.4		
Run No. 10-21, x = 2.006, T = 100°C, Room Temperature = 25.3°C			
0	100.0	15	48.0
0.25	85.3	40	42.6
0.50	77.5	100	35.8
1.0	68.8	990	21.5
2.0	61.9	1470	19.1
5.0	54.3	2580	16.7

TABLE 6 (CONT'D)

Time(minutes)	p_a(microns)	Time(minutes)	p_a(microns)
Run No. 18-8, x = 1.903, T = 300°C Room Temperature = 25.3°C			
0	101.7	100	64.5
0.25	93.8	360	58.6
1.0	85	1080	53.2
5.0	76.2	2220	48.3
30	68.2		
Run No. 18-9, x = 1.903, T = 300°C, Room Temperature = 24.2°C			
0	103.6	100	66
0.25	95.5	510	59.6
1.0	86.3	1250	56
5.0	78	1980	52.8
30.0	70.3		
Run No. 18-10, x = 1.903, T = 200°C, Room Temperature = 26.3°C			
0	107.2	100	78.5
0.25	100.3	380	73.2
1.0	95.3	1160	68.7
5.0	89.2	2620	65.5
30.0	82.3		
Run No. 18-11, x = 1.903, T = 200°C, Room Temperature = 25.2°C			
0	104.1	120	75.2
0.25	98.7	510	69.7
1.0	93.8	1430	66.0
5.0	87.8	2885	63.7
30.0	80.5		

TABLE 6 (CONT'D)

Time(minutes)	p_a(microns)	Time(minutes)	p_a(microns)
Run No. 18-15, x = 1.903, T = 100°C, Room Temperature = 24.4°C			
0	100	100	81.5
0.25	96.5	540	74.8
1.0	94.4	1460	70.1
5.0	90.2	2660	67.1
30.0	85.0		
Run No. 18-16, x = 1.903, T = 100°C, Room Temperature = 26.8°C			
0	101.9	100	84.2
0.25	98	360	79.3
1.0	96.2	0545	73.6
10.0	91.7	2615	70.3
40.0	87.4		
Run No. 17-1, x = 2.099, T = 300°C, Room Temperature = 25.1°C			
0	102.5	60	87.4
0.25	100.3	120	84.2
1.0	99.2	360	74.5
5.0	96	1140	65
20.0	90.6	2670	55.5
Run No. 17-2, x = 2.099, T = 300°C, Room Temperature = 25.1°C			
0	102.5	60	88.4
0.25	101.0	120	83.1
1.0	99.9	480	69.2
5.0	98	1330	51.1
20.0	93.8	2880	42.1

TABLE 6 (CONT'D)

Time(minutes)	p_a(microns)	Time(minutes)	p_a(microns)
Run No. 17-3, x = 2.099, T = 300°C, Room Temperature = 24.9°C			
0	100.6	120	84.7
0.25	98.8	280	76.6
1.0	93.2	530	68.6
5.0	96	1665	52.1
30.0	91.6	2995	45.2
60.0	88.9		
Run No. 17-5, x = 2.099, T = 200°C, Room Temperature = 24.5°C			
0	105.2	40	102.0
0.25	103.4	100	101.0
1.0	102.8	1560	99.2
5.0	102.6		
Run No. 17-6, x = 2.099, T = 400°C, Room Temperature = 25.2°C			
0	103.3	60	54.3
0.25	99.2	100	48.0
1.0	95.0	250	34.5
5.0	84.8	740	22.5
10.0	78.1	1440	17.7
30.0	64.5		

TABLE 6 (CONT'D)

Time(minutes)	p_a(microns)	Time(minutes)	p_a(microns)
Run No. 17-7, x = 2.099, T = 400°C, Room Temperature = 24.8°C			
0	98.8	60	50.6
0.25	95.5	170	38.1
1.0	89.7	300	31.0
5.0	79.1	650	24.6
10.0	71.3	1440	18.0
30.0	58.2		
Run No. 14-1, x = 1.954, T = 300°C, Room Temperature = 26.2°C			
0	102.0	160	90.1
0.25	100.3	500	87.9
1.0	98.1	1240	85.2
10.0	95.0	2730	82.3
30.0	93.0		
Run No. 14-2, x = 1.954, T = 300°C, Room Temperature = 25.3°C			
0	100.9	120	92.2
0.25	99.9	420	90.0
1.0	98.3	1500	87.8
10.0	96.0	2800	86.4
30.0	94.1		
Run No. 14-4, x = 1.954, T = 500°C, Room Temperature = 27.7°C			
0	103.6	30	65.7
0.25	98	100	55.2
1.0	88	180	49.8
5.0	77.9	560	40.6
10.0	74	1340	33.6

TABLE 6 (CONT'D)

Time(minutes)	p_a(microns)	Time(minutes)	p_a(microns)
Run No. 14-5, x = 1.954, T = 500°C, Room Temperature = 23.1°C			
0	103.3	90	57.0
0.25	97.5	180	51.7
1.0	87.8	690	42.2
10.0	74.2	1360	37.7
30.0	66		
Run No. 14-6, x = 1.954, T = 400°C, Room Temperature = 25.3°C			
0	105.7	100	76.6
0.25	102.0	260	70.7
1.0	93.8	620	64.2
5.0	88.0	1725	53.2
30.0	81.6		
Run No. 14-7, x = 1.954, T = 400°C, Room Temperature = 22.3°C			
0	105.2	30	81.0
0.25	101.0	120	74.8
1.0	93.0	580	64.0
5.0	87.4	1320	55.4
Run No. 15-3, x = 2.058, T = 400°C, Room Temperature = 25.1°C			
0	101.4	45	51.8
0.25	97.5	90	44.7
1.0	90.2	180	38.2
5.0	76.2	390	32.6
10.0	68.4	1430	28.0
20.0	60.1		

TABLE 6 (CONT'D)

Time(minutes)	p_a(microns)	Time(minutes)	p_a(microns)
Run No. 15-4, x = 2.058, T = 400°C, Room Temperature = 26.7°C			
0	100.9	20	61
0.25	97.7	50	52.2
1.0	89.6	110	44.8
5.0	75.8	210	39.3
10.0	68.3	1415	29.0
Run No. 15-6, x = 2.058, T = 350°C, Room Temperature = 26.7°C			
0	99.7	40	73.1
0.25	97.7	80	68.2
1.0	93.2	180	62.4
5.0	86.3	615	52.2
15.0	79.3	1395	44.4
Run No. 15-7, x = 2.058, T = 350°C, Room Temperature = 28.6°C			
0	99.4	30	72.2
0.25	97.0	60	67.9
1.0	92.2	100	64.2
5.0	84.5	390	55.4
15.0	77.3	1225	47.5
Run No. 15-8, x = 2.058, T = 300°C, Room Temperature = 28.7°C			
0	103.2	30	85.8
0.25	102.0	60	81.5
1.0	99.2	130	76.8
5.0	95	370	69.0
15.0	89.5	1255	60.8

C. Data of Oxygen Desorption

TABLE 7

EXPERIMENTAL DATA OF OXYGEN DESORPTION
FROM 50.000 GRAMS OF COBALT FERRITE

Time (minute)	p_a(micron)	Time(minute)	p_a(micron)
Run No. 10-14, x = 2.006, T = 300°C, Room Temperature = 23.1°C			
0	5.35	120	7.2
1	5.5	230	8.2
5	5.6	1390	12.8
60	6.48		
Run No. 10-15, x = 2.006, T = 300°C, Room Temperature = 24.7°C			
0	5.07	150	6.9
1	5.07	330	8.3
5	5.22	1410	11.7
30	5.65		
Run No. 10-19, x = 2.006, T = 200°C, Room Temperature = 24.4°C			
0	1.41	140	1.56
1	1.42	1390	2.6
50	1.47		
Run No. 10-20, x = 2.006, T = 200°C, Room Temperature = 25.5°C			
0	1.14	110	1.78
1	1.16	1510	4.27
10	1.31		
Run No. 10-21, x = 2.006, T = 100°C, Room Temperature = 26.0°C			
0	0.7	100	1.86
1	1.13	410	2.57
10	1.27	1230	3.17

TABLE 7 (CONT'D)

Time(minute)	p_a(micron)	Time(minute)	p_a(micron)
Run No. 10-21, x = 2.006, T = 100°C, Room Temperature = 26.0°C			
0	0.7	100	1.86
1	1.13	410	2.57
10	1.27	1230	3.17
Run No. 18-8, x = 1.903, T = 300°C, Room Temperature = 24.5°C			
0	16.28	140	19.7
1	16.43	420	21.8
5	16.93	1420	23.1
30	17.88		
Run No. 18-9, x = 1.903, T = 300°C, Room Temperature = 25.1°C			
0	16.3	290	21.0
1	17.2	1475	25.6
30	18.05		
Run No. 19-10, x= 1.903, T = 200°C, Room Temperature = 25.5°C			
0	27.0	270	29.2
1	28.4	2910	30.9
30	28.9		
Run No. 18-11, x = 1.903, T = 200°C, Room Temperature = 29.3°C			
0	17.2	505	19.6
1	18.4	2865	21.1
30	18.6		
Run No. 18-15, x = 1.903, T = 100°C, Room Temperature = 23.5°C			
0	20.1	105	21.4
1	21.3	1305	21.6

TABLE 7 (CONT'D)

Time(minute)	p_a(micron)	Time(minute)	p_a(micron)
Run No. 18-16, x = 1.903, T = 100°C, Room Temperature = 27.5°C			
0	16.8	240	18.1
1	17.9	2730	18.5
Run No. 17-1, x = 2.099, T = 300°C, Room Temperature = 25.5°C			
0	7.1	370	17.9
1	8.5	1420	22.0
30	10.4	2850	23.9
Run No. 17-2, x = 2.099, T = 300°C, Room Temperature = 24.2°C			
0	37.8	1380	41.0
1	38.7	2620	
250	39.1		
Run No. 17-5, x = 2.099, T = 200°C, Room Temperature = 24.5°C			
0	14.1	90	16.0
1	15.9	2885	16.1
Run No. 17-6, x = 2.099, T = 400°C, Room Temperature = 24.0°C			
0	7.3	120	23.1
1	8.8	540	33.8
5	11.7	1440	47.3
10	13.9	2940	50.2
30	18.0		
Run No. 17-7, x = 2.099, T = 400°C, Room Temperature = 24.7°C			
0	4.9	100	13.8
1	5.8	220	17.8
5	6.6	1320	36.2
40	10.4	3080	50.6

TABLE 7 (CONT'D)

Time(minute)	p_a(micron)	Time(minute)	p_a(micron)
Run No. 14-1, x = 1.954, T = 300°C, Room Temperature = 29.7°C			
0	9.0	60	12.5
1	10.5	530	16.0
5	10.8		
Run No. 14-2, x = 1.954, T = 300°C, Room Temperature = 26.2°C			
0	28.4	150	34.5
1	30.5	440	36.2
5	30.9	1320	37.8
40	32.3	2740	38.7
Run No. 14-4, x = 1.954, T = 500°C, Room Temperature = 23.9°C			
0	5.3	60	20.2
1	7.3	310	32.1
5	10.3	660	40.5
20	14.9	1635	53.2
Run No. 14-5, x = 1.954, T = 500°C, Room Temperature = 22.3°C			
0	5.3	280	31.5
1	7.9	690	42.2
5	10.7	1400	52.5
20	15.0	2880	65.0
70	21.4		
Run No. 14-6, x = 1.954, T = 400°C, Room Temperature = 24.5°C			
0	7.4	150	15.0
1	9.0	290	17.1
5	10.0	1430	23.2
40	12.3		

TABLE 7 (CONT'D)

Time(minute)	p_a(micron)	Time(minute)	p_a(micron)
Run No. 14-7, x = 1.954, T = 400°C, Room Temperature = 25.1°C			
0	7.6	40	12.8
1	9.5	280	17.9
5	10.5	1380	14.5
Run No. 15-3, x = 2.058, T = 400°C, Room Temperature = 24.1°C			
0	8.6	110	31.5
1	11.6	170	36.9
5	14.9	460	58.1
30	21.5	1270	90.1
Run No. 15-4, x = 2.058, T = 400°C, Room Temperature = 27.8°C			
0	5.9	60	21.8
1	7.8	160	31.6
10	12.9	1310	83.1
30	17.2		
Run No. 15-6, x = 2.058, T = 350°C, Room Temperature = 26.7°C			
0	7.8	100	20.5
1	9.3	350	28.2
5	10.1	640	35.4
30	15.5	1455	46.0
Run No. 15-7, x = 2.058, T = 350°C, Room Temperature = 27.0°C			
0	14.8	180	30.9
1	16.1	660	44.1
10	19.2	1410	52.8
60	25.0		

TABLE 7 (CONT'D)

Time (minute)	p_a(micron)	Time(minute)	p_a(micron)
Run No. 15-8, x = 2.058, T = 300°C, Room Temperature = 26.8°C			
0	10.6	100	15.9
1	11.8	310	19.8
30	13.4	1520	27.6

APPENDIX II SAMPLE CALCULATIONS

A. Exchange Reaction of CO_2 and CO

For a given run with constant ratio of CO_2 and CO at constant temperature, the rate constant $k(a_o)$ was calculated by applying equation (21).

$$\frac{V}{ART}\frac{d\ p1^4_{CO}}{dt} = k(a_o)\ [p^i{}_{14_{CO_2}} - (1 + a_o)\ p_{14_{CO}}] \qquad (21)$$

The following is a sample calculation of $k(a_o)$ for Run 17-21 (of Table 5) at a_o=2.565, T=350°C by two methods.

(i) Initial Rate Method:

At t=0, equation (21) can be simplified to

$$d\left(\frac{\left(\frac{p_{14_{CO}}}{p^i{}_{14_{CO_2}}}\right)}{dt}\right)_{t=0} = \frac{k(a_o)\ ART}{V} \qquad (74)$$

The raw date of $p_{14_{CO}}/p^i{}_{14_{CO_2}}$ versus time are plotted in Figure 4. They are tabulated in Table 8.

From Figure 16 of the plot $p_{14_{CO}}/p^i{}_{14_{CO_2}}$ versus t, the slope at t=0 was obtained, by equation (74)

$$\frac{k(a_o)\ ART}{V} = \frac{0.116}{1.0} = 0.116\ (-hr^{-1})$$

since A=2.48 x 10^4 cm^2 for 1.000 gm of catalyst

T=623°K

V=507 cm^3

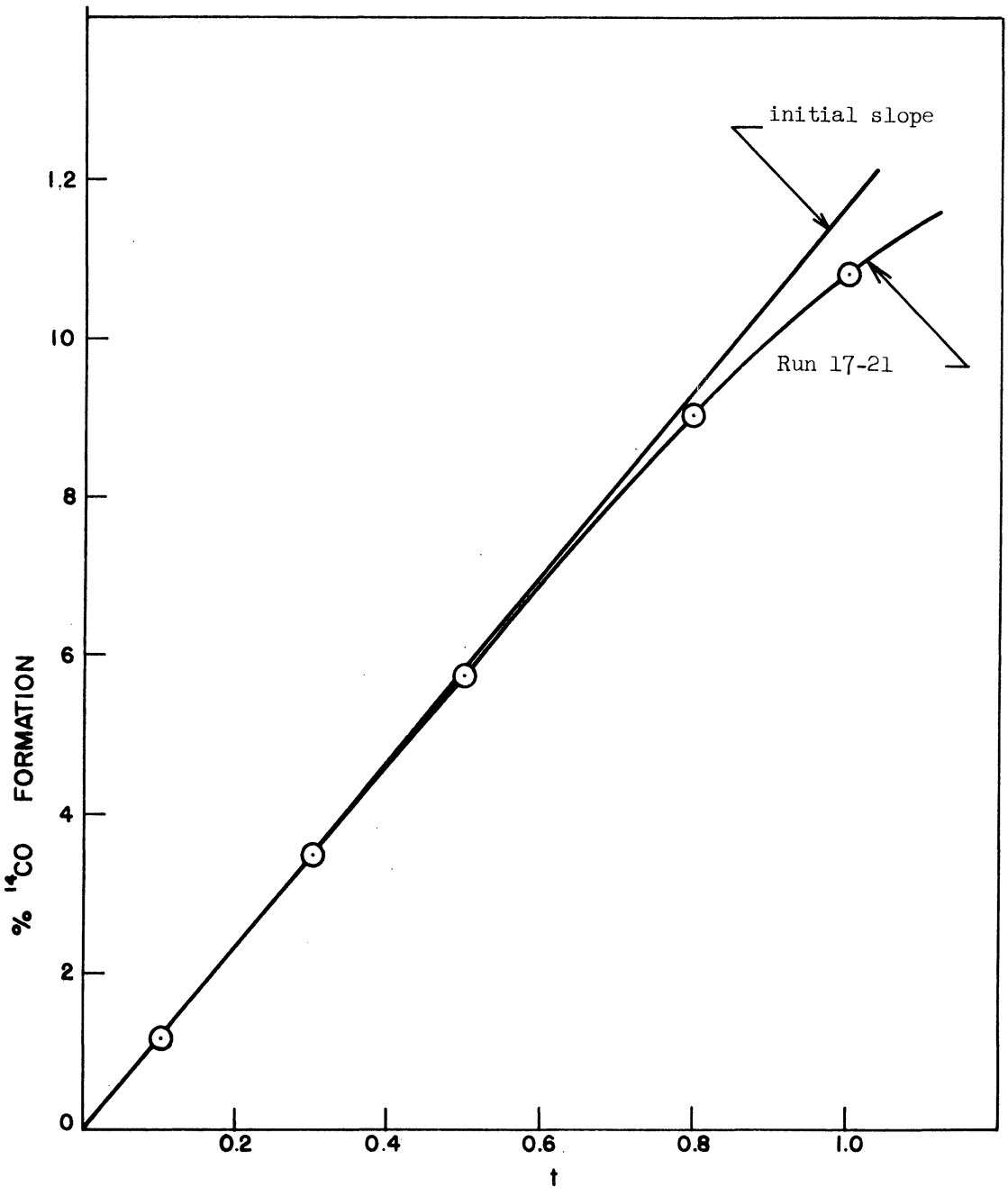

Figure 16. $\frac{p_{^{14}CO}}{p^{i}_{^{14}CO_2}}$ versus t for Run 17-21 and initial slope

$$k(a_o) = \frac{0.116 \times 507}{82.05 \times 623 \times 2.48 \times 10^4} = 0.464 \times 10^{-7} \left(\frac{\text{mole}}{\text{hr.atm cm}^2} \right)$$

In order to prove that $k(a_o)$ is not a function of time, the values of $k(a_o)$ are calculated from the raw data by applying equation (23) which is the integrated form of equation (21). The results are tabulated in Table 8.

$$\ell n\left[1-(1 + a_o) \frac{p_{^{14}CO}}{p^i_{^{14}CO_2}}\right] = - \frac{k(a_o)RTA(1+a_o)t}{V} \qquad (23)$$

The following is a sample calculation at $t=0.3$, $\frac{p_{^{14}CO}}{p^i_{^{14}CO_2}} = 0.035$.

$$k(a_o) = \frac{-507 \times \ell n\,[1-(1 + 2.565) \times 0.035]}{82.05 \times 623 \times 2.48 \times 10^4 \times 3.565 \times 0.3}$$

$$= 0.45 \times 10^{-7} \left(\frac{\text{mole}}{\text{hr} \cdot \text{ atm cm}^2} \right)$$

TABLE 8

THE RESULT OF RUN 17-21 OF THE EXCHANGE REACTION OF CO_2 AND CO.

t(hr)	0	0.1	0.3	0.5	0.8	1.0	2.0
$\frac{p_{^{14}CO}}{p^i_{^{14}CO_2}}$	0	0.012	0.035	0.057	0.090	0.109	0.163
calculated $k(a_o) \times 10^7$ $\left(\frac{\text{mole}}{\text{hr}\cdot\text{atm}\cdot\text{cm}^2}\right)$		0.46	0.45	0.46	0.48	0.46	0.47

(ii) Digital Computer Simulating Method:

Knowing the value of $k(a_o)$, the numerical relationship of $p_{l^4CO}/p^i_{l^4CO_2}$ versus t could be obtained from solving equation (21) by the finite difference method. Euler's method was applied to solve the first order differential equation. The calculation was done on a IBM 7090 computer. Different values of $k(a_o)$ ART/V were fed to the computer to simulate the experimental data. Figure 17 shows the result of Run 17-21, which also gives $k(a_o)$ ART/V = 0.116 [hr^{-1}]. The following is the main program written in MAD to solve for the numerical solution of equation (21) by Euler's method.

```
          INTEGER COUNT,  FREQ
          PRINT COMMENT  $ L EULERS METHOD SOLUTION $
START     READ AND PRINT DATA
          T = 0
          PCO = 0
          PRINT RESULTS T,  PCO
          COUNT = 0
          THROUGH STEP FOR  T = 0., H, T.G. TMAX
          COUNT = COUNT + 1
          PCO = PCO + H * (KFORW -(KFORW + KFORW * AO)* PCO)
STEP      WHENEVER (COUNT/FREQ) * FREQ. E. COUNT, PRINT RESULTS T+H, PCO
          TRANSFER TO START
          END OF PROGRAM
```

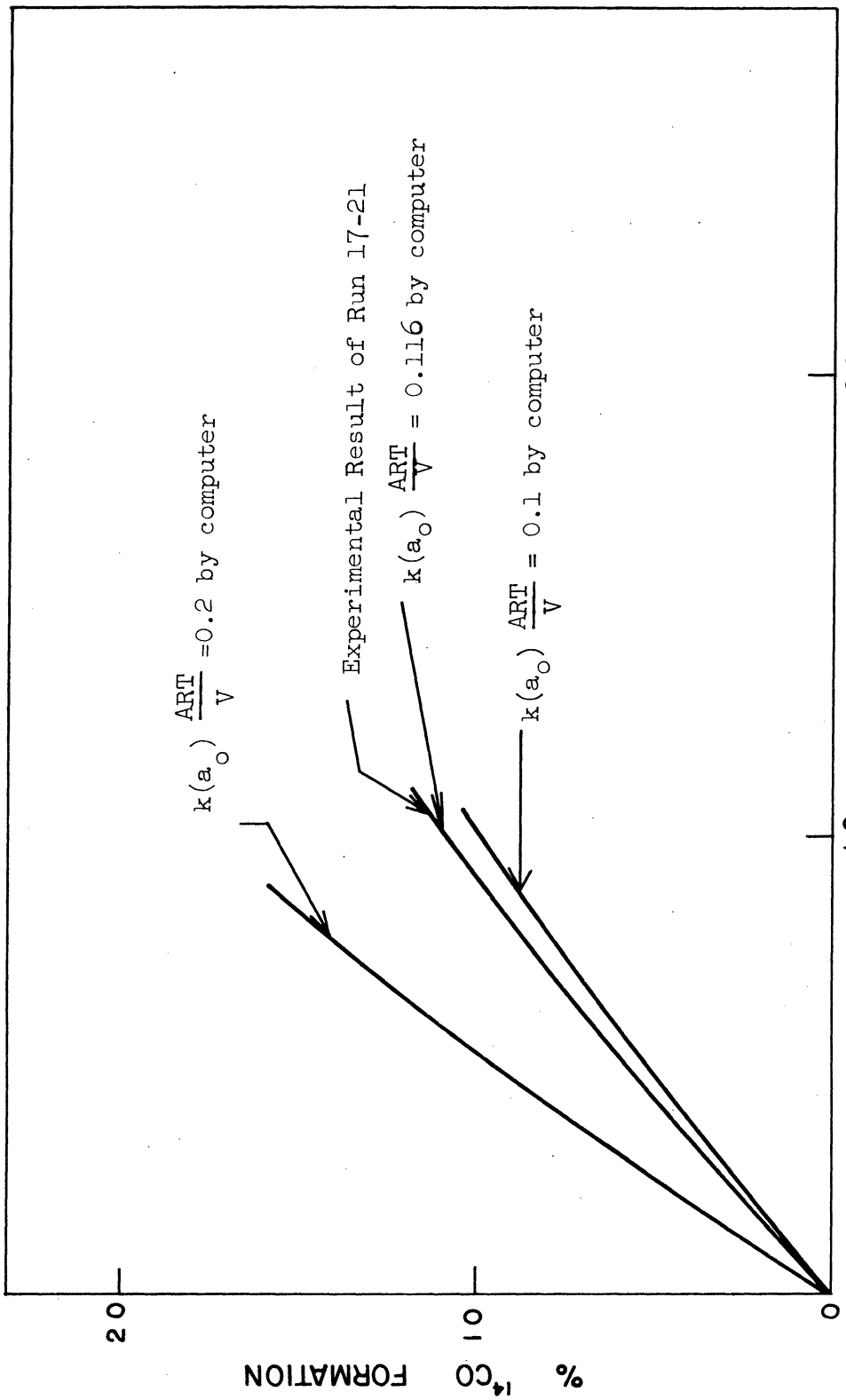

Figure 17. $\frac{p_{14CO}}{p^1_{14CO_2}}$ versus t for Run 17-21 and Results from Computer Simulating Method

The following is the list of variables in the program.

Program Symbol	Definition
PCO	$p_{^{14}CO}/p^{i}_{^{14}CO_2}$
KFORW	$k(a_o)_t \frac{ART}{V}$
T	
AO	a_o
COUNT	The number of times the algorithm has been applied
FREQ	A parameter which control the printing frequency
H	step size

B. Adsorption and Desorption of Oxygen

In Table 3, the amount of oxygen adsorbed per unit surface area of the sample, the initial rate of adsorption and the rate constant $K_{ads.}$ were calculated from equations (58), (48) and (59).

$$\frac{\Delta na}{A} = \frac{Va}{ART}(p_{ai} - p_{af}) \tag{58}$$

$$-\frac{Va}{ART}\frac{dpa}{dt} = k_{ads.}\{[Co^{+2}|B| - Fe^{+3}|B|]_{br} - \gamma(p_{ai} - pa)\}pa \tag{48}$$

and

$$-\left(\frac{dna}{Adt}\right)_{t=0} = K_{ads.}\ p_{ai} = k_{ads.}[Co^{+2}|B| - Fe^{+3}|B|]_{br}p_{ai} \tag{59}$$

The following is a sample calculation for Run 10-14 (of Table 6) with x=2.006 and T=300°C

$$\frac{\Delta na}{A} = \frac{5.302\ (102.3 - 2.15)}{50 \times 2.48 \times 10^4 \times 760{,}000 \times 0.08205 \times 298}$$

$$= 2.29 \times 10^{-11}\ (\frac{mole}{cm^2})$$

From equation (48) the values of $[Co^{+2}|B| - Fe^{+3}|B|]_{br}$ and k_{ads} were obtained by the digital computer simulating method. Sets of values of $[Co^{+2}|B| - Fe^{+3}|B|]$ and $k_{ads}ART/Va$ were fed to a IBM 7090 computer to solve equation (48) and to simulate the experimental data of p_a versus t. The value γ in equation (48) was defined by equation (47)

$$= \frac{Va\ N}{ART\beta} = \frac{5.302 \times 6.023 \times 10^{23}}{0.08205 \times 298 \times 50 \times 2.48 \times 10^{20} \times \frac{1}{23.4} \times 760{,}000}$$

$$= 3.35 \times 10^{-4}\ (\text{micron}^{-1})$$

Figure 18 shows the plot of experimental data of Run 10-14 and the plot of numerical solution of equation (48) with $[Co^{+2}|B| - Fe^{+3}|B|]_{br} = 0.0271$ and $k_{ads}\ ART/Va = 24.3\ (min^{-1})$. Then from equation (59),

$$K_{ads.} = \frac{24.3 \times 0.0271 \times 5.302 \times 60}{2.48 \times 10^{4} \times 0.08205 \times 298} = 3.46 \times 10^{-4}\ \left(\frac{\text{mole}}{\text{hr}\cdot\text{atm}\cdot\text{cm}^2}\right)$$

and

$$-\left(\frac{dn_a}{ART}\right)_{t=0} = \frac{3.46 \times 10^{-4} \times 102.3}{760{,}000} = 4.66 \times 10^{-10}\ \left(\frac{\text{mole}}{\text{hr}\cdot\text{cm}^2}\right)$$

The following is the MAD program to solve equation (48) by the IBM 7090 computer.

```
          INTEGER COUNT, FREQ
          PRINT COMMENT $ 1 EULERS METHOD SOLUTION $
START     READ AND PRINT DATA
          T = 0
          P02 = P020
```

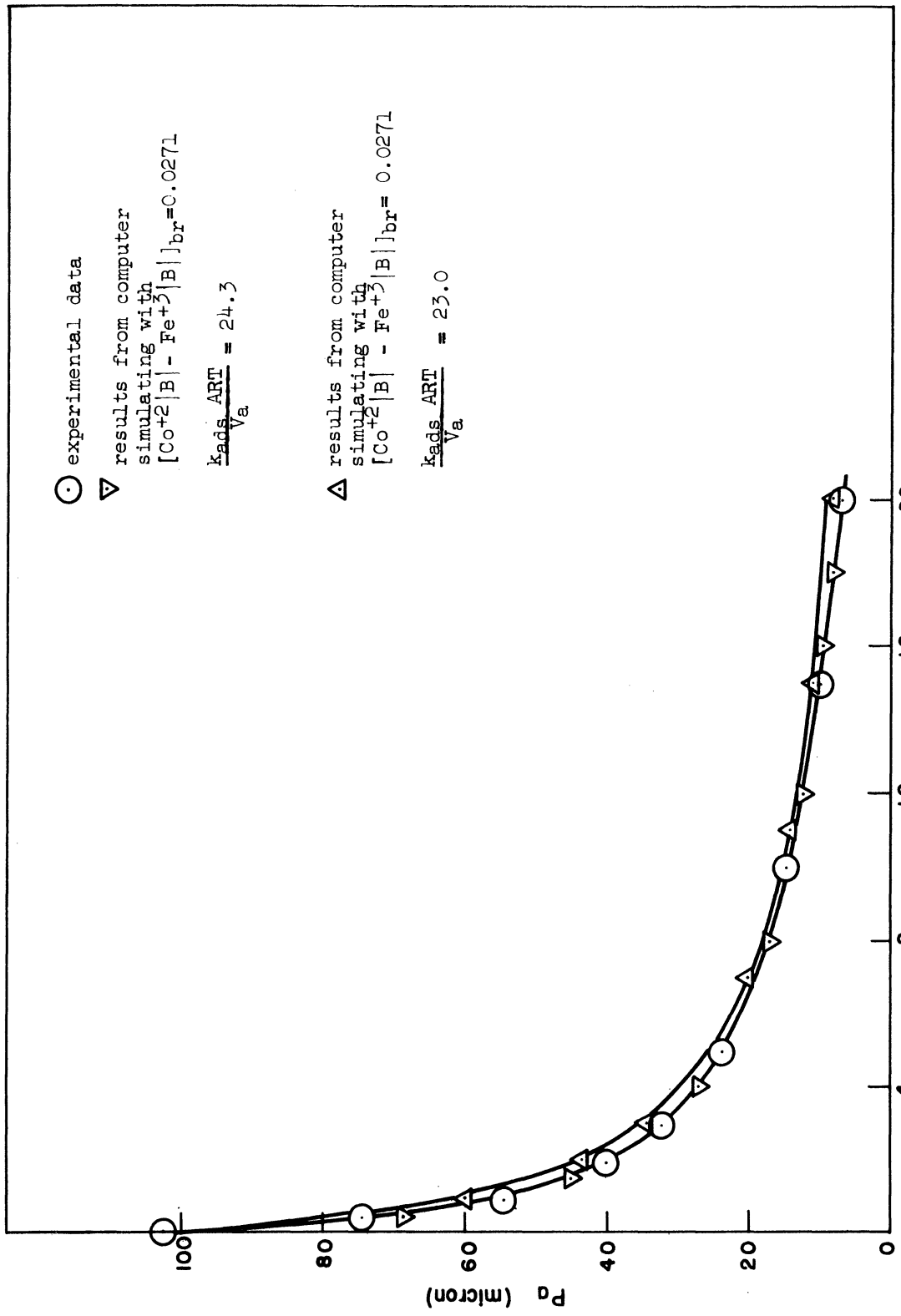

Figure 18. P_a versus t for Run 10-14 and Results from the Computer Simulating Method

```
        PRINT RESULTS T, PO2
        COUNT = 0
        THROUGH STEP, FOR T = 0., H, T.G. TMAX
        COUNT = COUNT + 1
        BRCNT = BRCNTR - GAMMA* (PO20 - PO2)
        PO2 = PO2 - H * KADS * BRCNT * PO2
STEP    WHENEVER (COUNT/FREQ) * FREQ.E.COUNT,PRINT RESULTS T+H, PO2
        TRANSFER TO START
        END OF PROGRAM
```

The following is the list of variables in the program.

Program Symbol	Definition
T	t
PO2	p_a
PO20	p_{ai}
GAMMA	γ
KADS	$\frac{k_{ads.}\ ART}{V_a}$
BRCNTR	$[Co^{+2}\|B\|-Fe^{+3}\|B\|]_{br}$
H	Step size
COUNT	The number of times the algorithm has been applied
FREQ	A parameter which controls the printing frequency

In Table 4, the amount of oxygen desorbed per unit surface area and the initial rate of desorption were calculated from equations (61) and (50). For Run 10-15 (of Table 7) with x=2.006 and T=300°C;

p_{df}=11.7 micron, p_{di}=5.07 micron, p_d=5.07 micron at t=1 min. and p_d=5.22 micron at t=5 min.

$$\frac{\Delta n_d}{A} = \frac{V_d(p_{df}-p_{di})}{ART}$$

$$= \frac{5.205 \times (11.7 - 5.07)}{760{,}000 \times 0.08205 \times 298 \times 50 \times 2.48 \times 10^4}$$

$$= 1.55 \times 10^{-12} \quad (\frac{\text{mole}}{\text{cm}^2})$$

$$\left(\frac{dn_d}{Adt}\right)_{t=0} = \frac{Va}{ART}\left(\frac{dp_d}{dt}\right)_{t=0}$$

$$= \frac{5.205 \times (5.22 - 5.07) \times \frac{60}{4}}{760{,}000 \times 0.08205 \times 298 \times 50 \times 2.48 \times 10^4}$$

$$= 0.725 \times 10^{-12} \frac{\text{mole}}{\text{hr}\cdot\text{cm}^2}$$

APPENDIX III STRUCTURE OF COBALT FERRITE

Cobalt ferrite exists in a structure of "inverse" spinel, $Fe^{+3}|A| - [Co^{+2}|B| Fe^{+3}|B|]O_4$ [44]. Figure 19 shows the composition of (100), (110) and $(\bar{1}10)$ planes in $CoFe_2O_4$ [64]. The value of a, the lattice parameter of $CoFe_2O_4$, is 8.39 Å.

The proposed active center, $Co^{+2}|B| - Fe^{+3}|B|$ cation pair, appears in plane (100). The inter-cation distance of $Co^{+2}|B| - Fe^{+3}|B|$ is $a\sqrt{2}/4 = 2.97$ Å as shown in Figure 19.

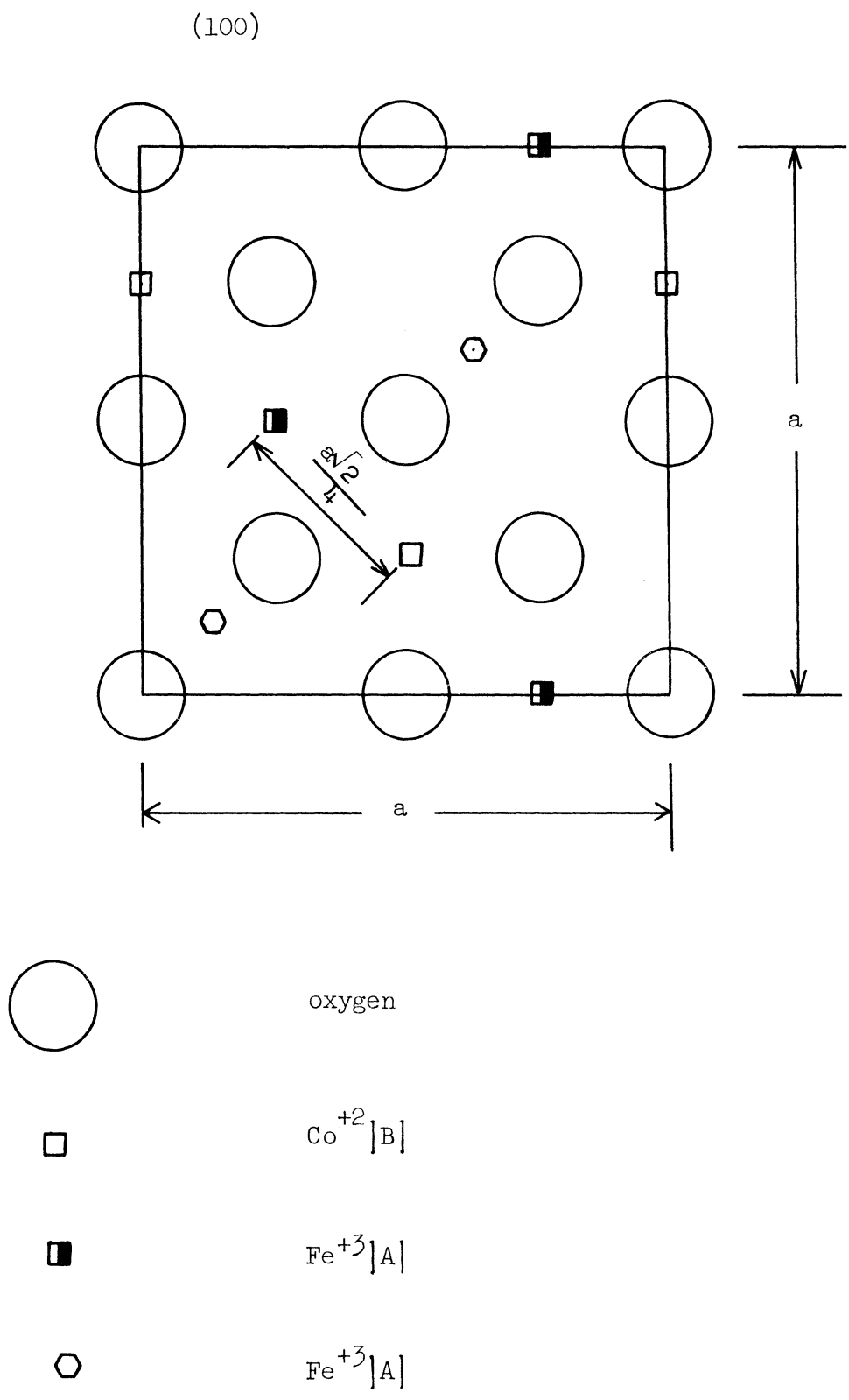

Figure 19. Composition of (100), (110) and ($\bar{1}$10) planes in $CoFe_2O_4$

(110)

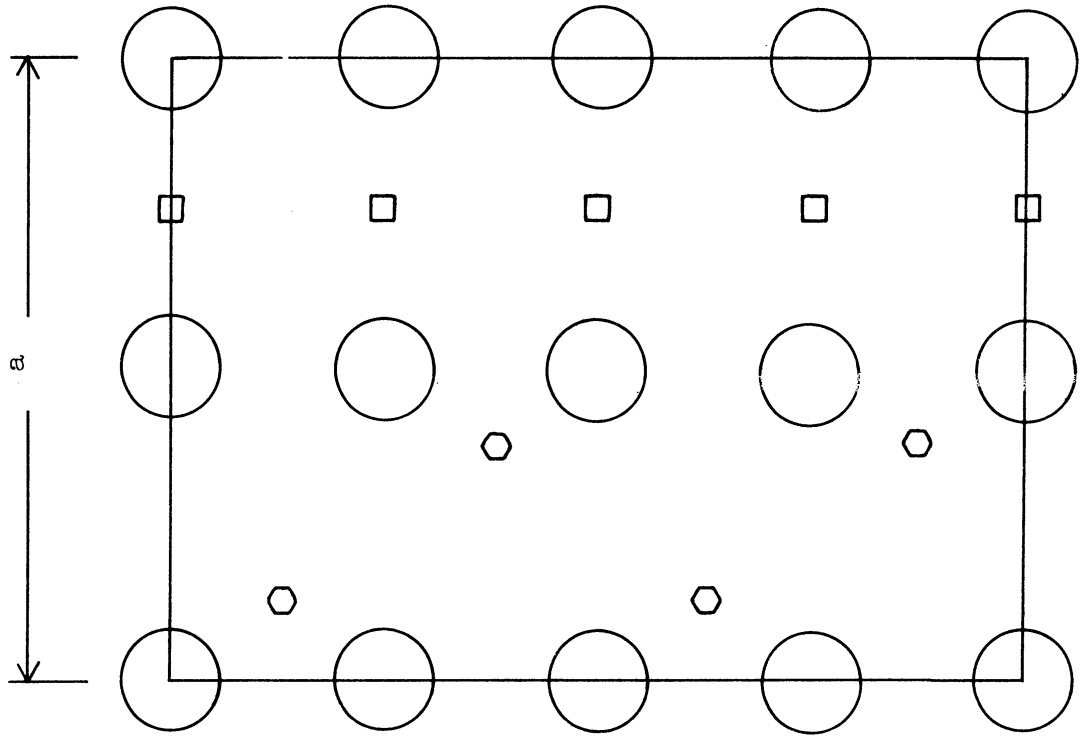

($\bar{1}$10)

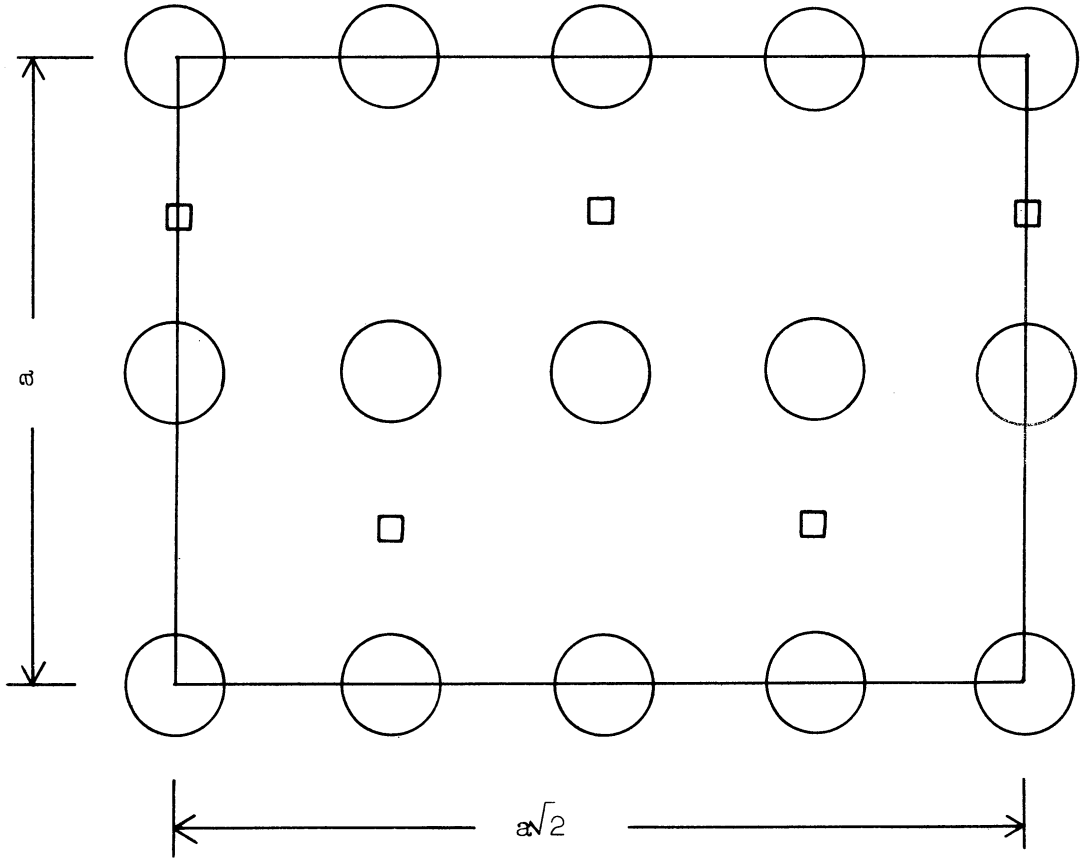

Figure 19. (CONT'D)

BIBLIOGRAPHY

1. Aigrain, P. and Dugas, C. Z., Elecktronchem, 56, 363 (1952).

2. Balandin, A. A., Catalysis and Chemical Kinetics, Academic Press, New York, (1964).

3. Barry, T. I., and Stone, F. S., Proc. Roy. Soc., A 255, 124, (1960).

4. Barth, T. F. W., and Posnjak, E., Zeits. f. Krist., 82, 235, (1932).

5. Bawn, C. E. H., and Ledwith, A., Chem. and Ind., 1329, (1958).

6. Beebe, R. A., and Dowden, D. A., J. Am. Chem. Soc., 60, 2912, (1938).

7. Bell, R. P., Acid-Base Catalysis, The Clarendon Press, London, (1941).

8. Boudart, M., J. Am. Chem. Soc., 74, 1531, (1952).

9. Bragg, W. H., Phil. Mag., 30, 305, (1915).

10. Brandner, J. D., and Urey, H. C., J. Chem. Phys., 13, No. 9, 351, (1945).

11. Brunauer, S., Love, K. S., and Keenan, R. G., J. Am. Chem. Soc., 64, 751, (1944).

12. Burwell, R. L., Jr., and Taylor, H. S., J. Am. Chem. Soc., 58, 697, (1936).

13. Dell, R. M., Stone, F. S., and Tiley, P. F., Trans. Faraday Soc., 49, 201, (1953).

14. Dowden, D. A., J. Chem. Soc., 1950, 242, (1950).

15. Dowden, D. A., Mackenzie, N., and Trapnell, B. M. W., Proc. Roy. Soc., A 237, 245, (1956).

16. Dzisyak, A. P., Boreskov, G. K., Kasatkina, L. A., and Kochurikhin, V. E. Kinetika i kataliz, 2, 386, (1961).

17. Elovich, S. Yu., and Zhabrova, G. M., Zh. Fiz. Khim., 13, 1761, (1939).

18. Engell, H. J., and Hauffe, Z., Elektrochem, 57, 773, (1953).

19. Faeth, P. A., and Willingham, C. B., Technical Bulletin on the Assembley, Calibration and Operation of a Gas Adsorption Aparatus for the Measurement of Surface Area, Pore Volume Distribution and Density of Finely Divided Solids, Mellon Institute of Industrial Research, Pittsburgh, (1955).

20. Garner, W. E., Stone, F. S., and Tiley, P. F., Proc. Roy. Soc., A 211, 472, (1952).

21. Garner, W. E., Advances in Catalysis, 9, 169, (1957).

22. Garner, W. E., J. Chem. Soc., p. 1239, (1947).

23. Garner, W. E., and Veal, F. J., J. Chem. Soc., 1487, (1935).

24. Glasstone, S., Laidler, K. J., and Euring, H., in The Theory of Rate Processes, McGraw-Hill, New York, 1941.

25. Gorter, E. W., Phil, Res. Rep., 9, 295, (1954).

26. Grabke, H. J., in Proc. Third. Inter. Congress on Catalysis, p. 928, (1964).

27. Grabke, H. J., Ber. Bunsenges. Physik. Chem. Bd., 69, Nr. 1, (1965).

28. Hauffe, K., Advances in Catalysis, 1, 213, (1955).

29. Hauffe, K., and Engell, H. J., Z. Elekrochem., 56, 366, (1952).

30. Hayakawa, T., Bull. Chem. Soc. Japan, 26, 165, (1953).

31. Hill, T. L., Introduction to Statistical Thermodynamics, Addison-Welsley, Reading, Massachusetts, (1960).

32. Howard, D. C., and Trapnell, B. M. W., Chemisorption, Butterworths and Co., London, (1964).

33. Hwang, S. T., Ph.D. Thesis, The University of Michigan, (1965).

34. Jennings, T. J., and Stone, F. S., Advances in Catalysis, 9, 441, (1957).

35. Jonker, G. H., J. Phys. Chem. Solids, 9, 165, (1959).

36. Jonker, G. H., and van Houten, S. in Halbleiterprobleme Band VI, p. 118, Verlag Friedr. Vieweg and Sohn, Braunschweig, (1961).

37. Laidler, K. J., J. Phys. Chem., 53, 712, (1949).

38. Langmuir, I., J. Am. Chem. Soc., 28, 2221 (1916; ibid. 40, 1361, (1918); Trans. Faraday Soc., 17, 607, (1922).

39. Langmuir, I., Phys. Rev., 22, 357, (1923).

40. Langmuir, I., J. Am. Chem. Soc., 54, 2798, (1932).

41. Law, J. T., J. Phys. Chem. Solids., 4, 91, (1958).

42. Ligenza, J. R., J. Phys. Chem., 64, 1017, (1960).

43. Low, M. J. D., Chem. Reviews, 60, 267, (1960).

44. Molinari, E., and Parravano, G., J. Am. Chem. Soc., 75, 5233, (1953).

45. Morrison, S. R., Advances in Catalysis, 7, 259, (1955).

46. Muller, E., and Huber-Emden, H., Ann., 649, 70, (1961).

47. Muller, W., Gehlordnungein, Koblatferrit, Diplomarbeit, Gottingen, (1963).

48. Muller, W., and Schmalzried, H., Berichte der Bunsengesellschaft fur Physikalische Chemie, Band 68, Helf 3, 270, (1964).

49. Pauling, L., The Nature of Chemical, the Bond, Cornell University Press, N.Y., (1960).

50. Parravano, G., and Boudart, M., Advances in Catalysis, 7, 50, (1955).

51. Parravano, G., unpublished paper.

52. Pietrzak, H., Gates, W. C., and Parravano, G., unpublished report.

53. Ratterman, F., unpublished work.

54. Robin, J., and Benard, J., Compt. rend. 232, 1830, (1951); Compt. rend. 234, 734, (1952).

55. Romeizn, F. C., Philips Research Rep. 8, 304, (1953).

56. Rudham, R., and Stone, F. S., in Chemisorption, ed. W. E. Garner, London, Butterworth, (1957).

57. Schmalzried, H., and Wagner, C., and Z. Physik. Chem. NF 31, 198, (1962).

58. Schmalzried, H.,"Point Defects in Ternary Ionic Crystals" in Progress in Chemistry of the Solid State, Pergamon Press, N.Y., (1965).

59. Scholten, J. J. F., Zwietering, P., Konvalinka, J. A., and deBoer, J. H., Trans. Faraday Soc., 55, 2166, (1959).

60. Schwab, G. M., and Block, J., Z. Elektrochem., 58, 756, (1954).

61. Schwab, G. M., Roth, E., Grintzos, C., and Mavrakis, N., in Structure and Properties of Solid Surfaces, p. 464, University of Chicago Press, Chicago, (1953).

62. Smiltens, R., J. Am. Chem. Soc., 79, 4481, (1957).

63. Squires, R. G., Ph.D. Thesis, The University of Michigan, (1962).

64. Squires, R. G., and Parravano, G., J. Catalysis, 2, 324, (1963).

65. Stone, F. S., Rudham, R., and Gale, R. L., Z. Elecktronchem., 63, 129, (1959).

66. Stone, F. S., Advances in Catalysis, 13, 1, (1962).

67. Taylor, H. A., and Thon, N., J. Am. Chem. Soc., 74, 4169, (1952).

68. Taylor, H. S., Z. Electrochem., 20, 201, (1914).

69. Taylor, H. S., J. Amer. Chem. Soc., 37, 551, (1915).

70. Taylor, H. S., and Williamson, A. T., J. Am. Chem. Soc., 53, 2168, (1931).

71. Taylor, H. S., and Ogden, G., Trans. Faraday Soc., 30, 1178, (1934).

72. Verwey, E. J. W., Haayman, P. W., and Romeijn, F. C., J. Chem. Phys., 15, 181, (1947).

73. Verwey, E. J. W., and Heilmann, E. L., J. Chem. Phys., 15, 174, (1947).

74. Wagner, D., J. Chem. Phys., 18, 69, (1950).

75. Wagner, C., Vorschlage zu Untersuchungen der Katalyse der Reaction $CO_2 + H_2 = CO + H_2O$ an Wustit, Mermorandum vom, Jan. 3, 1962.

76. Wagner, C., Vorschlage zu Untersuchungen uber die Reaktion $C^{14}O_2 + C^{12}O = C^{12}O_2 + C^{14}O$, Jan. 14, 1962.

77. Weisz, P. B., J. Chem. Phys.,20, 1483, (1952).

78. Weisz, P. B., J. Chem. Phys., 21, 1531, (1953).

79. Winter, E. R. S., J. Chem. Soc., p. 2726, (1955).

80. Winter, E. R. S., Advances in Catalysis, 10, 196, (1958).

81. Wolkenstein, Th., J. Chem. Phys., 54, 175, (1957).

82. Wolkenstein, Th., Advances in Catalysis, 9, 807, (1957).

83. Wolkenstein, Th., Advances in Catalysis, 12, 189, (1960).

84. Wolkenstein, Th., in The Electronic Theory of Catalysis on Semiconductors, Pergamon Press, 1963.